The Dissertation Committee for Evstati Georgiev Evstatiev
certifies that this is the approved version of the following dissertation:

A Model for Multi-Wave Beam–Plasma Interaction

Committee:

Philip J. Morrison, Supervisor

Wendell Horton

Boris Breizman

Richard D. Hazeltine

Rafael De La Llave

A Model for Multi-Wave Beam–Plasma Interaction

by

Evstati Georgiev Evstatiev, B.S; M.S.

Dissertation

Presented to the Faculty of the Graduate School of

The University of Texas at Austin

in Partial Fulfillment

of the Requirements

for the Degree of

Doctor of Philosophy

The University of Texas at Austin

December 2004

To my parents Georgi and Zlatka

Acknowledgments

I thank my supervisor, Philip Morrison, for his guidance and encouragement throughout my time at The University of Texas at Austin. I thank Boris Breizman and Swadesh Mahajan for useful discussions, and Paul Watson for a lot of help and advice with numerical simulations. I thank Tom Yudichak, Alex Wurm, Amit Apte, Todd Krause, and Chris Jones for many useful discussions.

I am grateful I came to Austin (the live music capital of the world), whose true faces are diversity, variety, and education. I thank my friends Gergana Drandova, Sergey Cheshkov, Nikola Petrov, Adriana Petrova, Ilian Iliev, and Hani Kaldass for helping me during my first years in Austin.

I thank my parents for all the support they have given me.

Evstati Georgiev Evstatiev

The University of Texas at Austin

December 2004

A Model for Multi-Wave Beam–Plasma Interaction

Publication No. _____

Evstati Georgiev Evstatiev, Ph.D.
The University of Texas at Austin, 2004

Supervisor: Philip J. Morrison

A system that describes the interaction of an electron beam, plasma waves, and electromagnetic waves in a cold plasma is presented and studied. A multi-wave model is developed that allows for efficient computational and analytical study. The model is based on the slow amplitude and phase change approximations. Using a Lagrangian approach, the continuous system of electron beam, background plasma, and waves is reduced to a finite degree-of-freedom system. This model, describes an efficient energy transfer mechanism between electromagnetic waves and the plasma wave, via the particles trapped in the plasma wave. It is suggested that this energy transfer be used in plasma-based accelerators to further increase the energy of the accelerated particles. Numerical and analytical studies of this mechanism are performed and an experimental test is proposed.

Contents

Chapter 1

Introduction

The subject of this thesis is the investigation of the interaction of a relatively small number of charged particles (electrons) with both electrostatic and electromagnetic waves in a cold unmagnetized plasma. In this introduction the basic ideas upon which the work hinges are introduced and previous results are summarized. The presentation here is concise, and it introduces the necessary notation and terminology.

An ionized gas in which all or considerable number of atoms have lost one or several of their electrons and turned into a mixture of free electrons and positive ions is called plasma. The charges interact via the Coulomb force i.e., the force between any two charges is proportional to the product of their charges and inversely proportional to the distance between them. Such a force is a long range force (compared to strong or weak forces, or intermolecular forces). The analysis in the early work of Tonks and Langmuir [1] led to explaining one of the fundamental characteristic vibrations observed in a plasma, the electron-plasma oscillations. To begin a more quantitative description, let us consider the fast electron oscillations in an infinite plasma. Suppose the

electron density is n, and the electron charge density, $-en$. Consider the portion of the plasma between two planes perpendicular to the z-axis of a Cartesian coordinate system. Suppose each electron between these two planes is displaced by a distance ξ which is independent of the x and y coordinates and is zero at each bounding plane. Let the displacement be a continuous function of z and $\partial\xi/\partial z$ be small compared to unity. The charge density caused by this displacement is given by

$$\delta n = n\frac{\partial \xi}{\partial z}.$$

Using Poisson's equation we find

$$\frac{\partial E}{\partial z} = 4\pi e\delta n = 4\pi ne\frac{\partial \xi}{\partial z},$$

where E is the electric field. Integrating the above and assuming that no external field is present, we obtain

$$E = 4\pi ne\xi. \tag{1.1}$$

Using the equation of motion $m_e\ddot{\xi} = -eE$, where m_e is the electron mass, yields

$$m_e\ddot{\xi} + 4\pi ne^2\xi = 0.$$

Therefore we conclude that the displaced electrons oscillate about their original position with a simple harmonic motion and frequency

$$\omega_p = \sqrt{\frac{4\pi ne^2}{m_e}},$$

which is called the electron plasma frequency. The electron plasma wave is an electrostatic wave and its group velocity, $v_g = d\omega/dk$, is zero. The wave

motion of this wave can be visualized using the following analogy. Let us think of the electrons as the bobs of equally spaced pendulums suspended from a rigid ceiling. If the swing amplitudes are small so that the pendulums do not collide, these pendulums resemble that of the electron oscillation. Now if a force sets those pendulums in motion (for example, passing horizontally a bar that slightly touches them), the resulting wave may be thought of as the electrostatic wave in a plasma. In a physical situation it is possible that the pendulums cross/collide and the force setting them in motion be a laser pulse or electron beam.

Considerations for the oscillations of the ions in the plasma yield a similar formula for the frequency, with the electron mass substituted by the ion mass. Since the electron-ion mass ratio is much smaller than unity, the ion plasma frequency is much lower than the electron plasma frequency. Therefore the ions have little time to respond to the electron oscillations and their motion can often be neglected. In this thesis the considered time scales are short enough so that the ions may be assumed to be immobile.

The electron-plasma oscillations (also referred to as plasma oscillations, or electron oscillations) are essentially plasma density oscillations resembling those of sound in air. However, there is an important difference between the two. In air, the particles interact via short range forces and many collisions occur during the period of an oscillation. Thus the short-time average of momentum transfer determines the mean motion of a particle. Similarly, the collisions in air are the reason that if a particle has velocity higher (slower) than that of the surrounding particles, it will be slowed down (accelerated) to the mean velocity of the flow, so that hydrodynamic description of air is appropriate.

In contrast, because of the long range Coulomb forces between the charges, a given particle collides with many particles at the same time continuously, but with small momentum transfer at each collision. Each particle moves almost freely with a gradual change of its velocity caused by the cumulative and simultaneous forces produced by all other particles. Therefore, to simplify the problem of description of a plasma as a medium, it is appropriate to smooth out the fluctuations resulting from the point character of the charges. This idea was used by Vlasov in his work [2] where he proposed a method, similar to that used by Hartree and Fock in quantum mechanics of the self-consistent fields. In this kinetic theory the description of the plasma is in terms of a distribution function $f(\mathbf{x}, \mathbf{v}, t)$, such that $\int d^3v f(\mathbf{x}, \mathbf{v}, t) = n(\mathbf{x}, t)$, where $n(\mathbf{x}, t)$ is the usual space number density (used in Eq. (1.1)). The distribution function satisfies the Vlasov equation

$$\frac{\partial f}{\partial t} + \mathbf{v} \cdot \nabla f + \mathbf{a} \cdot \nabla_v f = 0, \tag{1.2}$$

$\mathbf{a} = (q/m_e)(\mathbf{E} + (1/c)\mathbf{v} \times \mathbf{B})$, and q is the electric charge. To this system of equations we also attach Maxwell equations

$$\begin{aligned} &\nabla \cdot \mathbf{E} = 4\pi\rho, \qquad \nabla \cdot \mathbf{B} = 0, \\ &\nabla \times \mathbf{E} = -\frac{1}{c}\frac{\partial \mathbf{B}}{\partial t}, \qquad \nabla \times \mathbf{B} = \frac{4\pi}{c}\mathbf{j} + \frac{1}{c}\frac{\partial \mathbf{E}}{\partial t}. \end{aligned} \tag{1.3}$$

In the above system of equations, ρ and $\mathbf{j}$ are the charge and current density, respectively. Finally, we need the relations

$$\rho = q \int f d^3v, \qquad \mathbf{j} = q \int \mathbf{v} f d^3v. \tag{1.4}$$

Equations (1.2)–(1.4) are the Vlasov-Maxwell system. Having found the distribution function we can easily find quantities like space density, mean

velocity and momentum, energy, pressure, temperature, heat flow, etc., and these are basically moments of the distribution function. The Vlasov-Maxwell system becomes particularly simple when we consider waves in the system with phase velocities much larger than the thermal velocity of the plasma. In particular, the cold plasma model assumes that the temperature of the plasma is zero. Then the distribution function is a delta function in $\mathbf{v}$ and the system of equations simplifies to fluid equations for the plasma (i.e. involving only spatial variables), plus simple constitutive relations for the charges and currents. This model will also be employed in the present work.

Using the Vlasov equation we can consider the situation of wave damping (excitement) in a plasma. The main result is due to Landau [3]. When a wave propagates in a plasma at a velocity close to the average (thermal) velocity of the electrons in a plasma, then it experiences collisionless damping, called the Landau damping. The damping coefficient is found to be

$$\gamma_L = \frac{\pi\omega_L\omega_p^2}{2nk^2}\frac{\partial f}{\partial v}, \qquad \omega_L = \left(\omega_p^2 + 3k^2T/m_e\right)^{1/2}. \tag{1.5}$$

The second of formulas (1.5) is the so-called Bohm-Gross dispersion relation. It is the dispersion relation of plasma waves propagating in a warm plasma. We will not pursue the properties of warm plasma in the present work. What is important for the future development is the fact that if in the first of formulas (1.5) $\partial f/\partial v > 0$ a plasma wave gets excited. The physical process behind such excitation of plasma waves is energy transfer from a group of particles, with velocity larger than the thermal velocity of the background plasma, to the plasma wave. Following the plasma wave excitation is a process of particle trapping. More specifically, as the plasma wave amplitude grows, it becomes possible that some of electrons with velocities very close to the phase velocity

of the wave get trapped in the electrostatic potential of the plasma wave. Then the particles and the wave exchange momentum (energy) and particles can get accelerated if they have the appropriate phase relative to the phase of the wave. If, in addition, the density of the background plasma changes so that the phase velocity of the wave increases (increasing plasma density) this could result in particle acceleration to very high speeds. This mechanism was proposed as a possibility leading to cosmic-ray particle acceleration, see [4].

The idea of plasma based accelerators has drawn attention in recent years because plasmas can sustain extremely large acceleration gradients. Conventional linear accelerators have acceleration gradient limited to about 100 MV/m. A plasma based accelerator can sustain plasma waves with fields of the order $E_0 = cm_e\omega_p/e$ (see [5]), or

$$E_0\,[\mathrm{V/cm}] \simeq 0.96 n^{1/2}\left[\mathrm{cm}^{-3}\right]. \tag{1.6}$$

For example, if $n = 10^{18}\mathrm{cm}^{-3}$, $E_0 \simeq 100\mathrm{GV/m}$.

A plasma wave can be excited in four different ways. First, an electron beam propagating in a plasma can excite a plasma wave. The accelerators based on this method of excitation are called plasma-based accelerators [6, 7, 8, 9, 10, 11, 12, 13, 14, 15, 16, 17]. The next three methods of exciting a plasma wave are based on laser pulses. The main idea was that of Tajima and Dawson [18] and Chan [19]. One way of exciting a plasma wave by a laser pulse uses the beat wave of two long laser pulses offset by a plasma frequency. This type of accelerator is called a beat-wave accelerator. Another way of exciting a plasma wave is by a single short powerful pulse and the accelerators based on this scheme are called laser wakefield accelerators. And lastly, the plasma wave can be excited by one long powerful laser pulse undergoing self-modulation at

the plasma frequency; the corresponding accelerators are called self-modulated laser wakefield accelerators. There has been a tremendous amount of work in studying the interaction between plasma and laser pulses with respect to accelerator development [20, 21, 22, 23, 24, 25, 26, 27, 28, 29, 30]. An overview of plasma-based accelerators is given in [31].

The work of the present thesis can be understood in the context of plasma-based accelerators but it also makes a bridge to laser wakefield accelerators. The purpose of this thesis is to build a simplified model for particle-wave interaction. It considers the beam-excited plasma wave in the linear and non-linear stages, and the influence of external electromagnetic (laser) waves in the system. It builds upon a model referred to as "The single wave model" [9, 10, 32, 33]. The main virtue of this work is that it takes this model and generalizes it to include multiple waves, plasma and electromagnetic, and three spatial dimensions. In the derivation of it we use a Lagrangian and Hamiltonian approach. The Lagrangian approach to problems in plasma physics has been used successfully by many authors [34, 35, 36, 37]. The continuous beam-plasma system is simplified to a finite degree-of-freedom system described by a system of ordinary differential equations. This allows for computational efficiency and, with additional simplifications, to analytical treatment. Based on the predictions of our model we study the interaction of trapped particles, plasma waves, and external electromagnetic waves. The fact that the trapped particles have velocity nearly equal to the plasma wave phase velocity (resonant particles) is used to suggest an efficient way of energy transfer between electromagnetic (laser) waves and the plasma wave through the trapped particles. It is suggested that this energy transfer be used in plasma-based accelerators to further increase the energy of the accelerated particles. We show that even

with small intensity of the laser pulses a considerable amount of energy could be transferred, on the order of $17 - -60\%$. Our numerical and analytical studies show that before such a transfer can occur the electromagnetic waves amplitudes should exceed a certain threshold.

The structure of the thesis is as follows. Chapter 2 is dedicated to derivation of the multi-wave model for plasma-wave interaction in the non-relativistic case. It introduces the basic approximations and ideas that underlie such derivation. The model is investigated numerically and a system of one plasma and two electromagnetic waves is shown to have chaotic features.

In Chapter 3 the model is derived in its full generality i.e., with three dimensions and relativistic particles. Here the limitations of the model are discussed and a justification of the approximations used is given.

In Chapter 4 we perform numerical study of the relativistic multi-wave and multi-dimensional model. We study how the energy of the plasma wave scales with the linear growth rate of the wave. Our findings conform to well-known results. Then we study a system of one plasma and one or two electromagnetic waves. In the case of one electromagnetic wave we show that there is no resonant interaction (no resonant particles), but the electromagnetic wave behaves as an external force to the beam-plasma system. This fact is used later in Chapter 5 to further simplify the equations and make possible an analytical study. In Chapter 4 we also study the system of one plasma and two electromagnetic waves. Our results show that energy transfer between the plasma and the electromagnetic waves is present when a matching condition is satisfied, provided the electromagnetic waves have amplitudes that are larger that a certain threshold. An experimental test is proposed (see also [38]).

In the last Chapter 5 we preform further simplifications that allow us

to create a simple picture of phenomena observed numerically in the previous chapters. We use the "macroparticle" model (see [32]) and additional "external wave" approximation to reduce the system of equations to a two-degree-of-freedom system. We perform analysis using the island overlapping technique, make surfaces of section plots, and finally perform a linear analysis to explain our numerical results from the previous chapters.

Chapter 2

Non-Relativistic Multi-Wave Model

2.1 Introduction

In this chapter we begin with the derivation of a non-relativistic model that describes the interaction of a mono-energetic beam with a cold plasma in the presence of several electrostatic and electromagnetic waves. The positive ions in the background plasma are supposed to be immobile. The presentation here follows closely Ref. [33]. The model is derived assuming slowly changing wave amplitudes and phases (envelope approximation). We study some basic properties numerically, such as interaction of one electrostatic and one or two electromagnetic waves with the beam. The model we derive is highly non-linear and some features of chaotic behavior are encountered. We also see that although the electromagnetic waves are non-resonant with the beam particles, their presence in the system has non-trivial consequences, such as accelerated

growth of the electrostatic wave.

The derivations given in this chapter are with somewhat less details since emphasis will be given on the numerical study of the model. This is done in order to introduce the model in a simpler context and introduce the basic parameters of the problem. In the next Chapter 3 more details on the derivations will be given, as the model will be in its general form, namely, relativistic beam particles in three spatial dimensions.

2.2 Derivation of the model

We start with a Lagrangian for the system of background plasma, fields, and particles

$$\begin{aligned} L \;=\; & \int \mathrm{d}^3x \Bigg\{ \frac{1}{2} mn|\mathbf{v}|^2 + \frac{1}{8\pi}\left(\left| \nabla\phi + \frac{1}{c}\frac{\partial \mathbf{A}}{\partial t} \right|^2 - |\nabla \times \mathbf{A}|^2 \right) \\ & -\rho\phi + \frac{1}{c}\mathbf{j}\cdot\mathbf{A} \Bigg\} + \sum_{i=1}^{N} \Bigg\{ \frac{1}{2}\, m|\dot{\mathbf{r}}_i|^2 + e\phi(\mathbf{r}_i, t) \\ & -\frac{e}{c}\,\dot{\mathbf{r}}_i \cdot \mathbf{A}(\mathbf{r}_i, t) \Bigg\} \end{aligned} \tag{2.1}$$

where $\mathbf{v}$ is the Eulerian velocity field, n the particle density for the background plasma, ϕ and $\mathbf{A}$ are the scalar and vector potentials, respectively, $\mathbf{j}$ is the current, ρ is the charge density, and $-e$ is the electron charge. Quantities with a subscript refer to beam particles whereas those without to the background plasma. The Coulomb gauge $\nabla\cdot\mathbf{A} = 0$ is assumed.

Two kinds of waves are included: N_L longitudinal waves, which are described by the scalar potential, and N_T electromagnetic (linearly polarized) transverse waves, which are described by the vector potential. The number of particles is N.

Motivated by fluid theory and previous derivations for the beam-plasma model, we assume the following linear response relations for the background plasma:

$$\begin{aligned}
&\mathbf{v}_L = \frac{1}{4\pi ne}\,\frac{\partial \nabla\phi}{\partial t}, \qquad \mathbf{v}_T = \frac{e}{mc}\,\mathbf{A},\\
&\mathbf{j}_L = -en\mathbf{v}_L, \qquad \mathbf{j}_T = -ne\mathbf{v}_T,\\
&\rho = -\frac{1}{4\pi}\nabla^2\phi,\\
&\phi = \sum_{i=1}^{N_L}\phi_i, \qquad \mathbf{A} = \sum_{i=1}^{N_T}\mathbf{A}_i\,,
\end{aligned} \tag{2.2}$$

where $\mathbf{v}_L$ and $\mathbf{v}_T$ are the longitudinal and transverse velocities, respectively, in terms of which the currents $\mathbf{j}_L$ and $\mathbf{j}_T$ are described. We insert (2.2) into the action of (2.1).

The fields are constrained by assuming the following forms:

$$\begin{aligned}
\phi_i(\mathbf{r},t) &= \phi_i(t)\cos[k_{Li}x - \omega_{Li}t - \beta_i'(t)], \quad i = 1...N_L,\\
A_{yi}(\mathbf{r},t) &= a_i(t)\cos[k_i x - \omega_i t - \theta_i'(t)], \quad i = 1...N_T,
\end{aligned} \tag{2.3}$$

and $A_{xi} \equiv A_{zi} \equiv 0$. The longitudinal fields only have components in the x–direction. The amplitudes, $\phi_i(t)$ and $a_i(t)$, and the phases, $\beta_i'(t)$ and $\theta_i'(t)$, of (2.3) are assumed to be slowly varying functions of time (Whitham's envelope approximation, see Ref. [39]). We substitute (2.3) into (2.1) and keep only terms up to first (linear) order in the time derivatives of the phases and the amplitudes. Assuming periodic boundary conditions we perform the spatial integration (i.e. we average) of the Lagrangian (2.1) over a box of size l to

obtain

$$
\begin{aligned}
L(t) \quad =& \sum_{i=1}^{N} \frac{1}{2} m \left[\dot{x}_i^2(t) + \dot{y}_i^2(t) \right] \\
& + e \sum_{i=1}^{N} \sum_{j=1}^{N_L} \phi_j(t) \cos[k_{Lj} x_i(t) - \omega_{Lj} t - \beta'_j(t)] \\
& - \frac{e}{c} \sum_{i=1}^{N} \sum_{j=1}^{N_T} \dot{y}(t) a_j(t) \cos[k_j x_i(t) - \omega_j t - \theta'_j(t)] \\
& + \frac{l^3}{8\pi} \sum_{j=1}^{N_L} \frac{k_{Lj}^2 \dot{\beta'}_j(t) \phi_j^2(t)}{\omega_p} \\
& + \frac{l^3}{8\pi} \sum_{j=1}^{N_T} \frac{\omega_j \dot{\theta}'_j(t) a_j^2(t)}{c^2} \, .
\end{aligned} \tag{2.4}
$$

In the above calculation we have made use of the dispersion relations for electrostatic and electromagnetic waves in a cold plasma $\omega_{Li}^2 = \omega_p^2$ and $\omega_i^2 = \omega_p^2 + k_i^2 c^2$, respectively. We have also assumed that wave vectors for different waves are different.

In the next section we derive the Hamiltonian of the system and show that the energy and momentum are conserved.

2.3 Hamiltonian form and conservation laws

We write the Lagrangian (2.4) in dimensionless variables

$$\begin{aligned} L \;=\; & \sum_{i=1}^{N} \frac{1}{2}\left(\dot{\xi}_i^2 + \dot{\eta}_i^2\right) + \sum_{i=1}^{N}\sum_{j=1}^{N_L} \sqrt{\frac{J_j}{\nu_j^3 N}}\cos\left[\nu_j(\xi_i - \beta_j)\right] \\ & -\left(\frac{2n_b}{n}\right)^{\frac{1}{3}} \sum_{i=1}^{N}\sum_{j=1}^{N_T} \left(\frac{\omega_p}{\omega_j}\right)^{\frac{1}{2}} \sqrt{\frac{I_j}{\mu_j N}}\,\dot{\eta}_i \cos\left[\mu_j(\xi_i - \theta_j)\right] \\ & + \sum_{j=1}^{N_L} J_j\dot{\beta}_j + \sum_{j=1}^{N_T} I_j\dot{\theta}_j + \left(\frac{2n_b}{n}\right)^{-\frac{1}{3}} \sum_{j=1}^{N_L}\left(1 - \frac{1}{\nu_j}\right) J_j \\ & + \left(\frac{2n_b}{n}\right)^{-\frac{1}{3}} \sum_{j=1}^{N_T}\left(1 - \frac{\omega_j}{\mu_j\omega_p}\right) I_j\,, \end{aligned} \tag{2.5}$$

where a number of scalings have been performed, $\mu_j = k_j/k_{L1}$, $\nu_j = k_{Lj}/k_{L1}$, $n_b = N/l^3$, and the following substitutions have been made

$$\begin{aligned} & \xi_i = k_{L1}x_i - \omega_p t(\tau), \quad \eta_i = k_{L1}y_i, \\ & t = \omega_p^{-1}\left(2n_b/n\right)^{-\frac{1}{3}}\tau, \\ & \beta'(t) = \nu_j\beta_j(\tau) + \left(\nu_j - 1\right)\omega_p t(\tau), \\ & \theta'(t) = \mu_j\theta_j(\tau) + \left(\mu_j - \frac{\omega_j}{\omega_p}\right)\omega_p t(\tau), \\ & \phi_j^2 = \left(\frac{m\omega_p^2}{ek_{L1}^2}\right)^2 \left(\frac{2n_b}{n}\right)^{\frac{4}{3}} \frac{J_j}{\nu_j^3 N}, \\ & a_j^2 = \left(\frac{mc\omega_p}{ek_{L1}}\right)^2 \left(\frac{2n_b}{n}\right)^{\frac{4}{3}} \left(\frac{\omega_p}{\omega_j}\right) \frac{I_j}{\mu_j N}\,. \end{aligned} \tag{2.6}$$

Notice that by (2.6) we have changed to a reference frame traveling with the phase velocity of the $j = 1$ longitudinal wave; this means that the $j \neq 1$ waves will have additional time dependence. All transverse waves have such additional time dependence since their phase velocity is always greater than

the phase velocity of the longitudinal waves (and also grater than the speed of light).

From this Lagrangian, by the standard Legendre transform for the coordinates and the method presented in Appendix A we find the Hamiltonian of the system

$$\begin{aligned} H &= \sum_{i=1}^{N} \frac{p_{\xi_i}^2}{2} + \sum_{i=1}^{N} \frac{1}{2} \left[p_{\eta_i} + \left(\frac{2n_b}{n} \right)^{\frac{1}{3}} \sum_{j=1}^{N_T} \left(\frac{\omega_p}{\omega} \right)^{\frac{1}{2}} \sqrt{\frac{I_j}{\mu_j N}} \cos\left[\mu(\xi_i - \theta_j) \right] \right]^2 \\ &\quad - \sum_{i=1}^{N} \sum_{j=1}^{N_L} \sqrt{\frac{J_j}{\nu_j^3 N}} \cos\left[\nu_j \left(\xi_i - \beta_j \right) \right] \\ &\quad - \left(\frac{2n_b}{n} \right)^{-\frac{1}{3}} \sum_{j=1}^{N_L} \left(1 - \frac{1}{\nu_j} \right) J_j - \left(\frac{2n_b}{n} \right)^{-\frac{1}{3}} \sum_{j=1}^{N_T} \left(1 - \frac{\omega_j}{\mu_j \omega_p} \right) I_j \,. \end{aligned} \tag{2.7}$$

With this Hamiltonian the Poisson brackets are of canonical form and the conservation of energy, $\mathrm{d}H/\mathrm{d}\tau = 0$, is assured because the Hamiltonian contains no explicit τ dependence. To see conservation of momentum, we write out the equations of motion for N particles, N_L longitudinal waves, and N_T

transverse waves

$$
\begin{aligned}
\dot{\xi}_i &= p_{\xi_i}, \\
\dot{p}_{\xi_i} &= -\sum_{j=1}^{N_L} \sqrt{\frac{J_j}{\nu_j N}} \sin[\nu_j\,(\xi_i - \beta_j)] \\
&\quad + \left(\frac{2n_b}{n}\right)^{\frac{1}{3}} \sum_{j=1}^{N_T} \left(\frac{\omega_p}{\omega_j}\right)^{\frac{1}{2}} \sqrt{\frac{\mu_j I_j}{N}} \sin[\mu_j\,(\xi_i - \theta_j)] \\
&\quad \times \left[p_{\eta_i} + \left(\frac{2n_b}{n}\right)^{\frac{1}{3}} \sum_{j=1}^{N_T} \left(\frac{\omega_p}{\omega_j}\right)^{\frac{1}{2}} \sqrt{\frac{I_j}{\mu_j N}} \right. \\
&\quad \left. \times \cos[\mu_j\,(\xi_i - \theta_j)] \right], \qquad (2.8) \\
\dot{\eta}_i &= p_{\eta_i} + \left(\frac{2n_b}{n}\right)^{\frac{1}{3}} \sum_{j=1}^{N_T} \left(\frac{\omega_p}{\omega_j}\right)^{\frac{1}{2}} \sqrt{\frac{I_j}{\mu_j N}} \cos[\mu_j\,(\xi_i - \theta_j)]\,, \\
\dot{p}_{\eta_i} &= 0, \\
\dot{\beta}_i &= -\frac{1}{2} \frac{1}{\sqrt{\nu_i^3 J_i N}} \sum_{k=1}^{N} \cos[\nu_i\,(\xi_k - \beta_i)] - \left(\frac{2n_b}{n}\right)^{-\frac{1}{3}} \left(1 - \frac{1}{\nu_i}\right), \\
\dot{J}_i &= \sqrt{\frac{J_i}{\nu_i N}} \sum_{k=1}^{N} \sin[\nu_i\,(\xi_k - \beta_i)]\,, \\
\dot{\theta}_i &= \frac{1}{2} \frac{1}{\sqrt{\mu_i I_i N}} \left(\frac{\omega_p}{\omega_i}\right)^{\frac{1}{2}} \left(\frac{2n_b}{n}\right)^{\frac{1}{3}} \sum_{k=1}^{N} \cos[\mu_i\,(\xi_k - \theta_i)] \\
&\quad \times \left[p_{\eta_k} + \left(\frac{2n_b}{n}\right)^{\frac{1}{3}} \sum_{j=1}^{N_T} \left(\frac{\omega_p}{\omega_j}\right)^{\frac{1}{2}} \sqrt{\frac{I_j}{\mu_j N}} \cos[\mu_j\,(\xi_k - \theta_j)] \right] \\
&\quad - \left(\frac{2n_b}{n}\right)^{-\frac{1}{3}} \left(1 - \frac{\omega_i}{\mu_i \omega_p}\right), \\
\dot{I}_i &= -\sqrt{\frac{\mu_i I_i}{N}} \left(\frac{\omega_p}{\omega_i}\right)^{\frac{1}{2}} \left(\frac{2n_b}{n}\right)^{\frac{1}{3}} \sum_{k=1}^{N} \sin[\mu_i\,(\xi_k - \theta_i)] \\
&\quad \times \left[p_{\eta_k} + \left(\frac{2n_b}{n}\right)^{\frac{1}{3}} \sum_{j=1}^{N_T} \left(\frac{\omega_p}{\omega_j}\right)^{\frac{1}{2}} \sqrt{\frac{I_j}{\mu_j N}} \cos[\mu_j\,(\xi_k - \theta_j)] \right],
\end{aligned}
$$

The two components of the total wave-particle momentum are

$$P_\xi := \sum_{i=1}^{N} p_{\xi_i} + \sum_{j=1}^{N_L} J_j + \sum_{j=1}^{N_T} I_j \,, \tag{2.9}$$

$$P_\eta := \sum_{i=1}^{N} p_{\eta_i} \,. \tag{2.10}$$

$$\tag{2.11}$$

Using equations (2.8) it is easy to see that $dP_\xi/d\tau = dP_\eta/d\tau = 0$, hence these components of the total momentum are conserved. The third component (the momentum along the z-axis) is trivially conserved for a plane polarized wave.

Notice that the canonical coordinates for the waves are the phases β_j and θ_j, and the corresponding conjugate momenta are J_j and I_j, respectively. The variables η_i are ignorable and so the p_{η_i} are conserved. The number of degrees of freedom is thus reduced to $N + N_L + N_T$. When the transverse fields are set to zero, the Hamiltonian reduces to that given in Ref. [11] and Ref. [32].

From these equations we see that the coupling between waves only occurs by means of the particle dynamics. This kind of coupling suggests there will be a transfer of energy between particles and waves, and consequently through this process, between transverse and longitudinal waves. Because our model is non-relativistic, the interaction between electromagnetic waves and particles is generally expected to be small. The reason is that the terms with a small factor (v/c) are much smaller, for example in the Lorentz force, than the dominant electric force (in our case the electric force is due to the electrostatic wave). Everywhere transverse waves in the system enter with two small factors: $(\omega_p/\omega_i)^{\frac{1}{2}}$ and $(2n_b/n)^{\frac{1}{3}}$. The first small factor appears in laser wake field accelerator physics, where the laser frequency is usually much larger

than the longitudinal wave frequency. However, in our derivation of the model nowhere is its smallness used and so it can in general be chosen arbitrarily. The smallness of the second factor is required to ensure that no significant changes of the shape of the waves occurs. Therefore, generally the influence of the transverse waves is expected to be small, since it includes both small factors. To increase the coupling between particles (electrons) and transverse (electromagnetic) waves we have to consider relativistic velocities of the beam particles because the phase velocity of the transverse wave is always greater than c. However, as we will see in the next section, such coupling exists even in the non-relativistic case and is not negligible.

We note that the in variables in which the system of equations (2.8) is written, the linear analysis is not convenient, since a singularity occurs at the equilibrium point $J = 0$. Since the pairs (J, β) forms action-angle variables (similarly do the pairs (I, θ) for the transverse waves), the situation can be compared to the one where linear analysis is done in polar coordinates. When the radial variable goes to zero, the coordinate change form Cartesian to polar coordinates has a singularity and the angle can take any value. In the next chapter we will derive a similar system of equations for relativistic beam particles in different variables, which will allow us to perform the linear analysis around the equilibrium point $\xi_i(0) = 2\pi i/N$, $p_{\xi_i}(0) = v_0$, $J(0) = 0$, $\beta(0) = 0$ (in the absence of transverse waves) without difficulty.

2.4 Numerical results and discussion

In the absence of transverse waves the system has been extensively studied in a number of papers, see Refs. [11, 32, 9, 10, 40, 41, 42, 43]. In the present

section we give some preliminary numerical results that demonstrate the effect of the presence of transverse waves in the system. We analyze the system of equations (2.8) numerically for $N = 100$ electrons uniformly distributed over 2π, $n_b/n = 0.001$, $p_{\xi_i}(0) = 0$, $\beta_i(0) = 0$, and $J_i(0) = 0$ (in the actual simulation $J(0) = 10^{-8}$). The longitudinal waves grow up from instability. The initial velocity of the beam particles is taken equal to the phase velocity of the longitudinal wave (resonant electrons). Because the system of equations (2.8) is in a moving frame, the initial momenta (velocities) are zero. All momenta p_{η_i} are taken to be zero, and the frequencies are determined according to the formula,

$$\frac{\omega_i}{\omega_p} = \left(1 + \mu_i^2 \frac{c^2}{\omega_p^2/k_{L1}^2}\right)^{\frac{1}{2}} . \tag{2.12}$$

The ratio of the phase velocity ω_p/k_{L1} to c is taken to be equal to 0.1 to justify neglect of relativistic effects. Two quantities that are used in laser-plasma experiments are $|e\mathbf{E}_T/m\omega_i c|$ and $|e\mathbf{E}_L/m\omega_p c|$. Using the relations $|\mathbf{E}_L| = |\nabla\phi|$ and $|\mathbf{E}_T| = |(1/c)(\partial\mathbf{A}/\partial t)|$ for the longitudinal and transverse electric fields, and the relations (2.6), we find the following estimates:

$$\left|\frac{e\mathbf{E}_L}{m\omega_p c}\right| \simeq \left(\frac{\omega_p}{k_{L1}c}\right)\left(\frac{2n_b}{n}\right)^{\frac{2}{3}}\sqrt{\frac{J_i}{\nu_i N}}\,, \tag{2.13}$$

$$\left|\frac{e\mathbf{E}_T}{m\omega_i c}\right| \simeq \left(\frac{\omega_p}{k_{L1}c}\right)^{\frac{5}{2}}\left(\frac{2n_b}{n}\right)\sqrt{\frac{I_i}{\mu_i^4 N}}\,. \tag{2.14}$$

For the parameters we use in our numerical simulations, and assuming $J_i = 10^2$, $\nu_i = 1$, $I_i = 10^3$, and $\mu_i = 2$, we get the values of 10^{-3} and 2.5×10^{-6} for (2.13) and (2.14), respectively. From formulas (2.13) and (2.14) we can easily find the transverse-to-longitudinal energy ratio. For example, for the same parameters as above, this yields 4×10^{-3} for $I_i = 10^3$ and 0.4 for $I_i = 10^5$; in

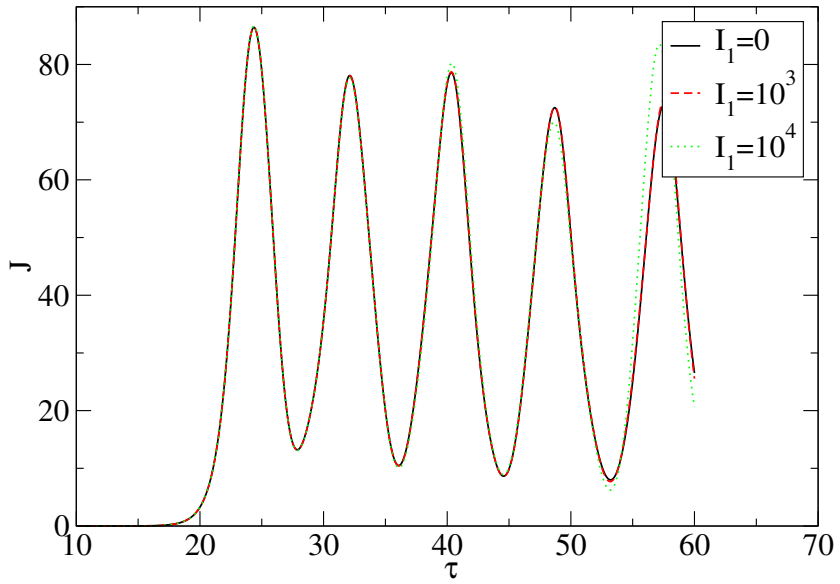

Figure 2.1: Case of one transverse wave and one longitudinal wave. Several runs with different transverse wave initial amplitude and $\mu_1 = 2.0$ are shown. No significant difference from the single wave model (solid line) is seen.

the second case the transverse waves have comparable energy to the longitudinal waves. Now let us consider numerical solutions of Eqs. (2.8). First we look at the case of one longitudinal and one transverse wave. In Fig. 2.1 we show results from several runs with various values of the transverse wave amplitude. We see very little influence of the transverse wave. With no transverse wave the longitudinal field evolves according to the equations for the longitudinal single-wave model. For example, the results agree with those shown in Ref. [32] (up to a change of variables). In Fig. 2.2, we show runs with two

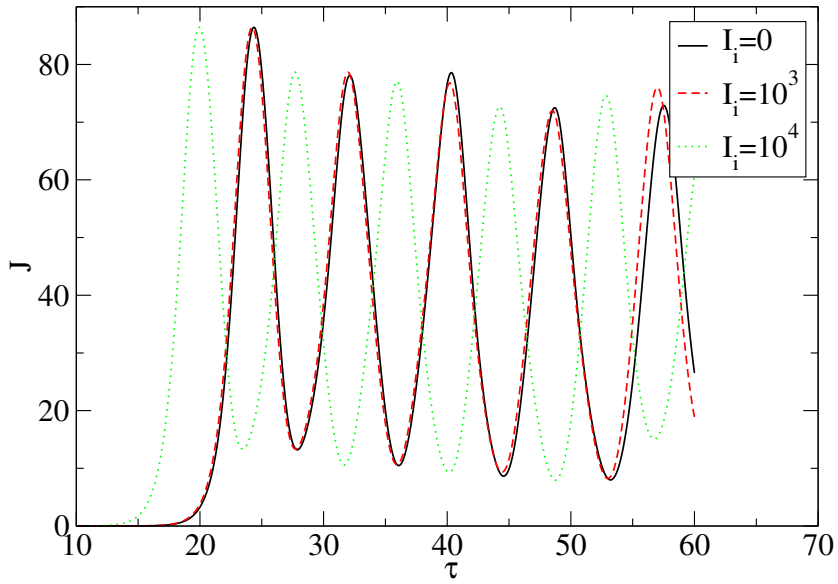

Figure 2.2: Case of two transverse wave and one longitudinal wave, $\mu_1 = 2.0$, $\mu_2 = 3.0$, and $\theta_1(0) = \theta_2(0) = 0.0$. The longitudinal wave exhibits faster growth with larger initial transverse wave amplitudes I_i.

transverse waves and one longitudinal wave. The transverse waves have equal initial amplitudes and phases, but different wave vectors. Now comparison with the single-wave case shows that the growth of the longitudinal wave occurs at an earlier time that depends on the value of the initial amplitudes of the transverse waves.

For a closer look at this phenomenon, we take the logarithm of the longitudinal waves in Fig. 2.2 and plot the result in Fig. 2.3. In Fig. 2.4 we plot the phase of the longitudinal wave. We see that the transverse waves influence

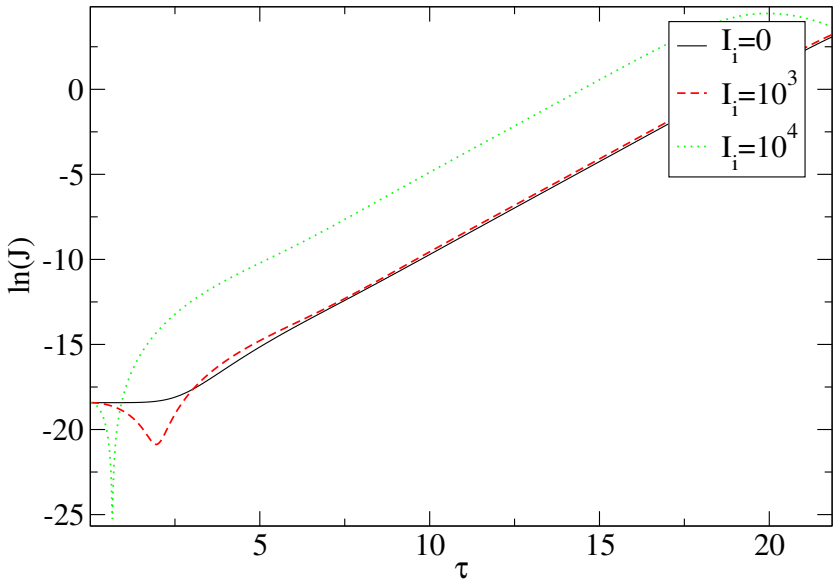

Figure 2.3: Case of two transverse waves and one longitudinal wave, $\mu_1 = 2.0$, $\mu_2 = 3.0$, and $\theta_1(0) = \theta_2(0) = 0.0$. Logarithm of the longitudinal waves from Fig. 2.2. The transverse waves have largest influence in the transient stage of the instability process.

the growth in the very beginning of the instability, when the instability process is still developing. At this time the solution of the system of equations (2.8) is still in a transient state. During this early time the beat wave of the transverse electromagnetic waves has the strongest influence. A resonant process takes place–see the large oscillation in Fig. 2.3 at times around $\tau = 0.6$ for $I_i = 10^4$ and $\tau = 2$ for $I_i = 10^3$. In Fig. 2.4 we see a sharp phase shift due to the transverse waves, which causes the offset of the linear regime toward earlier time. This phenomenon will be explained in Chapter 5 with the linear analysis

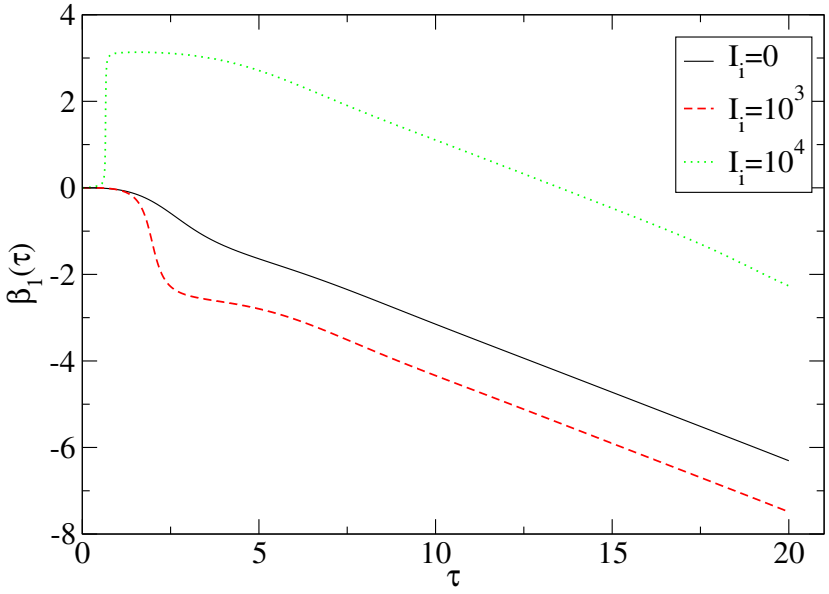

Figure 2.4: Case of two transverse and one longitudinal waves, $\mu_1 = 2.0$, $\mu_2 = 3.0$, and $\theta_1(0) = \theta_2(0) = 0.0$. Phases of the longitudinal wave from Fig. 2.2. The transverse waves have largest influence in the transient stage of the instability process.

of a simplified model. At a certain amplitude of the beat-wave of the two transverse waves, the transient behavior of this simplified system switches from oscillatory to exponentially growing. This results in the observed "jump" behavior. in addition to the phase shift, if the phase velocity of the longitudinal wave is relativistic, the coupling with the transverse waves will be stronger and transfer of energy can occur.

Further, we examine the behavior of the system for long times. In Fig. 2.5 we show the growth of the longitudinal wave for large initial amplitudes

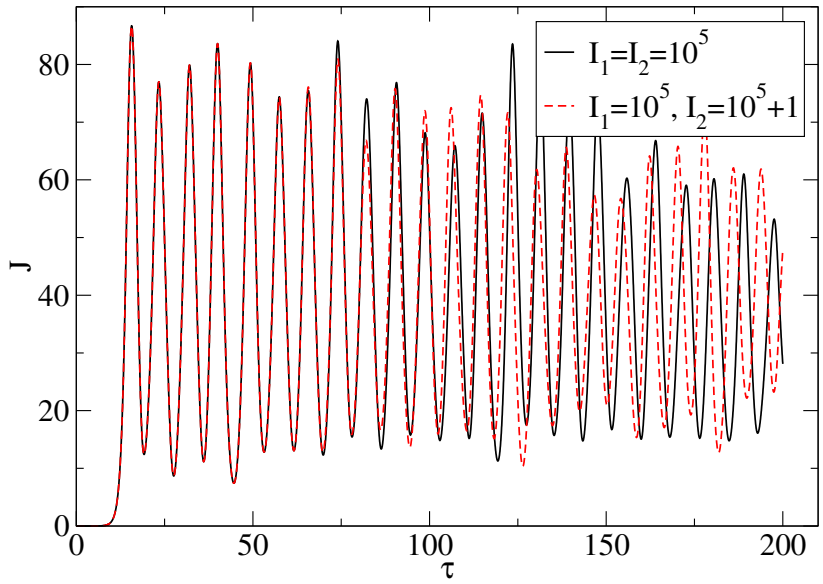

Figure 2.5: Case of two transverse waves and one longitudinal wave, $I_1 = 10^5$, $I_2 = 10^5 + 1$, $\mu_1 = 2.0$, $\mu_2 = 3.0$, and $\theta_1(0) = \theta_2(0) = 0.0$. The two transverse waves have slightly different large initial amplitudes. This figure shows sensitivity to the initial conditions.

of the two transverse waves. Figure 2.5 gives evidence for the chaotic behavior that is to be expected: a very small difference in one of the initial transverse waves amplitudes, a difference of one part in 10^5, causes a large difference in the subsequent evolution.

Figure 2.6 shows the evolution of the two transverse waves in the presence of one longitudinal wave and the beam electrons. As expected, the interaction between the transverse wave and the electrons is negligible.

The two curves in Fig. 2.7 show sensitivity to initial conditions—in this

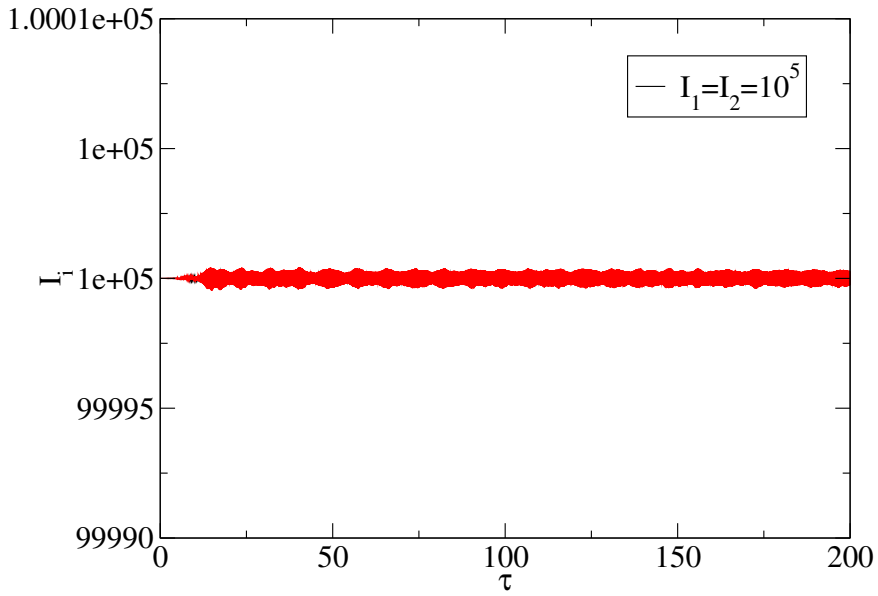

Figure 2.6: Case of two transverse waves and one longitudinal wave, $I_1 = I_2 = 10^3$, $\mu_1 = 2.0$, $\mu_2 = 3.0$, and $\theta_1(0) = \theta_2(0) = 0.0$. The evolution of the two transverse amplitudes is shown.

case due to truncation error. This, again, gives evidence for chaotic behavior of the system.

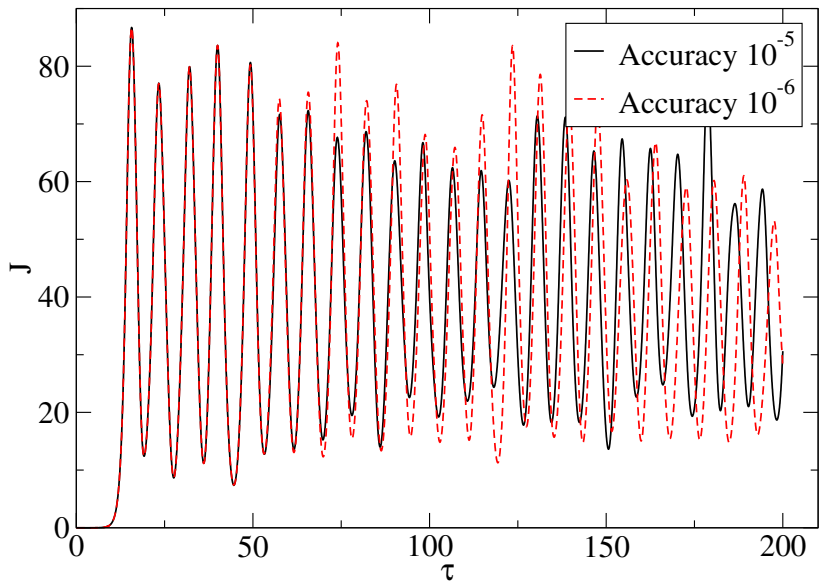

Figure 2.7: Case of two transverse and one longitudinal waves, $I_1 = I_2 = 10^3$, $\mu_1 = 2.0$, $\mu_2 = 3.0$, and $\theta_1(0) = \theta_2(0) = 0.0$. Divergence due to the exponential growth of the small truncation errors and leading to dynamical system chaos.

2.5 Conclusions

In this chapter we derived the non-relativistic model for multi-wave interaction. The model is based on the assumption of slowly changing amplitudes and phases (envelope approximation). The system of background plasma, waves and particles reduces to a finite-dimensional one that is described by a finite number of ordinary differential equations. It conserves energy and momentum and is in this sense self-consistent. The system goes through a stage of transient growth and a linear stage, followed by a saturation and trapping of particles. Subsequent evolution of the system involves (quasi)periodic exchange of momentum between particles and longitudinal, and particles and electromagnetic waves. The interaction with the transverse waves is strongest in the very beginning of the instability process and there it results in a phase shift leading to accelerated growth of the instability (of the longitudinal wave). We also showed that this system exhibits sensitivity to initial conditions or truncation from round off. This points to the chaotic behavior of this system that becomes more pronounced in the presence of transverse waves (see also [32]).

Chapter 3

Relativistic Multi-Wave Model

3.1 Introduction

In this chapter we generalize and further analyze the model introduced in Chapter 2. Here we derive our model in its full generality, allowing for three spatial dimensions and relativistic particles. As before, the background plasma is assumed to respond linearly and non-relativistically; in addition, the ions in the background plasma are, similarly to the development in Chapter 2, assumed to be immobile. These are good approximations because the resonant particles are assumed to constitute a very small fraction of the total plasma, and their velocities are assumed to be much larger than the thermal velocity of the background plasma. The waves described by the model are the plasma wave and external electromagnetic waves, which have a period of oscillation on the order of a plasma period. For this reason the motion of the heavy ions is neglected. The external electric fields are assumed small enough so that nonlinear effects in the background plasma can be neglected.

3.2 Derivation of the relativistic model

As in Section 2.2, start with the Lagrangian for the system of fields, background plasma, and relativistic beam particles,

$$\begin{aligned} L &= \int \mathrm{d}^3x \left\{ \frac{1}{2} mn|\mathbf{v}|^2 + \frac{1}{8\pi}\left(\left| \nabla\phi + \frac{1}{c}\frac{\partial \mathbf{A}}{\partial t} \right|^2 - |\nabla \times \mathbf{A}|^2 \right) - \rho\phi + \frac{1}{c}\,\mathbf{j}\cdot\mathbf{A} \right\} \\ &\quad + \sum_{j=1}^{N} \left\{ -mc^2\sqrt{1 - \frac{\dot{\mathbf{r}}_j^2}{c^2}} + e\phi(\mathbf{r}_j, t) - \frac{e}{c}\,\dot{\mathbf{r}}_j \cdot \mathbf{A}(\mathbf{r}_j, t) \right\}. \end{aligned} \tag{3.1}$$

As in Chapter 2, $\mathbf{v}$ is the Eulerian velocity field, n–the particle density of the background plasma, ϕ and $\mathbf{A}$ are the scalar and vector potentials associated with the N_L electrostatic and N_T electromagnetic waves, respectively, N is the number of particles, $\mathbf{j}$ is the current, ρ is the charge density, and $-e$ is the electron charge. The quantities m and e of the last three terms of (3.1) may be interpreted as follows. If the integration volume V is divided into N cells, e may be interpreted as the effective charge of the cell, or en_bV/N, whereas m as the effective mass equal to mn_bV/N, n_b being the beam density. Then the sum ranges over all cells. In what follows the nominal "particles" will be equivalent to "cells". Quantities with a subscript refer to particles whereas those without a subscript refer to the background plasma. Coulomb gauge $\nabla\cdot\mathbf{A} = 0$ is assumed.

Using fluid theory, the linear response of the background plasma is given

by

$$\begin{aligned}
\rho &= -\frac{1}{4\pi}\nabla^2\phi, \\
\mathbf{j}_L &= -\frac{1}{4\pi}\nabla\frac{\partial\phi}{\partial t}, \\
\mathbf{j}_T &= -\frac{c}{4\pi}\left(\nabla^2\mathbf{A} - \frac{1}{c^2}\frac{\partial^2\mathbf{A}}{\partial t^2}\right), \\
\mathbf{v} &= -\frac{1}{ne}\mathbf{j},
\end{aligned} \tag{3.2}$$

where $\mathbf{j}_L$ and $\mathbf{j}_T$ are the longitudinal and transverse parts of the current. Notice that Eqs. (3.2) are slightly different from (2.2) that we used in our non-relativistic model. The first three of (3.2) follow directly from Maxwell equations upon splitting the current into irrotational and solenoidal parts and using the Coulomb gauge (see e.g. Ref. [44]). Substituting the above relations into the Lagrangian (3.1) is incomplete because it amounts to the neglect of the fields due to the beam particles. The justification of our model is considered in more detail in Section 3.3. We now continue with the derivation of the model.

Suppose that the electrostatic and vector potentials are represented by three-dimensional Fourier series as (The model is flexible enough to accommodate the use of a different set of complete functions depending on the geometry of the specific problem. For example, a plasma channel formed by an intense laser pulse has a cylindrical shape, so decomposition of the fields in a cylindrical geometry would be more appropriate.)

$$\phi(\mathbf{r},t) = \sum_{\mathbf{k}_L>0}\left(f_{\mathbf{k}_L}e^{i\mathbf{k}_L\cdot\mathbf{r}} + f^*_{\mathbf{k}_L}e^{-i\mathbf{k}_L\cdot\mathbf{r}}\right), \tag{3.3}$$

$$\mathbf{A}(\mathbf{r},t) = \sum_{\mathbf{k}>0}\left(\mathbf{a}_{\mathbf{k}}e^{i\mathbf{k}\cdot\mathbf{r}} + \mathbf{a}^*_{\mathbf{k}}e^{-i\mathbf{k}\cdot\mathbf{r}}\right), \tag{3.4}$$

the star superscript denoting the complex conjugate. The sums $\mathbf{k}_L > 0$ and $\mathbf{k} > 0$ range over half of the corresponding wave vector spaces, and we have

$$\mathbf{k}_L = \left(\frac{2\pi\mu_{Lx}}{L_x}, \frac{2\pi\mu_{Ly}}{L_y}, \frac{2\pi\mu_{Lz}}{L_z} \right), \qquad \mathbf{k} = \left(\frac{2\pi\mu_x}{L_x}, \frac{2\pi\mu_y}{L_y}, \frac{2\pi\mu_z}{L_z} \right) \tag{3.5}$$

with $\mu_{Lx,y,z}$ and $\mu_{x,y,z}$ positive integers. L_x, L_y, L_z determine the size of the plasma, or the periodicity length; for example, they can be taken to be equal to the maximal wave length of the electrostatic wave. The sums exclude the zero components since they do not contribute to the equations of motion. The Coulomb gauge condition reads $\mathbf{k} \cdot \mathbf{a}_\mathbf{k} = 0$. Let the amplitudes $f_{\mathbf{k}_L}$ and $\mathbf{a}_\mathbf{k}$ contain a slow and a fast time scales. The derivatives will be

$$\begin{aligned} \dot{f}_{\mathbf{k}_L} &= -i\omega_{\mathbf{k}_L} f_{\mathbf{k}_L} + \underline{\dot{f}}_{\mathbf{k}_L}, \\ \dot{\mathbf{a}}_\mathbf{k} &= -i\omega_\mathbf{k} \mathbf{a}_\mathbf{k} + \underline{\dot{\mathbf{a}}}_\mathbf{k}. \end{aligned} \tag{3.6}$$

The underline notation means differentiation with respect to the slow time scale, i.e. if $f_{\mathbf{k}_L}(t) = F_{\mathbf{k}_L}(t) e^{-i\omega_{\mathbf{k}_L} t}$, $F_{\mathbf{k}_L}(t)$ representing the slow time dependence, then $\underline{\dot{f}}_{\mathbf{k}_L}(t) = \dot{F}_{\mathbf{k}_L}(t) e^{-i\omega_{\mathbf{k}_L} t}$. The second derivatives assume the form

$$\begin{aligned} \ddot{f}_{\mathbf{k}_L} &= (-i\omega_{\mathbf{k}_L})^2 f_{\mathbf{k}_L} - 2i\omega_{\mathbf{k}_L} \underline{\dot{f}}_{\mathbf{k}_L} + \underline{\ddot{f}}_{\mathbf{k}_L} \\ &\simeq -\omega_{\mathbf{k}_L}^2 f_{\mathbf{k}_L} - 2i\omega_{\mathbf{k}_L} \underline{\dot{f}}_{\mathbf{k}_L}, \\ \ddot{\mathbf{a}}_\mathbf{k} &\simeq -\omega_\mathbf{k}^2 \mathbf{a}_\mathbf{k} - 2i\omega_\mathbf{k} \underline{\dot{\mathbf{a}}}_\mathbf{k}. \end{aligned} \tag{3.7}$$

The second derivatives with respect to the slow time scale have been neglected according to the slow variation assumption; in particular, is is assumed that

$$\begin{aligned} |\ddot{f}_{\mathbf{k}_L}| &\ll \omega_{\mathbf{k}_L} \left| \dot{f}_{\mathbf{k}_L} \right| \ll \omega_{\mathbf{k}_L}^2 \left| f_{\mathbf{k}_L} \right|, \\ |\ddot{\mathbf{a}}_\mathbf{k}| &\ll \omega_\mathbf{k} |\dot{\mathbf{a}}_\mathbf{k}| \ll \omega_\mathbf{k}^2 |\mathbf{a}_\mathbf{k}|. \end{aligned} \tag{3.8}$$

The assumption of slowly varying amplitudes puts another restriction on the usage of the model in experimental context. In a typical plasma wake-field

acceleration experiment, the length of an electron bunch (or a laser pulse, in the case of a laser wake-field experiment) is normally on the order of a plasma wave period [28, 30]. Our model would describe experimental situations for which the length of the pulses is several plasma wavelengths long.

Now formulas (3.2) are substituted into (3.1). The cold plasma dispersion relations, $\omega^2_{\mathbf{k}_L} = \omega_p^2$ for electrostatic and $\omega^2_{\mathbf{k}} = \omega_p^2 + \mathbf{k}^2 c^2$ for electromagnetic waves, and the formulas for the derivatives, (3.6) and (3.7), are used. The integration is performed over a domain with periodic boundary conditions. Upon integrating the squares, terms which contain different wave vectors in the exponential $e^{i(\mathbf{k}\pm\mathbf{k}')\cdot\mathbf{r}}$ average to zero, and so do terms in which the wave vectors double, $e^{\pm 2i\mathbf{k}\cdot\mathbf{r}}$. Only terms with equal wave vectors but opposite sign of the exponent survive and for them the integration reduces to multiplication by the volume of integration. Use is made of the Coulomb gauge condition to reduce vector products to scalar products.

More quantitatively, we present the part of the derivation that only contains the vector potentials. First, consider the term in the Lagrangian (3.1) containing $|\mathbf{v}|^2$. Using formulas (3.2), (3.4), (3.6), and (3.7), and taking into account that $\mathbf{j}_L$ is perpendicular to $\mathbf{j}_T$ (only $\mathbf{j}_T$ contains the vector potential

$\mathbf{A}$) we have

$$\begin{aligned}
\int \mathrm{d}^3x\, \frac{1}{2} mn|\mathbf{v}|^2 &= \frac{c^2}{8\pi\omega_p^2} \int \mathrm{d}^3x \left| \nabla^2 \mathbf{A} - \frac{1}{c^2} \frac{\partial^2 \mathbf{A}}{\partial t^2} \right|^2 \\
&= \frac{c^2}{8\pi\omega_p^2} \int \mathrm{d}^3x \left| \sum_{\mathbf{k}>0} \left(\frac{\omega_{\mathbf{k}}^2}{c^2} - k^2 \right) \left(\mathbf{a}_{\mathbf{k}} e^{i\mathbf{k}\cdot\mathbf{r}} + \mathbf{a}_{\mathbf{k}}^* e^{-i\mathbf{k}\cdot\mathbf{r}} \right) \right. \\
&\qquad \left. + \frac{1}{c^2} \left(2i\omega_{\mathbf{k}} (\underline{\dot{\mathbf{a}}}_{\mathbf{k}} e^{i\mathbf{k}\cdot\mathbf{r}} - \underline{\dot{\mathbf{a}}}_{\mathbf{k}}^* e^{-i\mathbf{k}\cdot\mathbf{r}}) - (\underline{\ddot{\mathbf{a}}}_{\mathbf{k}} e^{i\mathbf{k}\cdot\mathbf{r}} + \underline{\ddot{\mathbf{a}}}_{\mathbf{k}}^* e^{-i\mathbf{k}\cdot\mathbf{r}}) \right) \right|^2 \\
&\simeq \frac{Vc^2}{8\pi\omega_p^2} \sum_{\mathbf{k}>0} \left(2 \left(\frac{\omega_p^2}{c^2} \right)^2 |\mathbf{a}_{\mathbf{k}}|^2 - 4i \frac{\omega_p^2}{c^2} \frac{\omega_{\mathbf{k}}}{c^2} \left(\mathbf{a}_{\mathbf{k}} \cdot \underline{\dot{\mathbf{a}}}_{\mathbf{k}}^* - \underline{\dot{\mathbf{a}}}_{\mathbf{k}} \cdot \mathbf{a}_{\mathbf{k}}^* \right) \right)
\end{aligned} \tag{3.9}$$

where we have neglected second order time derivatives of $\mathbf{a}_{\mathbf{k}}$, as well as products of first order time derivatives; the dispersion relation for electromagnetic waves has also been used. For the integration of the rest of the terms containing $\mathbf{A}$, notice that the current term in the Lagrangian may be transformed so that it equals twice the field term with a negative sign. Therefore for the rest of the calculation we need to evaluate as follows

$$\begin{aligned}
-\frac{1}{8\pi c^2} \int \mathrm{d}^3x \left| \frac{\partial \mathbf{A}}{\partial t} \right|^2 &= \int \mathrm{d}^3x \left| \sum_{\mathbf{k}>0} \left(-i\omega_{\mathbf{k}} \left(\mathbf{a}_{\mathbf{k}} e^{i\mathbf{k}\cdot\mathbf{r}} - \mathbf{a}_{\mathbf{k}}^* e^{-i\mathbf{k}\cdot\mathbf{r}} \right) + \right. \right. \\
&\qquad \left. \left. \underline{\dot{\mathbf{a}}}_{\mathbf{k}} e^{i\mathbf{k}\cdot\mathbf{r}} + \underline{\dot{\mathbf{a}}}_{\mathbf{k}}^* e^{-i\mathbf{k}\cdot\mathbf{r}} \right) \right|^2 \\
&\simeq -\frac{V}{8\pi c^2} \sum_{\mathbf{k}>0} \left(2\omega_{\mathbf{k}}^2 |\mathbf{a}_{\mathbf{k}}|^2 - 2i\omega_{\mathbf{k}} \left(\mathbf{a}_{\mathbf{k}} \cdot \underline{\dot{\mathbf{a}}}_{\mathbf{k}}^* - \mathbf{a}_{\mathbf{k}}^* \cdot \underline{\dot{\mathbf{a}}}_{\mathbf{k}} \right) \right)
\end{aligned} \tag{3.10}$$

and

$$\begin{aligned}
\frac{1}{8\pi} \int \mathrm{d}^3x\, |\nabla \times \mathbf{A}|^2 &= \frac{1}{8\pi} \int \mathrm{d}^3x \sum_{\mathbf{k}>0} \left| (i\mathbf{k} \times \mathbf{a}_{\mathbf{k}})\, e^{i\mathbf{k}\cdot\mathbf{r}} - (i\mathbf{k} \times \mathbf{a}_{\mathbf{k}}^*)\, e^{-i\mathbf{k}\cdot\mathbf{r}} \right|^2 \\
&= \frac{V}{8\pi} \sum_{\mathbf{k}>0} 2k^2 |\mathbf{a}_{\mathbf{k}}|^2.
\end{aligned} \tag{3.11}$$

In the last step the Coulomb gauge condition, $\mathbf{k}\cdot\mathbf{a}_\mathbf{k}=0$, was used. Adding (3.9), (3.10), and (3.11) we see that upon using the dispersion relation for electromagnetic waves, all terms with $|\mathbf{a}_\mathbf{k}|^2$ cancel, and the remaining terms combine into

$$\frac{V}{4i\pi}\sum_{\mathbf{k}>0}\frac{\omega_\mathbf{k}}{c^2}\left(\mathbf{a}_\mathbf{k}\cdot\underline{\dot{\mathbf{a}}}^*_\mathbf{k}-\dot{\mathbf{a}}_\mathbf{k}\cdot\mathbf{a}^*_\mathbf{k}\right). \tag{3.12}$$

By an analogous calculation for the terms involving the electrostatic potential one can show that upon using the cold plasma dispersion relation for electrostatic waves, terms with $|f_{\mathbf{k}_L}|^2$ cancel out and the remaining terms, after performing the integration over the spatial variables, are

$$\frac{V}{4i\pi}\sum_{\mathbf{k}_L>0}\frac{\mathbf{k}_L^2}{\omega_p}\left(f_{\mathbf{k}_L}\underline{\dot{f}}^*_{\mathbf{k}_L}-\underline{\dot{f}}_{\mathbf{k}_L}f^*_{\mathbf{k}_L}\right). \tag{3.13}$$

To include (3.12) and (3.13) into the Lagrangian (3.1), we make use of formulas (3.6) to express $\underline{\dot{\mathbf{a}}}_\mathbf{k}$ and $\underline{\dot{f}}_{\mathbf{k}_L}$ in terms of $\mathbf{a}_\mathbf{k}$, $\dot{\mathbf{a}}_\mathbf{k}$, $f_{\mathbf{k}_L}$, and $\dot{f}_{\mathbf{k}_L}$. Thus the Lagrangian (3.1) takes the form

$$\begin{aligned}
L &= -mc^2\sum_{j=1}^{N}\sqrt{1-\frac{\dot{\mathbf{r}}_j^2}{c^2}}+e\sum_{j=1}^{N}\sum_{\mathbf{k}_L>0}\left(f_{\mathbf{k}_L}e^{i\mathbf{k}_L\cdot\mathbf{r}_j}+f^*_{\mathbf{k}_L}e^{-i\mathbf{k}_L\cdot\mathbf{r}_j}\right)\\
&\quad-\frac{e}{c}\sum_{j=1}^{N}\sum_{\mathbf{k}>0}\dot{\mathbf{r}}_j\cdot\left(\mathbf{a}_\mathbf{k}e^{i\mathbf{k}\cdot\mathbf{r}_j}+\mathbf{a}^*_\mathbf{k}e^{-i\mathbf{k}\cdot\mathbf{r}_j}\right)\\
&\quad-\frac{V}{2\pi}\sum_{\mathbf{k}_L>0}\mathbf{k}_L^2(f_{\mathbf{k}_L}f^*_{\mathbf{k}_L})+\frac{V}{4i\pi}\sum_{\mathbf{k}_L>0}\frac{\mathbf{k}_L^2}{\omega_p}(f_{\mathbf{k}_L}\dot{f}^*_{\mathbf{k}_L}-f^*_{\mathbf{k}_L}\dot{f}_{\mathbf{k}_L})\\
&\quad-\frac{V}{2\pi}\sum_{\mathbf{k}>0}\frac{\omega_\mathbf{k}^2}{c^2}(\mathbf{a}_\mathbf{k}\cdot\mathbf{a}^*_\mathbf{k})+\frac{V}{4i\pi}\sum_{\mathbf{k}>0}\frac{\omega_\mathbf{k}}{c^2}(\mathbf{a}_\mathbf{k}\cdot\dot{\mathbf{a}}^*_\mathbf{k}-\mathbf{a}^*_\mathbf{k}\cdot\dot{\mathbf{a}}_\mathbf{k}).
\end{aligned} \tag{3.14}$$

Let us discuss again the time scales in the Lagrangian (3.14). In the single wave model, Refs. [9, 10], the slow time scale in the system is obtained by a Galilean transformation to a moving (with the initial beam velocity)

frame, or by a particular choice of variables. However, here this is not done because instead of a Galilean transformation, a Lorentz transformation should be used, and that would involve transformation of the fields as well. It is preferable that the fields be the ones in the laboratory (stationary) frame. All quantities in this Lagrangian contain both the fast time scale, on the order of the electron plasma period and the slow time scale, on which we assumed the amplitudes and phases of the waves vary. To obtain a quantity that varies on the slow time scale, we simply take instead of $f_{\mathbf{k}_L}$ and $\mathbf{a}_{\mathbf{k}}$, $|f_{\mathbf{k}_L}|$ and $|\mathbf{a}_{\mathbf{k}}|$.

One may attempt a different way of averaging the Lagrangian over the fast time scale and retaining only the small time scale. This has been done by several authors [45, 46, 47]. We can see that doing so will retain only terms for which the resonant condition,

$$\mathbf{v}_0 \cdot \mathbf{k}_L - \omega_p = 0, \tag{3.15}$$

is satisfied. Indeed, the terms with $f_{\mathbf{k}_L}$ contain a time dependence of the form $e^{i(\mathbf{v}_0 \cdot \mathbf{k}_L - \omega_p)t}$. If the phase velocity of the longitudinal wave equals that of the beam electrons, $\omega_p/k_L = v_0$, averaging over the time scale determined by ω_p and retaining the next small order corrections (remember that we have terms in the Lagrangian that contain small derivatives of amplitudes, and are therefore small compared to the rest of the terms) will retain only terms of zeroth and first order in $(n/n_b)^{1/3}$ (ratio which is proportional to the ratio of the fast and slow time scales). Consider now the electromagnetic terms. The fast time dependence for them has the form $e^{i(\mathbf{v}_0 \cdot \mathbf{k} - \omega_{\mathbf{k}})t}$. In this case the resonant condition (3.15) cannot be satisfied since the phase velocity of the electromagnetic wave is always greater than the speed of light (recall that $\omega_{\mathbf{k}}^2 = \omega_p^2 + \mathbf{k}^2 c^2$). However, terms with electromagnetic waves can still produce

slowly varying quantities. For example, if more than one electromagnetic wave are present, their frequencies can be chosen such that the resultant beat wave fulfills the necessary resonant condition. This case will be considered in Chapter 4.

To continue, it is convenient to write all variables in dimensionless form. Use formula (3.5) to define the dimensionless coordinates and longitudinal wave vectors as $\mathbf{k}_L \cdot \mathbf{r}_j = \boldsymbol{\mu}_L \cdot \boldsymbol{\rho}_j$, and similarly for the transverse wave vectors, $\mathbf{k} \cdot \mathbf{r}_j = \boldsymbol{\mu} \cdot \boldsymbol{\rho}_j$. Let the time scale be given by $1/\omega_p$ and length scale given by the maximal longitudinal wave length, i.e. choose $L_x = L_y = L_z = 2\pi/|\mathbf{k}_{L_{\min}}|$. Define $\beta = \omega_p/c|\mathbf{k}_{L_{\min}}|$. The dimensionless electrostatic potential and vector potentials are defined by

$$f_{\mathbf{k}_L} = \frac{mc^2 s_{\boldsymbol{\mu}_L} f_{\boldsymbol{\mu}_L}}{e}, \quad \mathbf{a}_{\mathbf{k}} = \frac{mc^2 s_{\boldsymbol{\mu}} \mathbf{a}_{\boldsymbol{\mu}}}{e}. \tag{3.16}$$

A Greek letter subscript denotes a dimensionless variable. The dimensionless coefficients $s_{\boldsymbol{\mu}_L}$ and $s_{\boldsymbol{\mu}}$ are given by

$$s_{\boldsymbol{\mu}_L} = \sqrt{\beta^2 n_b / 2Nn\boldsymbol{\mu}_L^2}, \quad s_{\boldsymbol{\mu}} = \sqrt{n_b/2Nn\omega_{\boldsymbol{\mu}}}, \tag{3.17}$$

where $\omega_{\boldsymbol{\mu}} = \omega_{\mathbf{k}}/\omega_p = (1 + \boldsymbol{\mu}^2/\beta^2)^{1/2}$. Rescaling by mc^2 and V, the dimensionless Lagrangian is obtained as

$$\begin{aligned} L \;=\; & -\sum_{j=1}^{N} \sqrt{1 - |\beta \dot{\boldsymbol{\rho}}_j|^2} + \sum_{j=1}^{N} \sum_{\boldsymbol{\mu}_L > 0} s_{\boldsymbol{\mu}_L} \left(f_{\boldsymbol{\mu}_L} e^{i\boldsymbol{\mu}_L \cdot \boldsymbol{\rho}_j} + f^*_{\boldsymbol{\mu}_L} e^{-i\boldsymbol{\mu}_L \cdot \boldsymbol{\rho}_j} \right) \\ & - \sum_{j=1}^{N} \beta \dot{\boldsymbol{\rho}}_j \cdot \sum_{\boldsymbol{\mu} > 0} s_{\boldsymbol{\mu}} \left(\mathbf{a}_{\boldsymbol{\mu}} e^{i\boldsymbol{\mu} \cdot \boldsymbol{\rho}_j} + \mathbf{a}^*_{\boldsymbol{\mu}} e^{-i\boldsymbol{\mu} \cdot \boldsymbol{\rho}_j} \right) \\ & - \sum_{\boldsymbol{\mu}_L > 0} \left(f_{\boldsymbol{\mu}_L} f^*_{\boldsymbol{\mu}_L} \right) + \frac{1}{2i} \sum_{\boldsymbol{\mu}_L > 0} \left(f_{\boldsymbol{\mu}_L} \dot{f}^*_{\boldsymbol{\mu}_L} - f^*_{\boldsymbol{\mu}_L} \dot{f}_{\boldsymbol{\mu}_L} \right) \\ & - \sum_{\boldsymbol{\mu} > 0} \omega_{\boldsymbol{\mu}} \left(\mathbf{a}_{\boldsymbol{\mu}} \cdot \mathbf{a}^*_{\boldsymbol{\mu}} \right) + \frac{1}{2i} \sum_{\boldsymbol{\mu} > 0} \left(\mathbf{a}_{\boldsymbol{\mu}} \cdot \dot{\mathbf{a}}^*_{\boldsymbol{\mu}} - \mathbf{a}^*_{\boldsymbol{\mu}} \cdot \dot{\mathbf{a}}_{\boldsymbol{\mu}} \right). \end{aligned} \tag{3.18}$$

The field variables, as in the system of equations in the non-relativistic case, see (2.8), enter either multiplied by small coefficients, or contain a small derivative. The small coefficients in front of the electrostatic variables depend on the ratio of beam and background plasma densities and on β whereas those in front of the electromagnetic variables depend in addition on the inverse of the large number $\omega_{\boldsymbol{\mu}}$. It follows that the coupling of fields and particles is stronger for fast particles, and for denser beams. The coupling between electromagnetic waves and particles is stronger for smaller frequency ratio $\omega_{\boldsymbol{\mu}}$.

3.3 Justification

Consider first the conditions which allow us to neglect the field of the beam particles compared to the electric field of the plasma wave. The electric and magnetic fields of a relativistic charge at a distance of the order $1/k_L$ (k_L being a typical wave vector of the electrostatic wave) are given by the formulas (see e.g. [48])

$$\mathbf{E}_e = e\frac{1-\dfrac{v^2}{c^2}}{\left(R-\dfrac{\mathbf{R}\cdot\mathbf{v}}{c}\right)^3}\left(\mathbf{R}-\frac{\mathbf{v}R}{c}\right)+\frac{e}{c^2\left(R-\dfrac{\mathbf{R}\cdot\mathbf{v}}{c}\right)}\mathbf{R}\times\left(\left(\mathbf{R}-\frac{\mathbf{v}R}{c}\right)\times\dot{\mathbf{v}}\right), \tag{3.19}$$

$$\mathbf{B}_e = \frac{1}{R}\left(\mathbf{R}\times\mathbf{E}\right). \tag{3.20}$$

In formulas (3.19) and (3.20) $\mathbf{R}$ is the vector from the point charge to the point where the fields are observed, and all quantities are taken at the moment t' in the system where the charge is at rest. An order of magnitude estimate follows, upon neglecting the term with $\dot{\mathbf{v}}$ as small by assumption, see (3.8),

compared to the first term on the right hand side of (3.19), as

$$E_b \sim n_b e \gamma^2 k_L^2. \tag{3.21}$$

where γ is the relativistic factor, $\gamma = (1-\beta^2)^{-1/2}$. From (3.21) we can find that the field of the beam is $E_b = n_b V E_e \sim n_b e \gamma^2 / k_L$, where we used the fact that the volume $V \sim k_L^{-3}$. With the maximum plasma wave amplitude given in [5], $E_0 = \sqrt{2}(\gamma-1)^{1/2} mc\omega_p/e$, we obtain the estimate

$$\frac{E_b}{E_0} \sim \frac{n_b e^2 \gamma^2}{\sqrt{2} mc k_L \omega_p (\gamma-1)^{1/2}} \sim \left(\frac{n_b}{n}\right) \frac{\beta\gamma^2}{\sqrt{2}(\gamma-1)^{1/2}}. \tag{3.22}$$

$\beta = \omega_p/k_L c$ is the dimensionless phase velocity of the longitudinal wave which is very close to that of the beam particles. For a non-relativistic beam, taking the limit $\beta \to 0$, we see that the condition that $E_b \ll E_0$ is equivalent to

$$\left(\frac{n_b}{n}\right) \ll 1. \tag{3.23}$$

To neglect the field of a relativistic electron beam, it is necessary that

$$\left(\frac{n_b}{n}\right) \ll \frac{\sqrt{2}}{\gamma^{3/2}}. \tag{3.24}$$

The latter condition puts a restriction on the beam–plasma density ratio: for fast particles this ratio needs to be small in order for such system to be described by the model.

To neglect the nonlinear response of the background plasma, it is necessary that

$$a_0 \equiv \left|\frac{e\mathbf{A}}{mc^2}\right| \ll 1. \tag{3.25}$$

To see why this is so, we can argue in the following way. The linear response of the plasma yields velocity that is linear in the electric field, $v_k^{(1)} \sim (ie/\omega_k m_e) E_k$; the non-linear response is quadratic with respect to the fields,

$v_k^{(2)} \sim (e^2/2m^2\omega_k^3)E_k^2$, see Ref. [49]. Upon using $E_T = (1/c)\partial\mathbf{A}/\partial t = (\omega_k/c)\mathbf{A}$, the condition that the linear velocity be much larger than the non-linear (quadratic) velocity, $v_k^{(1)} \gg v_k^{(2)}$, yields (3.25). The quantity on the left-hand-side of (3.25) is the so called normalized vector potential. In an experiment on wake-field acceleration, a powerful laser pulse can have a normalized vector potential on the order of unity, or even several units. Our model is not applicable to such experiments.

Next the Hamiltonian formulation will be given and conservation laws will be found.

3.4 Hamiltonian form and conservation laws

The Hamiltonian of the system can be found from the Lagrangian (3.18), by a Legendre transform. The canonical momentum is given by

$$\begin{aligned} \boldsymbol{\pi}_j &= \partial L/\partial\dot{\boldsymbol{\rho}}_j \\ &= \frac{\beta^2\dot{\boldsymbol{\rho}}_j}{\sqrt{1-\beta^2\dot{\boldsymbol{\rho}}_j^2}} - \beta\sum_{\boldsymbol{\mu}>0} s_{\boldsymbol{\mu}}\left(\mathbf{a}_{\boldsymbol{\mu}}e^{i\boldsymbol{\mu}\cdot\boldsymbol{\rho}_j} + \mathbf{a}^*_{\boldsymbol{\mu}}e^{-i\boldsymbol{\mu}\cdot\boldsymbol{\rho}_j}\right). \end{aligned} \tag{3.26}$$

Let us introduce the notations

$$\begin{aligned} a_{j\sigma} &= \sum_{\boldsymbol{\mu}>0} s_{\boldsymbol{\mu}}\left(a_{\boldsymbol{\mu}\sigma}e^{i\boldsymbol{\mu}\cdot\boldsymbol{\rho}_j} + a^*_{\boldsymbol{\mu}\sigma}e^{-i\boldsymbol{\mu}\cdot\boldsymbol{\rho}_j}\right) \\ \mathbf{a}_{,j\sigma} &= \sum_{\boldsymbol{\mu}>0} is_{\boldsymbol{\mu}}\left(a_{\boldsymbol{\mu}\sigma}e^{i\boldsymbol{\mu}\cdot\boldsymbol{\rho}_j} - a^*_{\boldsymbol{\mu}\sigma}e^{-i\boldsymbol{\mu}\cdot\boldsymbol{\rho}_j}\right)\boldsymbol{\mu}\,, \\ \mathbf{f}_{,j} &= \sum_{\boldsymbol{\mu}_L>0} is_{\boldsymbol{\mu}_L}\left(f_{\boldsymbol{\mu}_L}e^{i\boldsymbol{\mu}_L\cdot\boldsymbol{\rho}_j} - f^*_{\boldsymbol{\mu}_L}e^{-i\boldsymbol{\mu}_L\cdot\boldsymbol{\rho}_j}\right)\boldsymbol{\mu}_L\,, \quad \sigma = 1,2,3. \end{aligned} \tag{3.27}$$

Notice that the vectorial nature of $\mathbf{a}_{,j\sigma}$ and $\mathbf{f}_{,j}$ comes from $\boldsymbol{\mu}$ and $\boldsymbol{\mu}_L$, correspondingly. From (3.26) follows

$$\dot{\boldsymbol{\rho}}_j = \frac{1}{\beta}\frac{\boldsymbol{\pi}_j/\beta + \mathbf{a}_j}{\sqrt{1+\left(\boldsymbol{\pi}_j/\beta + \mathbf{a}_j\right)^2}}. \tag{3.28}$$

Using (3.26) and (3.28) for the particle variables, the Hamiltonian is found as

$$\begin{aligned} H &= \sum_{j=1}^{N}\sqrt{1+\left|\boldsymbol{\pi}_j/\beta + \sum_{\boldsymbol{\mu}>0} s_{\boldsymbol{\mu}}\left(\mathbf{a}_{\boldsymbol{\mu}}e^{i\boldsymbol{\mu}\cdot\boldsymbol{\rho}_j} + \mathbf{a}^*_{\boldsymbol{\mu}}e^{-i\boldsymbol{\mu}\cdot\boldsymbol{\rho}_j}\right)\right|^2} \\ &\quad - \sum_{j=1}^{N}\sum_{\boldsymbol{\mu}_L>0} s_{\boldsymbol{\mu}_L}\left(f_{\boldsymbol{\mu}_L}e^{i\boldsymbol{\mu}_L\cdot\boldsymbol{\rho}_j} + f^*_{\boldsymbol{\mu}_L}e^{-i\boldsymbol{\mu}_L\cdot\boldsymbol{\rho}_j}\right) \\ &\quad + \sum_{\boldsymbol{\mu}_L>0}\left(f_{\boldsymbol{\mu}_L}f^*_{\boldsymbol{\mu}_L}\right) + \sum_{\boldsymbol{\mu}>0}\omega_{\boldsymbol{\mu}}\left(\mathbf{a}_{\boldsymbol{\mu}}\cdot\mathbf{a}^*_{\boldsymbol{\mu}}\right) \end{aligned} \tag{3.29}$$

with Poisson brackets

$$\begin{aligned} \left[\rho_{i\sigma}, \pi_{j\sigma'}\right] &= \delta_{ij}\delta_{\sigma\sigma'}, \\ \left[f_{\boldsymbol{\mu}_L}, f^*_{\boldsymbol{\mu}'_L}\right] &= \frac{1}{i}\,\delta_{\boldsymbol{\mu}_L\boldsymbol{\mu}'_L}, \qquad \left[a_{\boldsymbol{\mu}\sigma}, a^*_{\boldsymbol{\mu}'\sigma'}\right] = \frac{1}{i}\,\delta_{\boldsymbol{\mu}\boldsymbol{\mu}'}\delta_{\sigma\sigma'}. \end{aligned} \tag{3.30}$$

$\sigma = 1, 2, 3$. Notice that the brackets for the field variables differ from the canonical brackets only by a factor of $1/i$. The calculation for the field part of the Hamiltonian is done in Appendix A.

The equations of motion that follow from (3.29) are

$$\begin{aligned} \dot{\boldsymbol{\rho}}_j &= \frac{1}{\beta}\frac{\boldsymbol{\pi}_j/\beta + \mathbf{a}_j}{\sqrt{1+\left(\boldsymbol{\pi}_j/\beta + \mathbf{a}_j\right)^2}}, \\ \dot{\boldsymbol{\pi}}_j &= -\frac{\left(\pi_{j\sigma}/\beta + a_{j\sigma}\right)\mathbf{a}_{,j\sigma}}{\sqrt{1+\left(\boldsymbol{\pi}_j/\beta + \mathbf{a}_j\right)^2}} + \mathbf{f}_{,j} \\ \dot{f}_{\boldsymbol{\mu}_L} &= -if_{\boldsymbol{\mu}_L} + \sum_{j=1}^{N} is_{\boldsymbol{\mu}_L}e^{-i\boldsymbol{\mu}_L\cdot\boldsymbol{\rho}_j}, \\ \dot{\mathbf{a}}_{\boldsymbol{\mu}} &= -i\omega_{\boldsymbol{\mu}}\mathbf{a}_{\boldsymbol{\mu}} - \sum_{j=1}^{N} is_{\boldsymbol{\mu}}e^{-i\boldsymbol{\mu}\cdot\boldsymbol{\rho}_j}\frac{\boldsymbol{\pi}_j/\beta + \mathbf{a}_j}{\sqrt{1+\left(\boldsymbol{\pi}_j/\beta + \mathbf{a}_j\right)^2}}, \end{aligned} \tag{3.31}$$

and two equations that are complex conjugates of the last two. Summation over the repeated index σ in the second of equations (3.31) is assumed. In addition to Eqs. (3.31), the gauge condition $\boldsymbol{\mu} \cdot \mathbf{a}_{\boldsymbol{\mu}} = 0$ must be added. The momentum equation has two terms. The first is the ponderomotive force due to the electromagnetic field, and the second is the electrostatic response of the plasma. It also shows that the particles are coupled to both, the electrostatic and the electromagnetic fields. Each of the field equations has two terms on the right-hand side. The first term is just the wave oscillation (varying on the fast time scale), whereas the second term describes the coupling of the plasma to the beam particles through the waves. The latter involves the small coefficients $s_{\boldsymbol{\mu}_L}$ and $s_{\boldsymbol{\mu}}$ and is responsible for the slowly changing amplitudes assumed in the beginning of the derivation.

It is easy to see that the total momentum of the system of particles and waves is conserved

$$\sum_{j=1}^{N} \boldsymbol{\pi}_j + \sum_{\boldsymbol{\mu}_L > 0} \boldsymbol{\mu}_L |f_{\boldsymbol{\mu}_L}|^2 + \sum_{\boldsymbol{\mu} > 0} \boldsymbol{\mu} \, |\mathbf{a}_{\boldsymbol{\mu}}|^2 = \text{const.} \tag{3.32}$$

It is also obvious that the total energy of fields and particles is a conserved quantity, since the Hamiltonian does not have explicit time dependence.

The system (3.31) is highly non-linear and integrability is unlikely even for one particle, one longitudinal, and one transverse waves; in fact, the system with one particle and one longitudinal wave is integrable (see [32]), but not so for one particle and one transverse wave, see Chapter 5. In the non-relativistic limit the chaotic behavior was noted in Ref. [33]. Linear analysis can be done in the absence of electromagnetic waves and in one spatial dimension. Further investigation is based on numerical solution. This is done in the next chapter.

Chapter 4

Analysis: Part One

4.1 Introduction

In the next two chapters we explore more fully the system of equations (3.31). In the present chapter emphasis is given to the numerical study of our model whereas in the next chapter we derive an approximation to the full system of equations, and the emphasis is on the analytical study of the system.

The model is used to study several problems. First, a formula for the linear growth rate is derived, thus corroborating previous results. It follows that the longitudinal growth rate decreases with increasing initial velocity of the beam, a result due to relativistic effects. On the other hand, computer runs with three spatial dimensions show that waves with nonzero transverse wave vectors grow faster then purely longitudinal waves. This is also in agreement with previous results. Next, we study the higher Fourier harmonics in the power spectrum, an find a correction to previous results because of the presence of multiple waves. We then study the scaling properties of the sat-

uration amplitude with the linear growth rate. In the non-relativistic case obtain the expected "trapping" scaling. Then we investigate the influence of electromagnetic waves on the beam-plasma system. The presence of one external electromagnetic wave stabilizes the beam-plasma instability. When two external electromagnetic waves are present simultaneously, beat-wave resonance is observed. This is used to suggest that particles may be accelerated via the transfer of energy from the electromagnetic waves since the relativistic particles and the beat wave can have matching velocities and thus can satisfy a resonance condition. Transfer of energy from the external electromagnetic waves to the plasma wave (through the beam particles) is observed only when a certain value of the initial vector potential is exceeded. This suggests that a "loss" mechanism is present, although our system is actually Hamiltonian; an explanation of this effect is given. Finally, an experimental test of the beat-wave resonance in the full system is suggested.

For numerical purposes it is convenient to rewrite the system (3.31) as a system of real equations by splitting the real and imaginary parts of each of its complex equations. We have

$$
\begin{aligned}
\dot{\boldsymbol{\rho}}_j &= \frac{1}{\beta}\frac{\boldsymbol{\pi}_j/\beta + 2\sum_{\boldsymbol{\mu}>0} s_{\boldsymbol{\mu}}\left(\mathbf{a}^0_{\boldsymbol{\mu}}\cos(\boldsymbol{\mu}\cdot\boldsymbol{\rho}_j) - \mathbf{a}^1_{\boldsymbol{\mu}}\sin(\boldsymbol{\mu}\cdot\boldsymbol{\rho}_j)\right)}{\sqrt{1+\left|\boldsymbol{\pi}_j/\beta + 2\sum_{\boldsymbol{\mu}>0}\left(\mathbf{a}^0_{\boldsymbol{\mu}}\cos(\boldsymbol{\mu}\cdot\boldsymbol{\rho}_j) - \mathbf{a}^1_{\boldsymbol{\mu}}\sin(\boldsymbol{\mu}\cdot\boldsymbol{\rho}_j)\right)\right|^2}}, \\
\dot{\boldsymbol{\pi}}_j &= \frac{\left[\boldsymbol{\pi}_j/\beta + 2\sum_{\boldsymbol{\nu}>0}\left(\mathbf{a}^0_{\boldsymbol{\nu}}\cos(\boldsymbol{\nu}\cdot\boldsymbol{\rho}_j) - \mathbf{a}^1_{\boldsymbol{\nu}}\sin(\boldsymbol{\nu}\cdot\boldsymbol{\rho}_j)\right)\right]}{\sqrt{1+\left|\boldsymbol{\pi}_j/\beta + 2\sum_{\boldsymbol{\mu}>0}\left(\mathbf{a}^0_{\boldsymbol{\mu}}\cos(\boldsymbol{\mu}\cdot\boldsymbol{\rho}_j) - \mathbf{a}^1_{\boldsymbol{\mu}}\sin(\boldsymbol{\mu}\cdot\boldsymbol{\rho}_j)\right)\right|^2}} \\
&\qquad\qquad \cdot\sum_{\boldsymbol{\mu}>0}\boldsymbol{\mu}\left[2s_{\boldsymbol{\mu}}\left(\mathbf{a}^0_{\boldsymbol{\mu}}\sin(\boldsymbol{\mu}\cdot\boldsymbol{\rho}_j) + \mathbf{a}^1_{\boldsymbol{\mu}}\cos(\boldsymbol{\mu}\cdot\boldsymbol{\rho}_j)\right)\right] \\
&\quad -2\sum_{\boldsymbol{\mu}_L>0}\boldsymbol{\mu}_L s_{\boldsymbol{\mu}_L}\left(f^0_{\boldsymbol{\mu}_L}\sin(\boldsymbol{\mu}_L\cdot\boldsymbol{\rho}_j) + f^1_{\boldsymbol{\mu}_L}\cos(\boldsymbol{\mu}_L\cdot\boldsymbol{\rho}_j)\right), \\
\dot{f}^0_{\boldsymbol{\mu}_L} &= f^1_{\boldsymbol{\mu}_L} + \sum_{j=1}^{N} s_{\boldsymbol{\mu}_L}\sin(\boldsymbol{\mu}_L\cdot\boldsymbol{\rho}_j), \\
\dot{f}^1_{\boldsymbol{\mu}_L} &= -f^0_{\boldsymbol{\mu}_L} + \sum_{j=1}^{N} s_{\boldsymbol{\mu}_L}\cos(\boldsymbol{\mu}_L\cdot\boldsymbol{\rho}_j),
\end{aligned}
$$

$$
\begin{aligned}
\dot{\mathbf{a}}^0_{\boldsymbol{\mu}} &= \omega_{\boldsymbol{\mu}}\mathbf{a}^1_{\boldsymbol{\mu}} \\
&\quad -\sum_{j=1}^{N}\frac{s_{\boldsymbol{\mu}}\sin(\boldsymbol{\mu}\cdot\boldsymbol{\rho}_j)\left[\boldsymbol{\pi}_j/\beta + 2\sum_{\boldsymbol{\nu}>0}\left(\mathbf{a}^0_{\boldsymbol{\nu}}\cos(\boldsymbol{\nu}\cdot\boldsymbol{\rho}_j) - \mathbf{a}^1_{\boldsymbol{\nu}}\sin(\boldsymbol{\nu}\cdot\boldsymbol{\rho}_j)\right)\right]}{\sqrt{1+\left|\boldsymbol{\pi}_j/\beta + 2\sum_{\boldsymbol{\nu}>0}\left(\mathbf{a}^0_{\boldsymbol{\nu}}\cos(\boldsymbol{\nu}\cdot\boldsymbol{\rho}_j) - \mathbf{a}^1_{\boldsymbol{\nu}}\sin(\boldsymbol{\nu}\cdot\boldsymbol{\rho}_j)\right)\right|^2}}, \\
\dot{\mathbf{a}}^1_{\boldsymbol{\mu}} &= -\omega_{\boldsymbol{\mu}}\mathbf{a}^0_{\boldsymbol{\mu}} \\
&\quad -\sum_{j=1}^{N}\frac{s_{\boldsymbol{\mu}}\cos(\boldsymbol{\mu}\cdot\boldsymbol{\rho}_j)\left[\boldsymbol{\pi}_j/\beta + 2\sum_{\boldsymbol{\nu}>0}\left(\mathbf{a}^0_{\boldsymbol{\nu}}\cos(\boldsymbol{\nu}\cdot\boldsymbol{\rho}_j) - \mathbf{a}^1_{\boldsymbol{\nu}}\sin(\boldsymbol{\nu}\cdot\boldsymbol{\rho}_j)\right)\right]}{\sqrt{1+\left|\boldsymbol{\pi}_j/\beta + 2\sum_{\boldsymbol{\nu}>0}\left(\mathbf{a}^0_{\boldsymbol{\nu}}\cos(\boldsymbol{\nu}\cdot\boldsymbol{\rho}_j) - \mathbf{a}^1_{\boldsymbol{\nu}}\sin(\boldsymbol{\nu}\cdot\boldsymbol{\rho}_j)\right)\right|^2}},
\end{aligned}
$$

where $f_{\boldsymbol{\mu}_L} = f^0_{\boldsymbol{\mu}_L} + if^1_{\boldsymbol{\mu}_L}$ and $\mathbf{a}_{\boldsymbol{\mu}} = \mathbf{a}^0_{\boldsymbol{\mu}} + i\mathbf{a}^1_{\boldsymbol{\mu}}$. The numerical simulations are done with an adaptive time step fourth order Runge-Kutta method. The time step is controlled by the greater of the absolute error, which is the C^2 norm of the vector made up from all dependent variables, and the relative error of the electrostatic field amplitude (this was chosen since the electrostatic field initial condition is a very small perturbation). The runs are done with

accuracies usually 10^{-5} to 10^{-6}. The difference in runs using two different accuracies is extremely small and only shows up at very long times. The system there exhibits its chaotic nature. Notice that the time units in the relativistic system differ from the non-relativistic one by a factor of $(2n_b/n)^{1/3}$, i.e. $\tau_{\text{non-rel}} = (2n_b/n)^{1/3}\tau_{\text{rel}}$. For example, if $n_b/n = 0.001$, as it is chosen in most runs, 1 unit of "non-relativistic time" would equal approximately 7.94 units of "relativistic" time.

4.2 Purely electrostatic case

4.2.1 Single wave, one dimensional electrostatic case

In this subsection the multi-wave model is used only in one spatial dimension and the electron beam is mono-energetic. The single wave model has been studied in a number of references, including the relativistic electron beam. In the Introduction it was mentioned that when a mono-energetic electron beam propagates in a plasma, an electrostatic wave grows because of the beam-plasma instability. Subsequently the wave saturates due to non-linear effects and traps some of the electrons from the electron beam. The trapped electrons and the wave periodically exchange momentum while the amplitude of the wave oscillates in time.

For a relativistic electron beam the linear growth rate is

$$\gamma_L^{\text{rel}} = \gamma_L\sqrt{1-\beta^2} = \frac{\sqrt{3}}{2}\left(\frac{n_b}{2n}\right)^{1/3}\sqrt{1-\beta^2}\,\omega_p, \tag{4.1}$$

where $\gamma_L = (\sqrt{3}/2)(n_b/2n)^{1/3}\omega_p$ is the non-relativistic growth rate (see e.g. [8, 9, 10, 32, 17]). In the context of the present model this result can be derived as follows. Consider the linearized equations of motion around the equilibrium

$f_{\boldsymbol{\mu}_L}(0) = 0$, $\boldsymbol{\pi}_j(0) \equiv \boldsymbol{\pi}_{0j} = \left(0, 0, \beta^2/\sqrt{1-\beta^2}\right)$, and a uniform distribution of beam particles. To emphasize the slow time scale we set $\boldsymbol{\rho}' = \boldsymbol{\rho} - \tau \hat{e}_z$, with $\hat{e}_z$ being the unit vector in the z-direction and $F_{\boldsymbol{\mu}_L} = f_{\boldsymbol{\mu}_L} e^{i\tau}$. In terms of these slowly changing quantities, the momentum is

$$P_j = \frac{\beta^2(1+\dot{\boldsymbol{\rho}}'_j)}{\sqrt{1-\beta^2(1+\boldsymbol{\rho}'_j)^2}}, \tag{4.2}$$

and the Hamiltonian becomes

$$H = \sum_{j=1}^{N} \sqrt{1+\left(\frac{P_j}{\beta}\right)^2} - \sum_{j=1}^{N} s_{\boldsymbol{\mu}_L} \left(F_{\boldsymbol{\mu}_L} e^{i\boldsymbol{\mu}_L \cdot \boldsymbol{\rho}'_j} + F^*_{\boldsymbol{\mu}_L} e^{-i\boldsymbol{\mu}_L \cdot \boldsymbol{\rho}'_j}\right) - \sum_{j=1}^{N} P_j. \tag{4.3}$$

From (4.3), the linearized equations of motion can be written as

$$\begin{aligned}
\delta\dot{\boldsymbol{\rho}}'_j &= \frac{1}{\beta^2}\frac{\delta\boldsymbol{\pi}_j}{\sqrt{1+\boldsymbol{\pi}^2_{0j}}} - \frac{1}{\beta^4}\frac{\boldsymbol{\pi}_{0j}\left(\boldsymbol{\pi}_{0j}\cdot\delta\boldsymbol{\pi}_j\right)}{\left(1+\boldsymbol{\pi}^2_{0j}\right)^{3/2}}, \\
\delta\dot{\boldsymbol{\pi}}_j &= \sum_{\boldsymbol{\mu}_L>0} i\boldsymbol{\mu}_L s_{\boldsymbol{\mu}_L}\left(\delta F_{\boldsymbol{\mu}_L} e^{i\boldsymbol{\mu}_L\cdot\boldsymbol{\rho}'_{0j}} - \delta F^*_{\boldsymbol{\mu}_L} e^{-i\boldsymbol{\mu}_L\cdot\boldsymbol{\rho}'_{0j}}\right), \\
\delta\dot{F}_{\boldsymbol{\mu}_L} &= \sum_{j=1}^{N}\left(\boldsymbol{\mu}_L\cdot\delta\boldsymbol{\rho}'_j\right) s_{\boldsymbol{\mu}_L} e^{-i\boldsymbol{\mu}_L\cdot\boldsymbol{\rho}'_{0j}},
\end{aligned} \tag{4.4}$$

and one equation that is complex conjugate of the last one. Assuming all linear quantities vary as $e^{\lambda t}$, the dispersion relation follows upon taking the

determinant of the following matrix:

$$\begin{pmatrix}
-\lambda & \dots & \dots & 0 & X_1 & \dots & \dots & 0 & 0 & 0 \\
0 & -\lambda & \dots & 0 & 0 & X_2 & \dots & 0 & 0 & 0 \\
\vdots & & & \vdots & \vdots & & & \vdots & \vdots & \vdots \\
0 & \dots & \dots & \lambda & 0 & \dots & \dots & X_N & 0 & 0 \\
0 & \dots & \dots & 0 & -\lambda & \dots & \dots & 0 & Y_1 & Y_1^* \\
\vdots & & & \vdots & 0 & -\lambda & & 0 & Y_2 & Y_2^* \\
\vdots & & & \vdots & \vdots & & & \vdots & \vdots & \vdots \\
0 & & & 0 & 0 & & & -\lambda & Y_N & Y_N^* \\
E_1^* & \dots & \dots & E_N^* & 0 & \dots & \dots & 0 & -\lambda & 0 \\
E_1 & \dots & \dots & E_N & 0 & \dots & \dots & 0 & 0 & -\lambda
\end{pmatrix}, \tag{4.5}$$

where we have used the abbreviations

$$\begin{aligned}
X_j &= \frac{1}{\beta^2}\frac{1}{\sqrt{1+(P_{0j}/\beta)^2}} - \frac{1}{\beta^4}\frac{P_{0j}^2}{(1+(P_{0j}/\beta)^2)^{3/2}}, \\
E_j &= s_{\boldsymbol{\mu}} e^{i\boldsymbol{\mu}_L\cdot\boldsymbol{\rho}'_{0j}}, \\
Y_j &= iE_j.
\end{aligned} \tag{4.6}$$

After diagonalizing (4.5), its determinant is found to give

$$\begin{aligned}
(-\lambda)^{2N}\Bigg[\left(-\lambda+\sum_{j=1}^{N}\frac{X_jE_j^*Y_j}{\lambda^2}\right)\left(-\lambda+\sum_{j=1}^{N}\frac{X_jE_jY_j^*}{\lambda^2}\right) \\
-\left(\sum_{j=1}^{N}\frac{X_jE_j^*Y_j^*}{\lambda^2}\right)\left(\sum_{j=1}^{N}\frac{X_jE_jY_j}{\lambda^2}\right)\Bigg] = 0.
\end{aligned} \tag{4.7}$$

Evaluating the relations (4.6) at the initial conditions $\boldsymbol{\rho}'_{0j} = (0, 0, 2\pi j/N)$, $P_{0j}= \beta^2/\sqrt{1-\beta^2}$ ($\dot{\boldsymbol{\rho}}'_{0j} = 0$ for particles moving with the phase velocity of the

wave), we get

$$\begin{aligned} X_j &= \frac{(1-\beta^2)^{3/2}}{\beta^2}, \\ \sum_{j=1}^{N} X_j E_j^* Y_j &= \frac{iNs_{\boldsymbol{\mu}}^2(1-\beta^2)^{3/2}}{\beta^2}, \\ \sum_{j=1}^{N} X_j E_j Y_j^* &= \frac{-iNs_{\boldsymbol{\mu}}^2(1-\beta^2)^{3/2}}{\beta^2}, \\ \sum_{j=1}^{N} X_j E_j Y_j &= \sum_{j=1}^{N} X_j E_j^* Y_j^* = 0. \end{aligned} \tag{4.8}$$

Finally, substituting (4.8) in (4.7) we obtain the equation for the eigenvalues,

$$\lambda^{2N-4}\left(\lambda^6 + \frac{1}{4}\left(\frac{n_b}{n}\right)^2(1-\beta^2)^3\right) = 0. \tag{4.9}$$

(Note that only the coordinates and momenta in the z-direction are relevant, and therefore the total number of variables is effectively $2N+2$, which equals the order of the polynomial equation.) From Eq. (4.9) a formula for the eigenvalue with the maximal positive real part is found to be

$$\Re\mathrm{e}\,(\lambda)_{\max} = \left(\frac{n_b}{2n}\right)^{1/3}(1-\beta^2)^{1/2}\cos(\pi/6). \tag{4.10}$$

In dimensional variables formula (4.10) becomes (4.1). Thus our result (4.1), for one longitudinal wave, agrees with the previously known result from the relativistic single wave model (see e.g. [10, 17]). It is seen that for a β approaching unity relativistic effects reduce the growth rate of the electrostatic wave. This is due to the increased relativistic longitudinal mass of the particles; the transverse mass remains unchanged since the motion is non-relativistic in directions perpendicular to $\hat{e}_z$.

In Fig. 4.1 we give an example of a numerical solution of the relativistic single wave model. This figure shows the growth and saturation of the fundamental mode (more precisely, $|f_{\boldsymbol{\mu}_L}|/\sqrt{N}$ is plotted, since it depends only on

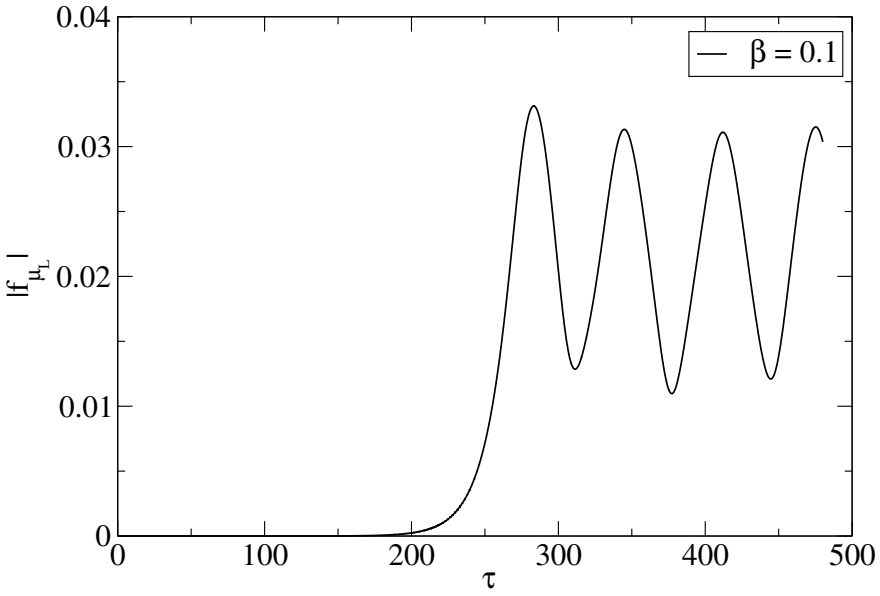

Figure 4.1: This figure shows initial linear growth of the electric potential followed by saturation with trapping oscillations. 300 particles are uniformly distributed over a distance of 2π in the z-direction and their initial velocity equals that of the wave.

the slow time scale and is a quantity independent of the number of particles). The initial condition of the run is as follows: The initial disturbance (initial amplitude) of the waves is 10^{-8} (both for the real and imaginary parts of $f_{\boldsymbol{\mu}_L}$), 300 particles are uniformly distributed over a distance of 2π in the z-direction and their initial velocity equals that of the wave. In this Fig. 4.1, as well as in Fig. 4.2, $\beta = 0.1$ for a weakly relativistic beam. For larger β the single wave model has similar behavior. The only difference is that the growth of the electrostatic wave occurs at later times because of the relativistic mass effect

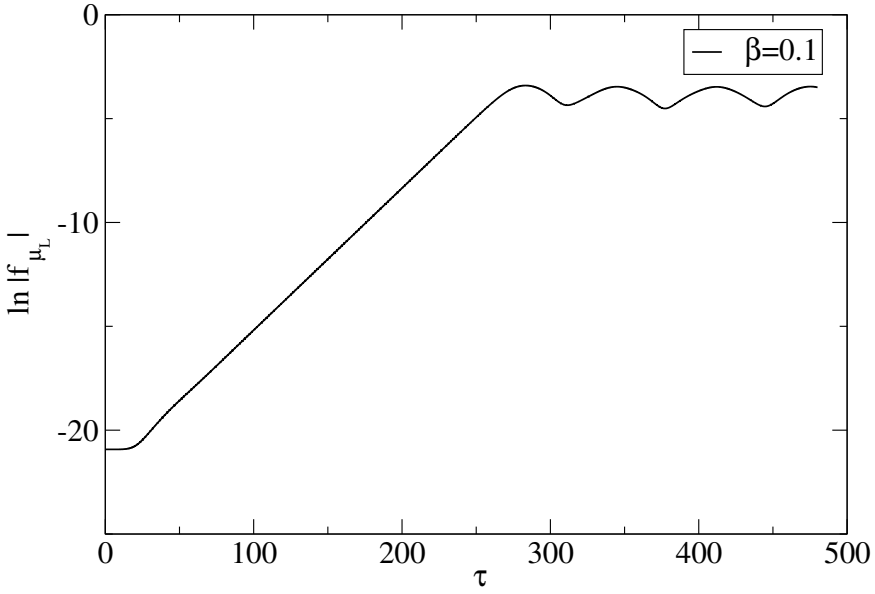

Figure 4.2: Logarithm, $\ln|f_{\mathbf{k}_L}|$, of the electrostatic potential versus normalized time for the case in Fig. 4.1. The numerical value of the slope is 0.0684, whereas that value given by Eq. (4.10) is 0.06839.

mentioned above. It is seen from Fig. 4.2, that the match between the numerical and theoretical values of the slope is within 0.1%: The numerical value of the slope is 0.0684, whereas that value given by formula (4.10) is 0.06839.

4.2.2 Multi-wave, one dimensional electrostatic case

We next consider the multi-wave pure electrostatic case in one spatial dimension. In Fig. 4.3 the growth and saturation of high Fourier field harmonics is shown (note that because of the normalization of the dimensionless field

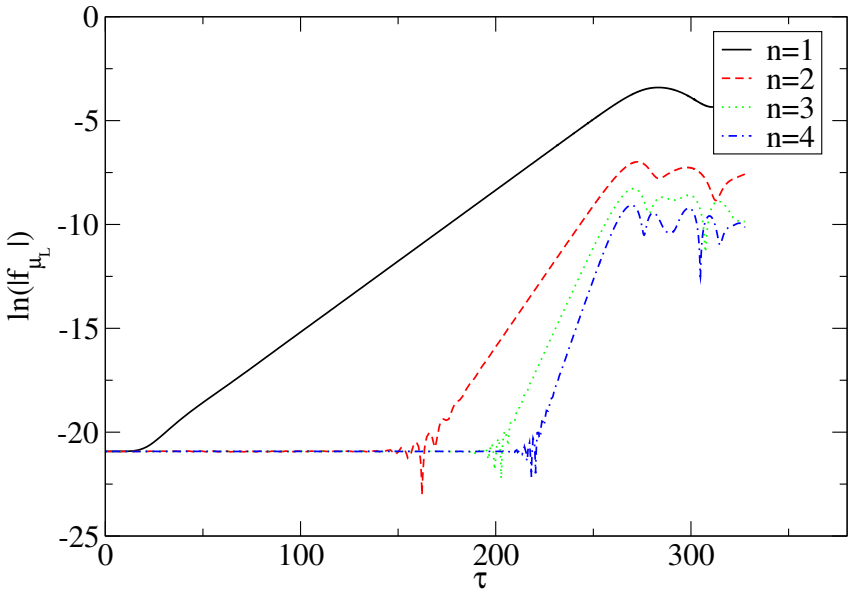

Figure 4.3: Logarithm of the electrostatic field, $\ln\left(|f_{\boldsymbol{\mu}_L}|\right)$, vs. time, $\beta = 0.1$

variables the amplitude the electric field is given by $|E_{\mathbf{k}_L}| \sim |f_{\boldsymbol{\mu}_L}|$). The high harmonics (the terminology high harmonics refers to spatial Fourier, *not* to frequency (temporal Fourier) harmonics) are non-resonant, since their phase velocity is n times smaller than that of the fundamental, where n is the number of the harmonic. This means that the high harmonics will grow much slower than the fundamental. The dielectric for higher harmonics is $\epsilon(k,\omega) = \epsilon(nk_{L\min}, \omega + (n-1)k_{L\min}v_0) \simeq 1 - \omega_p^2/(\omega + (n-1)k_{L\min}v_0)^2 \simeq 1$ for $n > 1$ (see Ref. [9]). From Coulomb's law then it follows that the harmonics

of the field evolve approximately according to

$$E_{\mathbf{k}_L}(t) \simeq \frac{4\pi n_{b\,k_L}(t)}{ik_L},$$

where $n_{b\,k_L}(t)$ stands for the time evolving harmonics of the beam charge density; equivalently one could say that the harmonics of the electric field reflect the harmonics of the beam charge density. Hence in dimensionless variables we have

$$E_{\mathbf{k}_L}(t) \sim \frac{\sum_{j=1}^{N} e^{i\boldsymbol{\mu}_L \cdot \boldsymbol{\rho}'_j(t)}}{i\mu_L}. \tag{4.11}$$

From (4.11) it follows upon setting $\boldsymbol{\mu}_L = (0, 0, n)$ that the energy spectrum obeys an n^{-2} law, i.e. $|E_n|^2/8\pi \sim An^{-2}$, with $A = \text{const.}$. The authors of Ref. [9] used the single wave model to calculate $\boldsymbol{\rho}'_j(t)$ and then substituted in formula (4.11) to verify the n^{-2} law for the non-relativistic case. They found that the actual exponent was -2.5 instead of -2. With the present model the spectrum can be directly calculated numerically. Moreover, dependence on the initial beam velocity can be studied, i.e. the spectrum of the field in the case of a relativistic beam can be found. In Fig. 4.4 the logarithm of the energy harmonics, $\ln |f_{\mathbf{k}_L}|^2$ (one-half of this quantity used for convenience), vs. n is shown ($\boldsymbol{\mu}_L = (0, 0, n)$, $n = 2, 3, \dots$). Notice that it is not a straight line. Only the initial slope of the curve (which is -2.6 for $\beta = 0.1$, a weakly relativistic case and, -2.5 for $\beta = 0.9$) agrees with the slope calculated in that reference. The reason for disagreement is that in Ref. [9] the influence of the higher field harmonics on the beam particles was neglected; having these harmonics could be significant enough to change the shape of the energy spectral distribution. Another possible reason for this difference is the fact that fine scale mixing occurs as the nonlinear regime is established. Since the high harmonics amplitudes are much smaller than the fundamental (roughly

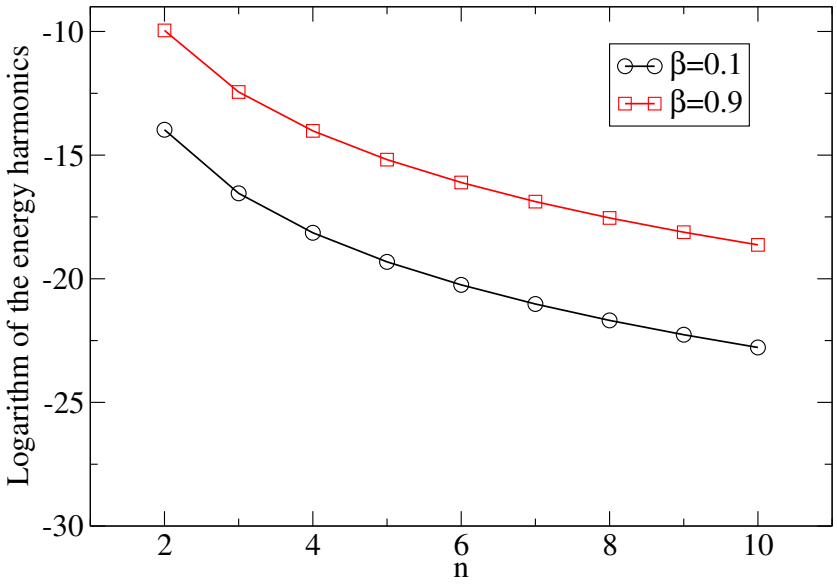

Figure 4.4: Energy spectrum. There is a deviation from a constant slope predicted in a previous work: Only the initial slope agrees with previous prediction.

by a factor of $(n_b/n)^{1/3}$) influence on them could be much larger. Another way to say this is that fine scale mixing for the high harmonics occurs at much smaller amplitudes (see Ref. [50]).

4.2.3 Multi-wave, multi-dimensional electrostatic case

In three dimensions it is possible that the boundary conditions can favor growth of waves with wave vectors that have non-zero components in the x- and y-directions. Suppose the initial velocity of the electron beam only has

a component along the z-direction. Then the resonant condition is satisfied for a certain component of the wave vector in the z-direction. The other two components of the wave vectors of such waves are not determined by the resonant condition. They may be determined by boundary conditions. Another important condition that influences the linear growth rate in transverse directions compared with that of the longitudinal growth rate was mentioned above. Namely, in the longitudinal direction the increased mass of a relativistic beam decreases the linear growth rate in that direction. However, in the transverse direction the velocities are still non-relativistic, and therefore the transverse gorwth rate may become larger than the longitudinal growth rate for an ultrarelativistic electron beam (see Ref. [8]). To examine this situation numerically, a simulation was done with 8x8x8 particles in which the waves have wave vectors in the range $(-3, -3, 1)$ to $(3, 3, 3)$, i.e. the total number of waves is 7x7x3 = 147. These waves divide in three major groups: Wave vectors with components in the z-direction equal to 1, 2, and 3. Figure 4.5 shows the linear growth of the waves. There are clearly three groups of waves growing at a similar growth rate. This figure should be compared with Fig. 4.3 where the waves with $n = 1, 2, 3$ have no x- and y-component of $\mathbf{k}_L$. This behavior is to be expected for a non-relativistic beam. In the next Fig. 4.6 we examine the same system for a relativistic beam with $\beta = 0.9$ and $\beta = 0.98$. Only the spread in the fundamental harmonics is shown. It is clear, that the more relativistic beam has larger spread. The green lines indicate the wave with wave vector $(0, 0, 1)$ and is seen to have the lowest growth rate. In Fig. 4.7 the total energy of all waves is shown. It is seen that, compared to when the waves have no components in the k_{Lx}- and k_{Ly}-directions (solid curve in Fig. 4.7), the (energy of) the electrostatic wave becomes more erratic and the amplitude of

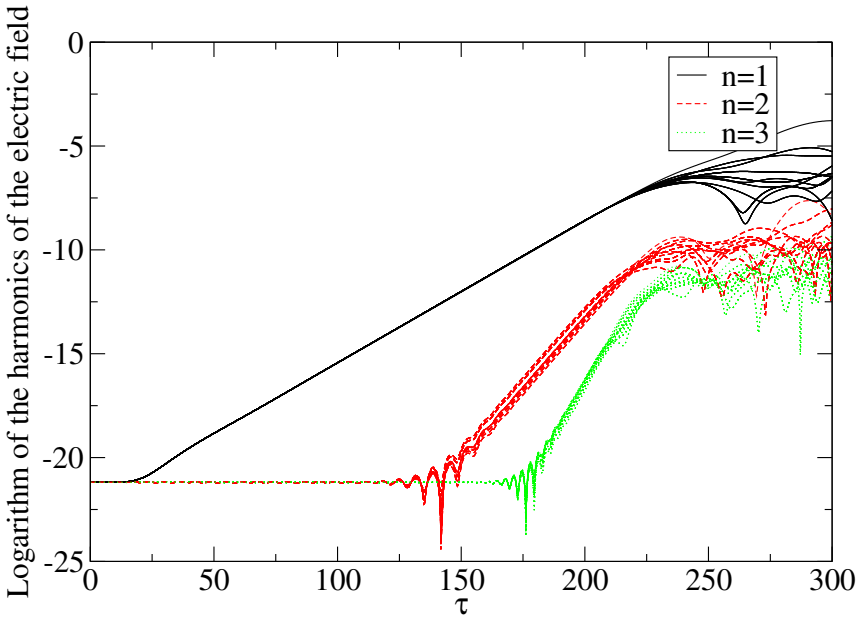

Figure 4.5: Linear growth of waves with wave numbers in the range $(-3, -3, 1)$ to $(3, 3, 3)$. Three major groups of growing waves correspond to wave numbers with z-component equal to $n = 1$, 2, and 3, $\beta = 0.1$.

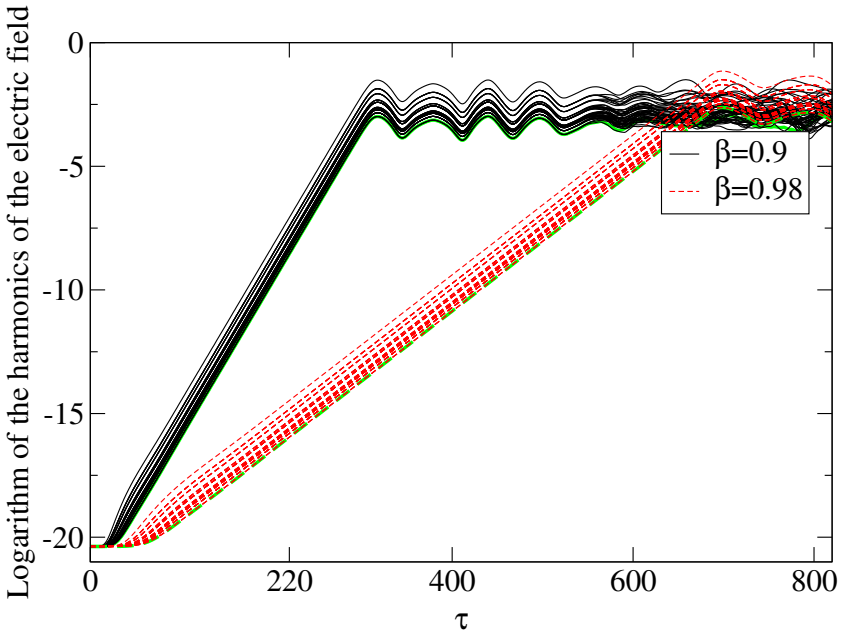

Figure 4.6: Linear growth of waves with wave numbers in the range $(-3, -3, 1)$ to $(3, 3, 3)$. Only group of growing waves with z-component of their wave numbers $n = 1$ are shown for two values of β: $\beta = 0.9$ and $\beta = 0.98$. There is much larger spread in the waves with present transverse components of their wave vectors.

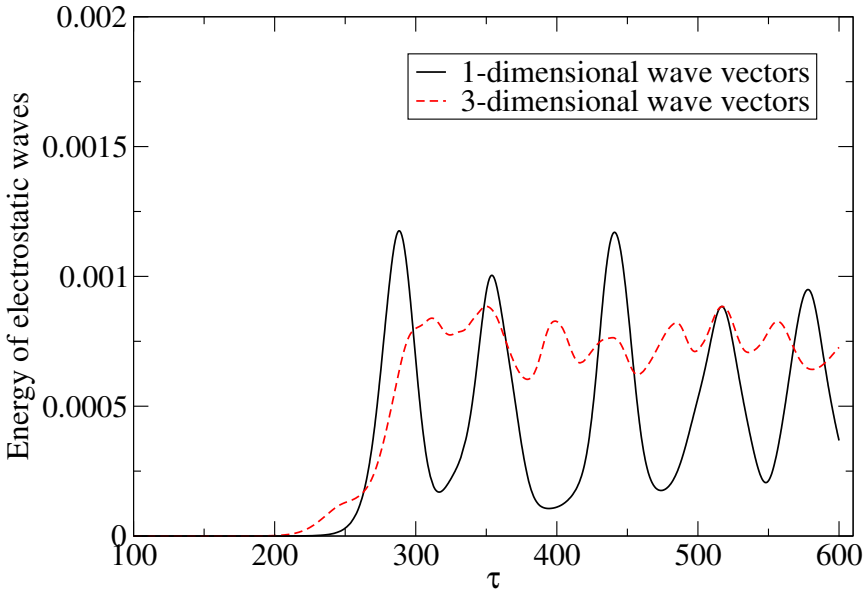

Figure 4.7: Energy of the electrostatic waves with non-zero x- and y-components of the wave vectors, solid line, compared with waves with components of wave vectors only in the z-direction, dashed line, $\beta = 0.1$.

the oscillations become smaller, i.e. the energy exchange between the electron beam and the electrostatic wave is smaller (dashed curve) and the coherence is violated by the growth of the higher harmonics. For a large number of modes (larger $|\mathbf{k}_L|$) the linear regime shortens. This could be explained by noting that fine scale mixing occurs when the amplitude of the corresponding mode exceeds the value of the order $1/|\mathbf{k}_L|$, as shown in Ref. [40]. Therefore even small amplitudes of higher modes can contribute nonlinearly to the growth of the energy at early times. Numerical simulations by other authors similarly

show only a few oscillations before the plasma wave is damped by fine scale mixing (see for example Refs. [17, 25]).

4.2.4 Scaling properties of the single wave model

As a last case of pure electrostatic wave-particle interaction, let us examine the scaling properties of the relativistic single wave model. By "scaling properties" we mean the following. It was shown in the earlier numerical examples, e.g. see Fig. 2.1, that the growth of the amplitude of the electrostatic wave goes through a linear regime, with a subsequent saturation. The saturation amplitude can be shown to scale as a certain power of the linear growth rate. This is what we would like to examine in this subsection.

The scaling of the single wave model in the non-relativistic case was first considered in Ref. [51]. The authors found that the saturation amplitude scales as the $1/2$ power of the linear growth rate. The same result was also found later in Ref. [52]. The method that was used in these works was based on considering the Vlasov equation for the problem of the bump on tail instability. It is known that the eigenfunction has a singularity at the resonant wave velocity. The eigenfunction has the same singularity. In the cited references the authors tried to regularize the eigenfunction using an appropriate regularization procedures from the theory of distributions. This behavior is now refered to as Hopf scaling.

A much simpler physical argument showed that the electrostatic wave grows until it reaches an amplitude such, as to trap the beam particles in its potential well. Then the energy balance between the kinetic energy of the beam particles and the electrostatic energy of the wave yields a relation between the

saturation amplitude and the linear growth rate. This argument was first used in Ref. [4] in relation to considering of wave-particle interaction and particle trapping, and later in the context of the single wave model, by [6, 9, 53]. The scaling properties of the saturation amplitude in the relativistic single wave model were considered in Refs. [8, 10]. The argument is as follows. In the linear regime, we have for the growth rate and frequency of the electrostatic wave (consider first non-relativistic beam)

$$\gamma_L = \Re\mathrm{e}\lambda = \frac{\sqrt{3}}{2}\left(\frac{n_b}{2n}\right)^{1/3}\omega_p, \tag{4.12}$$

$$\omega = \omega_p + \Im\mathrm{m}\lambda = \omega_p\left(1 - \frac{1}{2}\left(\frac{n_b}{2n}\right)^{1/3}\right). \tag{4.13}$$

The velocity of the beam particles, relative to the wave phase velocity is

$$\Delta v = v_0 - \frac{\omega}{k_L} = \frac{1}{2}\left(\frac{n_b}{n}\right)^{1/3} v_0. \tag{4.14}$$

Then the electrostatic wave will grow until it reaches amplitude large enough to trap the beam particles, i.e.

$$\phi \sim \frac{m(\Delta v)^2}{e} \sim \frac{m v_0^2 (n_b/n)^{2/3}}{e}. \tag{4.15}$$

Therefore we see that the saturation amplitude scales as the square of the linear growth rate–so-called trapping scaling.

In our model $|E_{\mathbf{k}_L}| \sim |f_{\boldsymbol{\mu}_L}|$. Noting that $v_0 = \omega_p/k_L$ and $E_{\mathbf{k}_L} \sim k_L\phi$, we have

$$E_{\mathbf{k}_L} \sim \frac{R(\tau)}{k_L}, \tag{4.16}$$

where $R(\tau)$ is a universal function for all different growth rates. Since $R(\tau)$ saturates at the same value for all electrostatic waves, we can test the scaling law by looking at the ratios $|E_{\mathbf{k}_{L1}}|/|E_{\mathbf{k}_{L2}}|$. In the non-relativistic case we

should have the dependence

$$\frac{|E_{\mathbf{k}_{L1}}|}{|E_{\mathbf{k}_{L2}}|} = \frac{\mu_{L2}}{\mu_{L1}}, \tag{4.17}$$

μ_{L1} and μ_{L2} determining different initial beam velocities (and hence different growth rates) through $v_0 = \omega_p/k_L$.

In the relativistic beam case a similar argument shows dependence on the relativistic factor γ. More precisely, the linear increment then is given by formula (4.1). The main difference from the non-relativistic case comes from the large mass increase as the beam particles move at relativistic velocities, namely, $m_L = m\gamma^3$ (see Ref. [48]). The particles transfer energy to the wave

$$\Delta\varepsilon = v_0 \Delta p \simeq m v_0^2 \left(\frac{n_b}{n}\right)^{1/3} \gamma^2 \tag{4.18}$$

and the oscillation energy is

$$|E_{\mathbf{k}_L}|^2 \sim n_b m v_0^2 \left(\frac{n_b}{n}\right)^{1/3} \gamma^2. \tag{4.19}$$

The relation (4.17) becomes then

$$\frac{|E_{\mathbf{k}_{L1}}|}{|E_{\mathbf{k}_{L2}}|} = \frac{\mu_{L2}}{\mu_{L1}} \frac{\gamma_1}{\gamma_2}, \tag{4.20}$$

The above relation (4.19) holds only for

$$\left(\frac{n_b}{n}\right)^{1/3} \gamma \ll 1, \tag{4.21}$$

when $\Delta p/p \ll 1$. If, on the other hand, $\Delta p/p \geq 1$, a different amount of energy is transfered to the wave

$$|E_{\mathbf{k}_L}|^2 \sim v_0 p \simeq n_b m v_0^2 \gamma \tag{4.22}$$

and the relation (4.20) becomes

$$\frac{|E_{\mathbf{k}_{L1}}|}{|E_{\mathbf{k}_{L2}}|} = \frac{\mu_{L2}}{\mu_{L1}} \frac{\gamma_1^{1/2}}{\gamma_2^{1/2}}. \tag{4.23}$$

$n_b/n = 10^{-3}$					
β	0.96	0.48	0.24	0.12	0.06
0.96	0.7751	4.43	9.57	19.47	39.15
		6.27	13.87	28.36	57.04
0.48		0.175	2.16	4.40	8.84
			2.21	4.53	9.10
0.24			0.0810	2.04	4.09
				2.05	4.11
0.12				0.0398	2.01
					2.01
0.06					0.0198

Table 4.1: Scaling relations. The theoretical formula used in the lower boxes is (4.20). The value $(n_b/n)^{1/3}\,\gamma = 0.36$ for $\beta = 0.96$.

Notice that the scaling property in the non-relativistic case was derived in a frame moving with the initial beam velocity, whereas in the relativistic case it is derived in the stationary frame. This explains the apparent difference in the scalings in formulas (4.15) and (4.20), (4.23); our model describes the system evolution in the stationary frame, and so the latter formulas will be used for comparison with numerical simulations. Note that the relativistic estimates go into the non-relativistic for $\gamma \to 1$. The relativistic scaling relations have been previously derived in Refs. [8, 10].

Next we present the results of several runs with different initial beam velocities and different beam-plasma density ratios. The results are presented in Tables 4.1, 4.2, 4.3 where the number in the upper box is the numerical value of the ratios $|f_{\boldsymbol{\mu}_{L1}}|/|f_{\boldsymbol{\mu}_{L2}}|$, the number in the lower box is the theoretical number according to formula (4.20) or (4.23), whereas on the diagonal are the values of $|f_{\boldsymbol{\mu}_{L1}}|/\sqrt{N}$.

$n_b/n = 10^{-5}$					
β	0.96	0.48	0.24	0.12	0.06
0.96	0.481	5.78	12.72	26.0	52.28
		6.27	13.87	28.36	57.04
0.48		0.0832	2.20	4.50	9.04
			2.21	4.53	9.10
0.24			0.0378	2.04	4.11
				2.05	4.11
0.12				0.0185	2.01
					2.01
0.06					0.0092

Table 4.2: Scaling relations. The theoretical formula used in the lower boxes is (4.20). The value $(n_b/n)^{1/3}\,\gamma = 0.02$ for $\beta = 0.96$. The agreement is much better for smaller values of β, and is overall better compared to the case in Table 4.1

Table 4.1 compares numerical runs with formula (4.20). Since the condition (4.21) is not very well satisfied for large values of β, we do not have very good agreement with the theoretical scaling relation.

In Table 4.2 we have a much lower value for $(n_b/n)^{1/3}\gamma = 0.02$ (for the maximal $\beta = 0.96$) and thus the scaling condition (4.21) is much better satisfied, therefore we see much better overall agreement, as well as much better agreement when β is smaller than 0.5. The good agreement in this case signifies the validity of our model in describing the beam-plasma system for this range of physical parameters.

In Table 4.3 we have runs with $(n_b/n)^{1/3} = 0.46$ and therefore the scaling condition (4.21) is not satisfied. Then we test the numerical simulations against formula (4.23). We see better agreement than with formula (4.20), however overall this there is no good agreement, except for small β, when the

$n_b/n = 0.1$					
β	0.96	0.48	0.24	0.12	0.06
0.96	0.770	2.24	4.50	9.02	18.03
		3.54	7.45	15.06	30.2
0.48		0.344	2.01	4.03	8.06
			2.10	4.26	8.53
0.24			0.171	2.00	4.00
				2.02	4.06
0.12				0.0854	2.00
					2.01
0.06					0.0427

Table 4.3: Scaling relations. The theoretical formula used in the lower boxes is (4.23). The value $(n_b/n)^{1/3}\,\gamma = 0.46$ for $\beta = 0.96$.

system becomes weakly relativistic. In addition, our model does not suite the description of the beam–plasma system when the ratio $(n_b/n)^{1/3}$ is of the order of unity since this violates one of the basic assumptions in the derivation.

The relation (4.16) has been derived in a more mathematically rigorous way in Refs. [54, 55] where the authors manage to eliminate the singularities in the distribution function to all orders by appropriately rescaling the field amplitude. The result confirms the trapping scaling. The authors of these papers also consider mobile ions, and the scaling law in this case turns out to be 5/3 instead of 2. These scalings have also been considered in Ref. [56] where an extensive numerical study is performed.

4.3 Effect of the electromagnetic waves

It was noted in Chapter 2 (see also Ref. [33]) that two electromagnetic waves of different wave vectors can have a noticeable effect on the linear growth of a non-relativistic electrostatic wave. It is expected that similar, and in fact much more significant effect, will take place in the relativistic case. We first study this numerically along the lines this was done in section 2.4. We will have one electrostatic and one or two electromagnetic waves in a one-dimensional system.

4.3.1 One electrostatic and one electromagnetic wave

First, consider one electromagnetic wave. For the runs in this subsection, we take $N = 100$ particles, $\boldsymbol{\mu}_L = (0, 0, \mu_L)$, $\boldsymbol{\mu} = (0, 0, \mu)$ with $\mu_L = 1$, $\mu = 2, 3, \ldots$, and $n_b/n = 0.001$. The dimensionless coefficients (3.17) have the order of magnitude value of $s_{\boldsymbol{\mu}} \simeq 2.2 \times 10^{-3}\sqrt{\beta/\mu}$ and $s_{\boldsymbol{\mu}_L} \simeq 2.2 \times 10^{-3}\beta/\mu_L$. For an estimate of how large the normalized vector potential $a_0 = s_{\boldsymbol{\mu}} a_{\boldsymbol{\mu}}$ (see (3.16)), is for given values of the parameters, let us take $\mu = 5$, and $\beta = 0.1$. Then for $|\mathbf{a}_{\boldsymbol{\mu}}| = 50$, $a_0 = 0.016$, for $|\mathbf{a}_{\boldsymbol{\mu}}| = 400$, $a_0 = 0.12$ i.e., our model still applies according to condition (3.25). It is also clear that for larger β, a_0 has larger value. For example if $\beta = 0.96$ and $\mu = 3$, for $|\mathbf{a}_{\boldsymbol{\mu}}| = 20$, $a_0 = 0.025$, and for $|\mathbf{a}_{\boldsymbol{\mu}}| = 200$, $a_0 = 0.25$. It also follows that faster particles will interact stronger with the electromagnetic waves (larger coupling coefficient $s_{\boldsymbol{\mu}}$).

In Figure 4.8 numerical solutions with one electrostatic wave and one electromagnetic wave are given for several different values of the transverse amplitude. It is seen that larger amplitude of the electromagnetic wave causes a bit larger saturation amplitude for the electrostatic wave, however, at the same

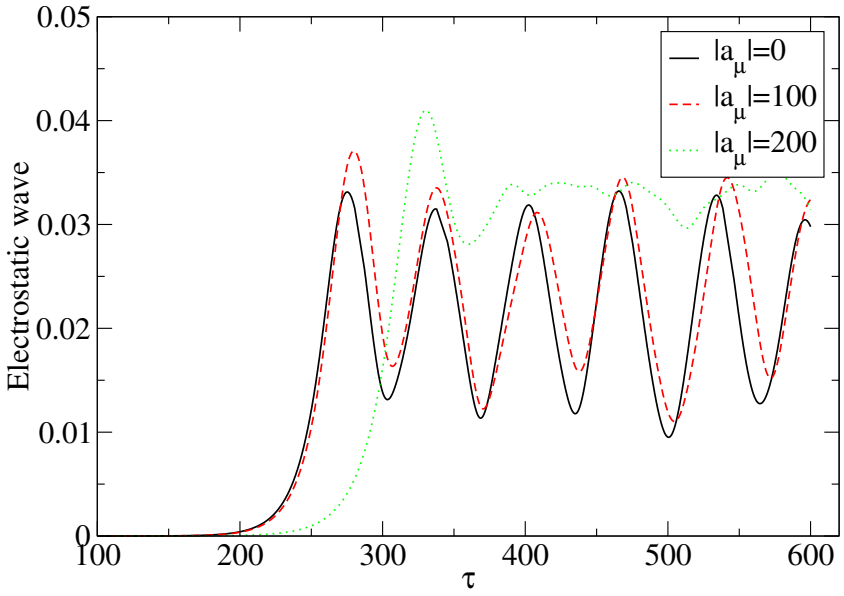

Figure 4.8: One electrostatic wave, one electromagnetic wave, 100 particles, $\mu = 5$, and $\beta = 0.1$.

time there is a tendency to destroy the regularity of the oscillation. Notice also that for $|\mathbf{a}_{\boldsymbol{\mu}}| = 200$ there is a significant delay of the instability process. In the next Fig. 4.9 the electromagnetic wave has even larger amplitude. As a result, a stabilizing effect is observed: The delay in the growth of the electrostatic wave is very significant, and the amplitude of saturation of the electrostatic wave is more than an order of magnitude smaller than for $|\mathbf{a}_{\boldsymbol{\mu}}| = 0$. This behavior can be explained by analogy with the forced reversed mathematical pendulum. Its unstable equilibrium becomes stable when an external periodic force of certain frequency is applied [57]. This suggests an important idea: As

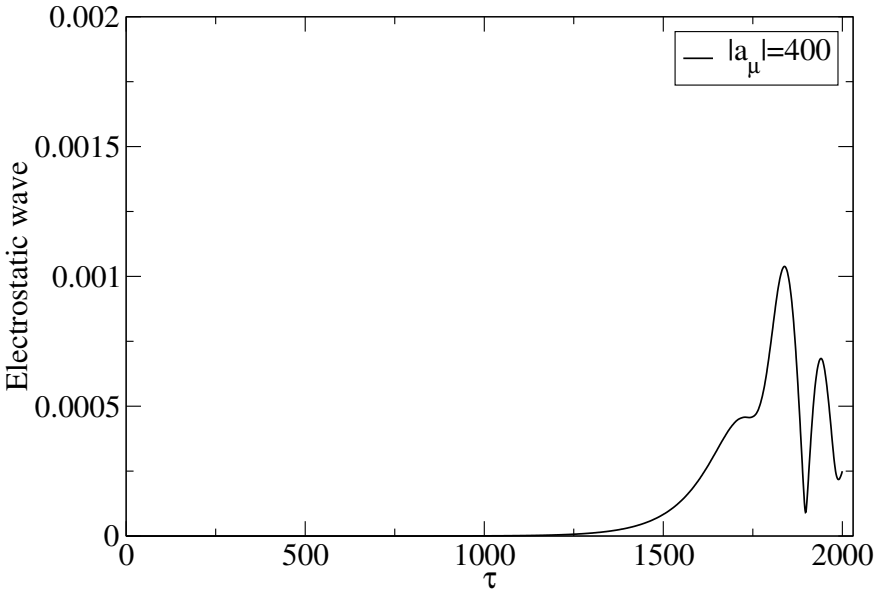

Figure 4.9: One electrostatic and one electromagnetic waves. For larger amplitude the electromagnetic wave has a stabilizing influence on the electrostatic wave, $\mu = 5$, and $\beta = 0.1$.

an approximation, the electromagnetic waves can be considered as an external force to the system of beam particles and electrostatic waves. This idea will be utilized later to draw some analytical conclusions about the system of equations (3.31).

4.3.2 Two electromagnetic and one electrostatic waves

A single electromagnetic wave has a phase velocity greater than the speed of light, and therefore cannot be used to resonantly drive the beam particles. On

μ	1	2	3	4	5
β	0.828	0.928	0.961	0.976	0.984

Table 4.4: Solutions of (4.25), β, for various values of given μ.

the other hand, if two waves are present, their frequencies and wave vectors can be chosen to satisfy

$$\omega_{\mathbf{k}+\mathbf{k}_L} - \omega_{\mathbf{k}} = \omega_p. \tag{4.24}$$

Such matching condition can be used to obtain resonant driving of the plasma wave (and the beam particles). To see if this holds for the system (3.31), expand the above matching condition for $\mu_L/\mu \ll 1$ and use the definition $\beta = \omega_p/k_L c$ to obtain

$$\mu^2 + \mu - \frac{\beta^2}{2(1-\beta)} = 0. \tag{4.25}$$

This quadratic equation, if solved for β with given values of μ, gives values for the matching condition. For example, if $\mu = 1$, the solution yields a value $\beta = 0.83$. The electromagnetic waves must have higher frequency than the electrostatic wave in order to propagate in the plasma. Therefore $\mu \geq 1$, and the the above value of β is a lower bound on the beam velocity, for which the matching condition (4.24) can be satisfied. Table 4.4 gives more values of β as a function of μ defined by equation (4.25). To test for such beat wave resonance, we choose different values of μ and fix β to equal some of the values in Table 4.4. We expect to observe a resonant curve similar to this of a forced mathematical pendulum [57].

The plots in Fig. 4.10 show how the saturation amplitude is affected by the presence of two electromagnetic waves with equal amplitudes, but different wave vectors. Only the wave vector with $\mu = 3$ (for the first wave, and $\mu = 4$ for

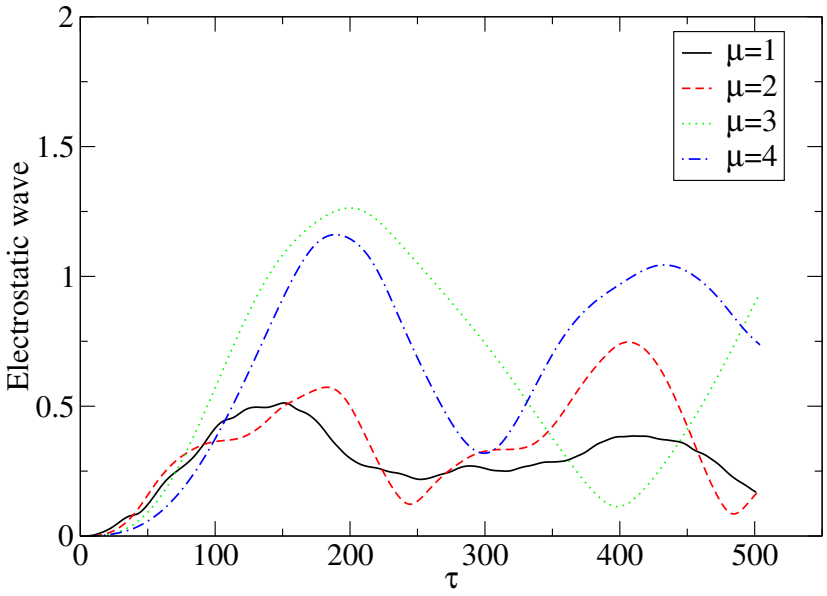

Figure 4.10: Electrostatic wave in the presence of two electromagnetic waves with $|\mathbf{a}_{\boldsymbol{\mu}}| = 200$ and $\beta = 0.961$.

the second) satisfies the matching condition, and we see that the electrostatic wave has the largest saturation amplitude for it. The rest of the curves are slightly off resonance, but still have a much stronger influence than a single electromagnetic wave, see Fig. 4.8. In the next Fig. 4.11 we show the resonant curve, i.e. the saturation amplitude as a function of the electromagnetic waves wave vector ($\omega_k/\omega_p \simeq \mu$). In Fig. 4.12 we see that the electromagnetic waves for $\mu = 3$ have the largest oscillation of their amplitudes. Note that we have plotted the electromagnetic wave's amplitudes $|\mathbf{a}_{\boldsymbol{\mu}}|/\sqrt{N}$ to make the plotted quantity independent of the number of beam particles. Since $N = 100$, the

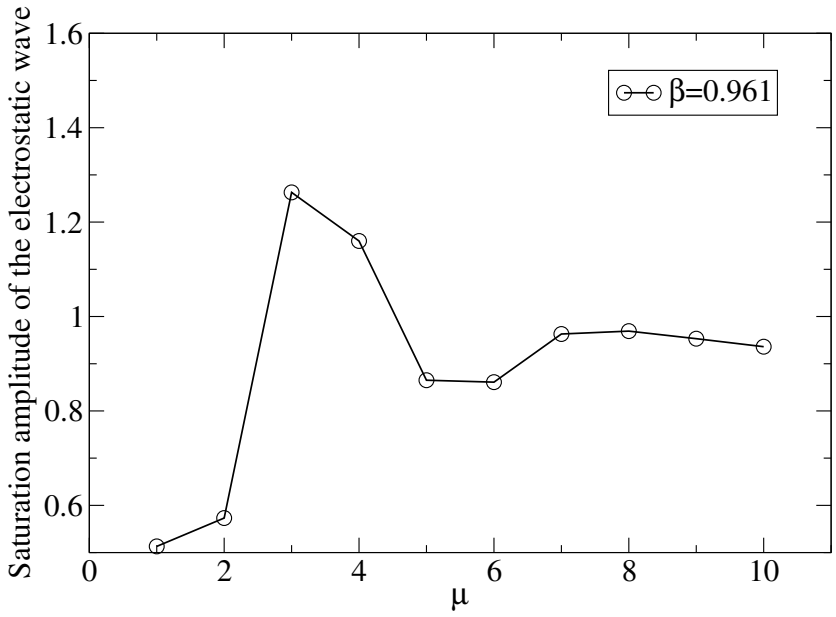

Figure 4.11: Resonance curve for $\beta = 0.961$ and $|\mathbf{a}_{\boldsymbol{\mu}}| = 200|$.

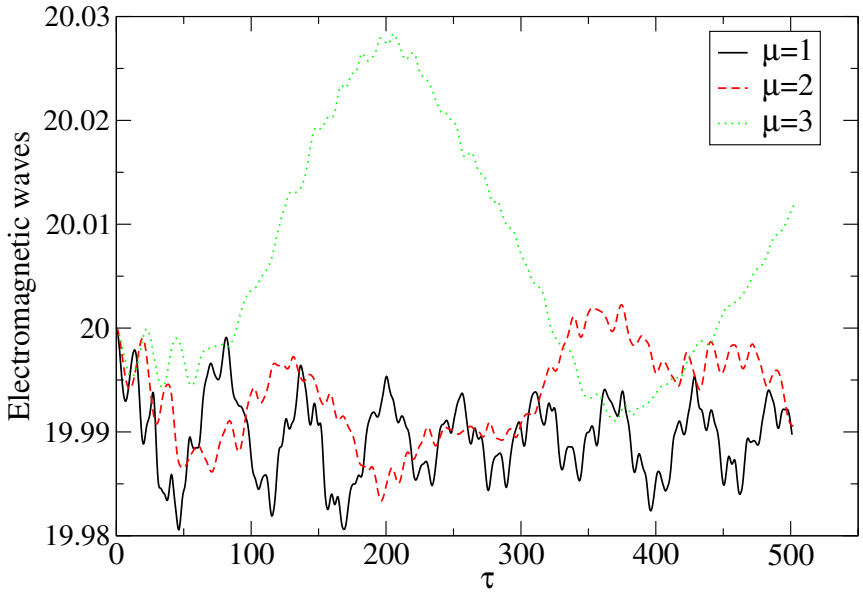

Figure 4.12: The change in the electromagnetic waves. The largest change is for the waves with $\mu_{1,2} = 3, 4$ that satisfy the matching condition (4.25) for $\beta = 0.961$ and $|\mathbf{a}_{\boldsymbol{\mu}}| = 200|$.

scale on the graph shows 1/10th of the actual value of $|\mathbf{a}_{\boldsymbol{\mu}}|$.

Next, in Fig. 4.13 we see the dependence of the electrostatic wave saturation amplitude on the amplitude of the electromagnetic waves. The two electromagnetic waves satisfy the matching condition (4.24). When the electromagnetic waves amplitudes are small, the electrostatic wave only responds with a phase shift, but with no change in its saturation amplitude (see also Fig. 4.14). Starting at the value of $|\mathbf{a}_{\boldsymbol{\mu}}| \simeq 20$, the electrostatic wave saturation amplitude starts increasing; at the same time the phase shift increases toward early growth of the instability similar to what was observed in Chapter 2. The existence of such a threshold of the electromagnetic waves initial amplitudes beyond which the electrostatic wave starts growing is equivalent to some kind of effective "loss" or "damping". In our model there is no loss of energy in the system. However, recall that the electromagnetic waves only interact with the beam particles, and not directly with the electrostatic waves. Similarly, the electrostatic waves interact with the beam particles, exchanging energy and momentum with them. The physical explanation of this fact is the following. The electromagnetic waves transfer momentum to the beam particles, thus "heating" the beam. However it requires a certain minimal value of the "heating" before the beam particles can transfer any energy to the electrostatic wave. This minimal value is determined by comparing the rates of "heating" by the electromagnetic waves, and rate of transferring "beam energy" to the electrostatic wave. When the "heating" rate exceeds the rate of transfer of "beam energy", the electrostatic wave gains energy from both, the beam kinetic energy, and the electromagnetic waves energy. The situation when a threshold exists in a system without energy loss is similar to plasma parametric instabilities in inhomogeneous medium: There is no loss of energy in the

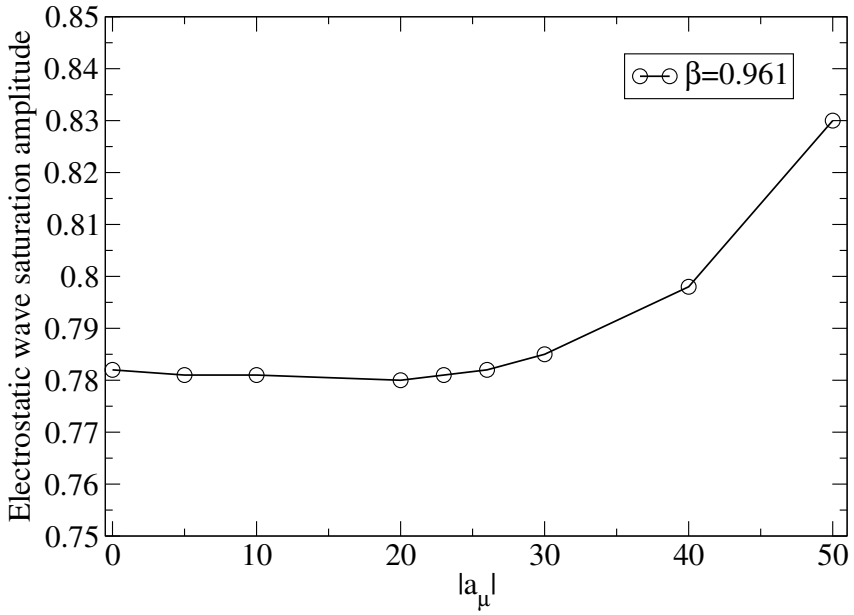

Figure 4.13: Threshold of instability of the electrostatic wave in the presence of two electromagnetic waves with $\mu_{1,2} = 3, 4$, $\beta = 0.961$.

system, but threshold for instability can arise from spatial inhomogeneities. If the region of instability is of the order of a plasma wavelength, and the electromagnetic wave period is close to the plasma wave period, energy can escape from the unstable region into the stable region on a time scale of a plasma period, and thus can provide an effective "loss" mechanism. This 'loss" results in the existence of a threshold for the electromagnetic wave amplitude, below which a plasma wave cannot be excited, see Ref. [58].

In Fig. 4.14 we see severall cases: The curves with $|\mathbf{a}_{\boldsymbol{\mu}}| = 5$ and 200 represent the growth of the electrostatic waves in the presence of electromag-

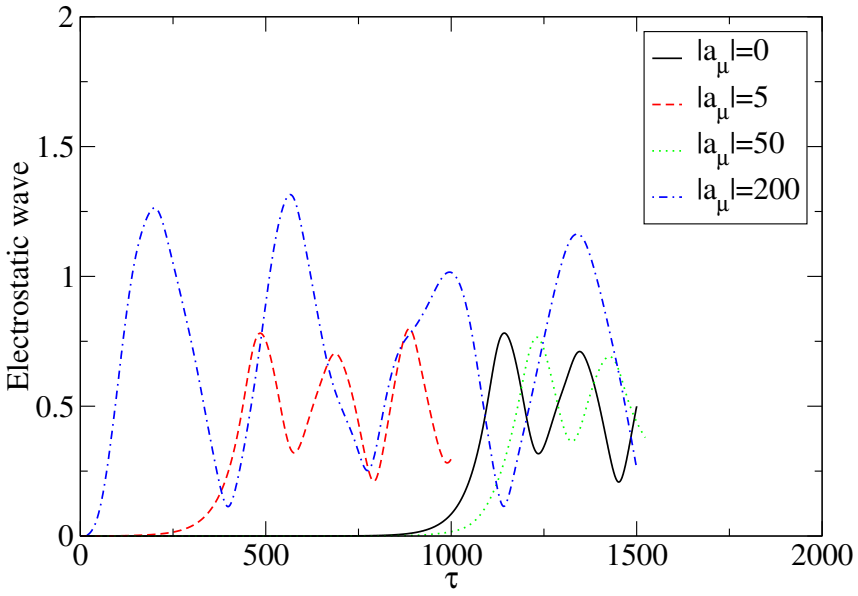

Figure 4.14: Resonant amplification and phase shift of the electrostatic wave in the presence of two electromagnetic waves with $|\mathbf{a_\mu}| = 5, 200$, and $\mu_1 = 3, \mu_2 = 4$. The curve with $|\mathbf{a_\mu}| = 50$, $\mu_1 = 3, \mu_2 = 5$ does not satisfy the resonant condition (4.25) for $\beta = 0.961$, and is seen to not cause any transfer of energy (amplification) to the electrostatic wave.

netic waves satisfying the matching condition (4.25). The curve with $|\mathbf{a_\mu}| = 5$ has no influence on the amplitude of the electrostatic wave, but has results in a big phase shift, similar to the one conisdered in Chapter 2, Sec. 2.4. The curve with $|\mathbf{a_\mu}| = 200$ has a considerable effect resulting in both, increase in the saturation amplitude of the electrostatic wave by about 60% and a big phase shift. The curve with $|\mathbf{a_\mu}| = 50$ does not satisfy the matching condition (4.25) since in this case $\mu_1 = 3, \mu_2 = 5$. We see effect similar to the effect of

only one electromagnetic wave present in the system in Fig. 4.8: No significant change in the saturation amplitude, and a delay in the instability.

4.4 Experimental application

It is important to emphasize that our model does not include background plasma nonlinearities because the electromagnetic waves are too small to interact with each other non-linearly. Therefore the only means of coupling of electromagnetic waves with each other and with electrostatic waves is by means of beam particles. The waves and particles must satisfy the matching condition (4.24). In our particular model the resonant particles are the beam particles, but similar considerations can show that a few particles from the background plasma can play the same role as long as their velocity is large enough to satisfy (4.24). It follows that a more effective mechanism for amplifying the plasma wave using small electromagnetic waves is through resonant particles.

In Ref. [38] the following idea for creating ultrashort electron bunches was suggested. First, a large laser pulse generates a plasma wake. A forward propagating injection laser pulse and a backward propagating laser pulse collide some distance behind the large laser pulse. The two injection pulses have small amplitudes $a_{i0} \ll 1$, and frequency offset $\Delta\omega = \omega_1 - \omega_2$. When the two injection pulses collide, their beat-wave has very small phase velocity $v_b = \Delta\omega/\Delta k \simeq \Delta\omega/2k_0$. During the collision process, the small beat wave injects electrons into the plasma wake for acceleration to high energies.

A schematic diagram of this is given in Fig. 4.15. Our suggestion extends this scheme in the following way. Suppose the two small injection pulses

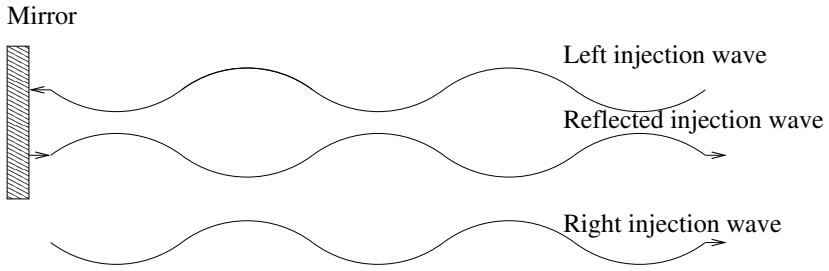

Figure 4.15: Schematic diagram for experimental application of the beat wave amplification of the electrostatic wave.

have frequencies that (approximately) satisfy the matching condition (4.24). Then after the two counter propagating pulses collide and inject electrons in the plasma wake, one of the pulses is reflected by the mirror, and sent back into the plasma. In the course of its propagation it creates a beat wave that can be used to further amplify the plasma wake. Of course, the amplitudes of the two injection pulses must be greater than the threshold amplitude. Depending on what the density of the injected electrons is, the transfered energy will vary. In our simulations the beam-background plasma density ratio was 10^{-3} and the amplification was about 60%. For a smaller density ratio of 10^{-5}

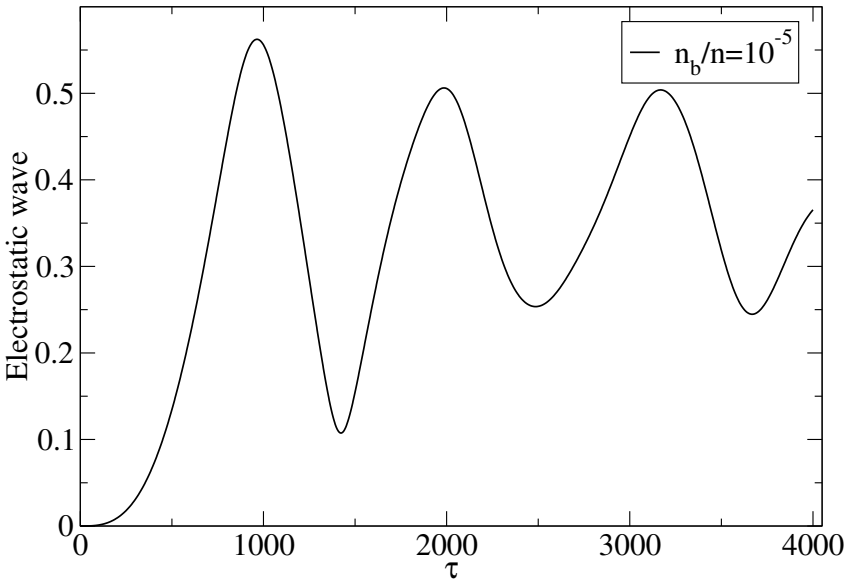

Figure 4.16: Resonant amplification of the electrostatic wave in the presence of two electromagnetic waves with $|\mathbf{a}_{\boldsymbol{\mu}}| = 200$, $\mu_1 = 3, \mu_2 = 4$, $\beta = 0.961$, and a small density ratio of $n_b/n = 10^{-5}$.

the wake amplitude only decreased by a factor of two, see Table 4.2; relative to the value in Table 4.2, which is the case without electromagnetic waves, the increase is also significant–about 17%. Since the growth rate of the plasma wave also decreases for smaller density ratios, the threshold will also decrease and the "heating" of the electron bunch will be smaller, so there will be smaller energy spread too. A numerical simulation for density ratio $n_b/n = 10^{-5}$ and with similar other initial conditions as in Fig. 4.10 is given in Fig. 4.16. We see that after about 1000 wave periods the electrostatic wave reaches satura-

tion. For a wavelength of 10μm the max amplification is reached after 1cm of propagation.

4.5 Conclusions

On the basis of the generalized model derived in Chapter 3 we first studied the purely electrostatic beam–plasma system. We showed that the growth rate of our model in one dimension agrees with previous derivations. In the three dimensional simulations we showed that the transverse growth rate becomes more significant as the velocity of the beam becomes more relativistic. We found a correction to previous results in the shape of the (Fourier) energy spectrum because of our more accurate picture included many waves. In the presence of one external electromagnetic wave the beam-plasma instability can be stabilized, provided the amplitude of the electromagnetic wave is large enough. In the presence of two external electromagnetic waves, beat wave resonance was observed. It was suggested that this phenomenon be used for plasma wake amplification thus extending previous ideas for generating ultrashort electron bunches.

Chapter 5

Analysis: Part Two

5.1 Introduction

In this chapter we will derive an analytically tractable model from the system of non-linear equations (3.31). The basis for such derivation comes from the observation that in the course of the evolution of the system of particles and fields, a significant number of the particles get trapped in the well of the electrostatic wave; these particles then propagate while clumped together and move as one big "macroparticle", as shown in Ref. [32]. In the context of the single wave model this approximation, together with the conservation of the total momentum of particles and fields, reduces the system of equations to a one-degree-of-freedom system that is integrable.

In Fig. 5.1 we show snapshots of the evolution of the full system at various times. The number of particles is 1000 and $\beta = 0.1$. On the y-axis we plot the momenta of the particles and on the x-axis their coordinates. The first panel shows the initial state which corresponds to an undisturbed electron

beam propagating in a plasma. The second panel shows the development of the beam-plasma instability in its linear stage. The third panel shows the beginning of the nonlinear stage. These first three panels of Fig. 5.1 illustrate the behavior that underlies the so-called "rotating bar" model as introduced in Ref. [11]. This model assumes that most of the particles stay on a finite segment of a straight line (the bar) in phase space that rotates rigidly in time. The rotating bar model is an approximation which is only valid for a limited period of time. As we can see in the next three panels of Fig. 5.1 the "bar" changes its shape from a straight line and more and more particles enter the chaotic region. Thus the rotating bar model is no longer applicable.

In the last three panels we show graphs of the phase space of the system after several oscillations (on the slow time scale) of the electric field. The macroparticle has formed and the conglomerate of particles simply rotates in phase space. The percent of the particles in the clump is about 71% and if we neglect the chaotic particles, the system is described by a single macroparticle in a given periodic (cosine) potential.

It was noted in the previous chapter that the electromagnetic waves can be considered as "external" to the system of particles and electrostatic waves. The reason for this was that in the one-electromagnetic-wave case, the electromagnetic wave acted in a manner similar to an external force on a reversed mathematical pendulum (causing it, for example, to stabilize the unstable equilibrium). In the two-electromagnetic-wave case we studied the beat wave resonance phenomenon, resulting in a resonant curve similar to that of a forced mathematical pendulum. Although the electromagnetic waves did not remain unchanged in the process of interaction, if they have large enough amplitudes then their relative changes are small (cf. Fig. 4.12). The latter

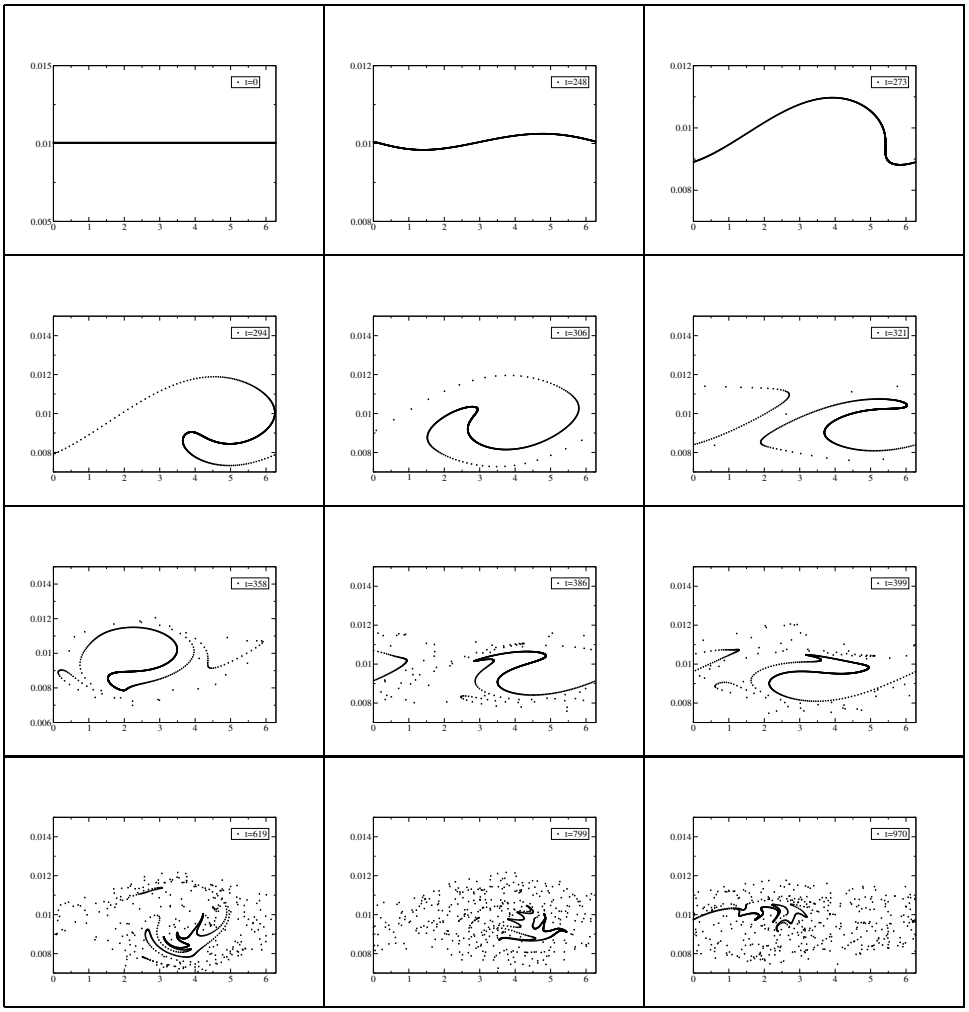

Figure 5.1: Evolution of the beam-plasma system for various times; $N = 1000$ and $\beta = 0.1$. In the first three panels the particles can be approximated by the rotating bar model, but the next three panels show that this model becomes invalid. In the last three panels the idea of the "macroparticle" model is illustrated. The clump of particles simply rotates in phase space leading to the idea of a single (macro-) particle approximation (see Ref. [32]).

warrants the assumption of the "external wave" approximation. In this chapter we combine the "macroparticle" model and the "external wave" approximation to derive a simple model that allows an analytical treatment. We shall try to quantitatively describe some of the features discussed in the previous chapters on the basis of our numerical analysis.

5.2 Derivation

To begin the derivation, consider the non-relativistic Lagrangian (3.18)

$$\begin{aligned} L &= -\sum_{j=1}^{N}\sqrt{1-|\beta\dot{\boldsymbol{\rho}}_j|^2}+\sum_{j=1}^{N}\sum_{\boldsymbol{\mu}_L>0} s_{\boldsymbol{\mu}_L}\left(f_{\boldsymbol{\mu}_L}e^{i\boldsymbol{\mu}_L\cdot\boldsymbol{\rho}_j}+f^*_{\boldsymbol{\mu}_L}e^{-i\boldsymbol{\mu}_L\cdot\boldsymbol{\rho}_j}\right) \\ &\quad -\sum_{j=1}^{N}\beta\dot{\boldsymbol{\rho}}_j\cdot\sum_{\boldsymbol{\mu}>0}s_{\boldsymbol{\mu}}\left(\mathbf{a}_{\boldsymbol{\mu}}e^{i\boldsymbol{\mu}\cdot\boldsymbol{\rho}_j}+\mathbf{a}^*_{\boldsymbol{\mu}}e^{-i\boldsymbol{\mu}\cdot\boldsymbol{\rho}_j}\right) \\ &\quad -\sum_{\boldsymbol{\mu}_L>0}\left(f_{\boldsymbol{\mu}_L}f^*_{\boldsymbol{\mu}_L}\right)+\frac{1}{2i}\sum_{\boldsymbol{\mu}_L>0}\left(f_{\boldsymbol{\mu}_L}\dot{f}^*_{\boldsymbol{\mu}_L}-f^*_{\boldsymbol{\mu}_L}\dot{f}_{\boldsymbol{\mu}_L}\right) \\ &\quad -\sum_{\boldsymbol{\mu}>0}\omega_{\boldsymbol{\mu}}\left(\mathbf{a}_{\boldsymbol{\mu}}\cdot\mathbf{a}^*_{\boldsymbol{\mu}}\right)+\frac{1}{2i}\sum_{\boldsymbol{\mu}>0}\left(\mathbf{a}_{\boldsymbol{\mu}}\cdot\dot{\mathbf{a}}^*_{\boldsymbol{\mu}}-\mathbf{a}^*_{\boldsymbol{\mu}}\cdot\dot{\mathbf{a}}_{\boldsymbol{\mu}}\right). \end{aligned} \tag{5.1}$$

From now on we assume that quantities vary only with the z-coordinate. Further, we put $\boldsymbol{\mu}_L=(0,0,\mu_L)$, $\mu_L=1$ and $\boldsymbol{\mu}=(0,0,\mu)$, the transverse waves being linearly polarized along the y-axis. We perform a coordinate change to a moving frame in (5.1), i.e.

$$\boldsymbol{\rho}=\boldsymbol{\rho}'_j+t,\qquad \dot{\boldsymbol{\rho}}=\dot{\boldsymbol{\rho}}'_j+1, \tag{5.2}$$

and make a change of field variables,

$$\begin{aligned} &f_{\boldsymbol{\mu}_L}=f'_{\boldsymbol{\mu}_L}e^{-i\mu_L t},\quad \dot{f}_{\boldsymbol{\mu}_L}=\dot{f}'_{\boldsymbol{\mu}_L}e^{-i\mu_L t}-(i\mu_L)f'_{\boldsymbol{\mu}_L}e^{-i\mu_L t} \\ &\mathbf{a}_{\boldsymbol{\mu}}=\mathbf{a}'_{\boldsymbol{\mu}}e^{-i\mu t},\qquad \dot{\mathbf{a}}_{\boldsymbol{\mu}}=\dot{\mathbf{a}}'_{\boldsymbol{\mu}}e^{-i\mu t}-(i\mu)\mathbf{a}_{\boldsymbol{\mu}}e^{-i\mu t}. \end{aligned} \tag{5.3}$$

The substitution of (5.3) into the corresponding terms in the Lagrangian (5.1) yields

$$f_{\boldsymbol{\mu}_L} f^*_{\boldsymbol{\mu}_L} = f'_{\boldsymbol{\mu}_L} f'^*_{\boldsymbol{\mu}_L}, \qquad \mathbf{a}_{\boldsymbol{\mu}} \cdot \mathbf{a}^*_{\boldsymbol{\mu}} = \mathbf{a}'_{\boldsymbol{\mu}} \cdot \mathbf{a}'^*_{\boldsymbol{\mu}} \tag{5.4}$$

and

$$\begin{aligned} \frac{1}{2i}\left(f_{\boldsymbol{\mu}_L}\dot{f}^*_{\boldsymbol{\mu}_L} - f^*_{\boldsymbol{\mu}_L}\dot{f}_{\boldsymbol{\mu}_L}\right) &= \mu_L\left(f'_{\boldsymbol{\mu}_L} f'^*_{\boldsymbol{\mu}_L}\right) + \frac{1}{2i}\left(f'_{\boldsymbol{\mu}_L}\dot{f}'^*_{\boldsymbol{\mu}_L} - f'^*_{\boldsymbol{\mu}_L}\dot{f}'_{\boldsymbol{\mu}_L}\right), \\ \frac{1}{2i}\left(\mathbf{a}_{\boldsymbol{\mu}} \cdot \dot{\mathbf{a}}^*_{\boldsymbol{\mu}} - \mathbf{a}^*_{\boldsymbol{\mu}} \cdot \dot{\mathbf{a}}_{\boldsymbol{\mu}}\right) &= \mu\left(\mathbf{a}'_{\boldsymbol{\mu}} \cdot \mathbf{a}'^*_{\boldsymbol{\mu}}\right) + \frac{1}{2i}\left(\mathbf{a}'_{\boldsymbol{\mu}} \cdot \dot{\mathbf{a}}'^*_{\boldsymbol{\mu}} - \mathbf{a}'^*_{\boldsymbol{\mu}} \cdot \dot{\mathbf{a}}'_{\boldsymbol{\mu}}\right). \end{aligned} \tag{5.5}$$

After expanding the kinetic term in (5.1) and keeping the non-relativistic part, a substitution of (5.4) and (5.5) yields

$$\begin{aligned} L &= \sum_{j=1}^{N} \frac{1}{2}\beta^2 \dot{\boldsymbol{\rho}}'^2_j + \sum_{j=1}^{N}\sum_{\mu_L>0} s_{\mu_L}\left(f'_{\mu_L} e^{i\boldsymbol{\mu}_L\cdot\boldsymbol{\rho}'_j} + f'^*_{\mu_L} e^{-i\boldsymbol{\mu}_L\cdot\boldsymbol{\rho}'_j}\right) \\ &\quad - \sum_{j=1}^{N} \beta\dot{\boldsymbol{\rho}}'_j \cdot \sum_{\mu>0} s_{\mu}\left(\mathbf{a}'_{\mu} e^{i\boldsymbol{\mu}\cdot\boldsymbol{\rho}'_j} + \mathbf{a}'^*_{\mu} e^{-i\boldsymbol{\mu}\cdot\boldsymbol{\rho}'_j}\right) \\ &\quad + \frac{1}{2i}\sum_{\mu_L>0}\left(f'_{\mu_L}\dot{f}'^*_{\mu_L} - f'^*_{\mu_L}\dot{f}'_{\boldsymbol{\mu}_L}\right) \\ &\quad + \frac{1}{2i}\sum_{\mu>0}\left(\mathbf{a}'_{\mu}\cdot\dot{\mathbf{a}}'^*_{\mu} - \mathbf{a}'^*_{\mu}\cdot\dot{\mathbf{a}}'_{\mu}\right) - \sum_{\mu>0}\left(\omega_{\mu}-\mu\right)\left(\mathbf{a}'_{\mu}\cdot\mathbf{a}'^*_{\mu}\right), \end{aligned} \tag{5.6}$$

where we have used $\mu_L = 1$ to cancel certain terms involving the fields f_{μ_L}.

We proceed with another assumption and another change of variables. The assumption is that the transverse waves have constant amplitudes. This is a good assumption as shown by our numerical investigation in previous chapters, see e.g. Fig. 4.12. The change of variables concerns the longitudinal field (which is assumed to be only one from now on) and has the form

$$f'_{\mu_L} = \sqrt{J}\, e^{-i\theta_L}. \tag{5.7}$$

This is a similar notation to that adopted in Chapter 2. With this, the third line in (5.6) becomes simply $J\dot{\theta}_L$. The constant amplitudes of the transverse

waves mean that we can omit the last line in (5.6), it being a known function of time. The transverse fields have the form

$$\mathbf{a}'_\mu = \mathbf{a}^0_\mu e^{-i(\omega_\mu - \mu)}, \tag{5.8}$$

and we can set the constant amplitude as $\mathbf{a}^0_\mu = (0, a_\mu, 0)$. Further, we represent the coordinates as

$$\boldsymbol{\rho}'_j = (\xi_j, \eta_j, \zeta_j). \tag{5.9}$$

With these assumptions the Lagrangian(5.6) becomes

$$\begin{aligned} L &= \sum_{j=1}^{N} \frac{1}{2}\beta^2 \left(\dot{\xi}_j^2 + \dot{\eta}_j^2 + \dot{\zeta}_j^2\right) + \sum_{j=1}^{N} \sum_{\mu_L > 0} 2 s_{\mu_L} \sqrt{J} \cos(\zeta_j - \theta_L) \\ &\quad - \sum_{j=1}^{N} \beta \dot{\eta}_j \sum_{\mu > 0} s_\mu \left(a_\mu e^{i\mu\xi_j} + a^*_\mu e^{-i\mu\xi_j}\right) + J\dot{\theta}_L. \end{aligned} \tag{5.10}$$

Notice that we do not use bold face for subscripts anymore according to the assumption that variables only depend on one coordinate, the z-coordinate (or ζ in our dimensionless notation).

To continue, notice that the equations of motion for ξ_j are just $\ddot{\xi}_j = 0$. With initial conditions $\xi_j(0) = \dot{\xi}_j(0) = 0$, we have $\xi_j = 0$ for all time. Next we write out the equations of motion for η_j

$$\begin{aligned} 0 &= \frac{d}{dt}\left(\frac{\partial L}{\partial \dot{\eta}_j}\right) - \frac{\partial L}{\partial \eta_j} \\ &= \frac{d}{dt}\left(\beta^2 \dot{\eta}_j - \beta \sum_{\mu > 0} s_\mu \left(a_\mu e^{i\mu\xi_j} + a^*_\mu e^{-i\mu\xi_j}\right)\right). \end{aligned} \tag{5.11}$$

It is clear the we can define constants of motion C_j as

$$\beta^2 \dot{\eta}_j - \beta \sum_{\mu > 0} s_\mu \left(a_\mu e^{i\mu\xi_j} + a^*_\mu e^{-i\mu\xi_j}\right) =: \beta C_j. \tag{5.12}$$

Thus from Eqs. (5.11) and (5.12) we can solve for $\dot{\eta}_j$ and substitute the result into the Lagrangian (5.10). In doing so, the following quantities appear quadratically

$$A_j := \left(a_\mu e^{i\mu\xi_j} + a_\mu^* e^{-i\mu\xi_j}\right). \tag{5.13}$$

One further simplification comes with the assumption that the two transverse waves have equal amplitudes, i.e. $a_\mu = A$. The squares of A_j contain the beat wave with frequency

$$\Delta = \Omega_{\mu_2} - \Omega_{\mu_1}, \quad \text{where} \quad \Omega_\mu = \omega_\mu - \mu. \tag{5.14}$$

Therefore the Lagrangian (5.10) can be rewritten in terms of only the ζ_j variables, as well as the longitudinal field variables (J, θ_L)

$$L = \sum_{j=1}^{N} \frac{1}{2}\beta^2\dot{\zeta}_j^2 + \sum_{j=1}^{N} 2s_{\mu_L}\sqrt{J}\cos(\zeta_j - \theta_L) - \epsilon\sum_{j=1}^{N}\cos(\zeta_j - \Delta t). \tag{5.15}$$

In (5.15), $\epsilon = 2A^2 s_{\mu_1} s_{\mu_2}$ is the beat wave amplitude. It is easy to see that putting $\Delta = 0$ is equivalent to the resonance (matching) condition (4.24); we will assume in further considerations that $\Delta = 0$. The rest of the terms quadratic in A_j are not included in (5.15), since it can be assumed that they vary on a fast time scale so that averaging of the Lagrangian over a period of the fast time scale will result in their vanishing.

We now apply the "macroparticle" assumption discussed in the introductory section of this chapter. We assume that N_m particles are clumped together as shown in the last three panels of Fig. 5.1. The particles that are not trapped are neglected. This is a crude approximation, but important features of the general system can still be captured. The Lagrangian (5.15) is thus reduced to a two-degree-of-freedom system and assumes the form

$$L = \frac{1}{2}N_m\beta^2\dot{\zeta}^2 + 2N_m s_{\mu_L}\sqrt{J}\cos(\zeta - \theta_L) - \epsilon N_m\cos(\zeta) + J\dot{\theta}_L. \tag{5.16}$$

We can perform further scalings and a change of variables so that (5.16) is left with a minimal number of parameters. Letting

$$\frac{t}{\beta\sqrt{N_m}} = t', \qquad \frac{J}{\beta\sqrt{N_m}} = J', \tag{5.17}$$

and then dropping the primes on the new variables produces the final form of the Lagrangian,

$$L = \frac{1}{2}\dot{\zeta}^2 + \epsilon_L\sqrt{J}\cos(\zeta - \theta_L) - \epsilon_T\cos(\zeta) + J\dot{\theta}_L. \tag{5.18}$$

The definitions of the parameters are

$$\epsilon_L = 2s_{\mu_L}N_m^{5/4}\beta^{1/2}, \qquad \epsilon_T = \epsilon N_m. \tag{5.19}$$

It is convenient to work with the Hamiltonian form of our reduced system. The transition from the Lagrangian (5.18) to a Hamiltonian form is made through a Legendre transform. The coordinates are transformed in the usual way, whereas the field is transformed as shown in Appendix A. The resulting Hamiltonian is

$$H = \frac{1}{2}p^2 - \epsilon_L\sqrt{J}\,\cos(\zeta - \theta_L) + \epsilon_T\cos(\zeta). \tag{5.20}$$

Another form of the Hamiltonian (5.20) is also convenient. It is achieved by a canonical change from variables (ζ, θ_L) and (p, J) to variables (q, Q) and (p, P), using a generating function of the second kind

$$F_2 = P\theta_L + p'(\zeta - \theta_L). \tag{5.21}$$

It follows that

$$\begin{aligned} p &= \frac{\partial F_2}{\partial \zeta} = p', \qquad & J &= \frac{\partial F_2}{\partial \theta_L} = P - p, \\ q &= \frac{\partial F_2}{\partial p'} = \zeta - \theta_L, \qquad & Q &= \frac{\partial F_2}{\partial P} = \theta_L. \end{aligned} \tag{5.22}$$

Whence, the other form of the Hamiltonian is

$$H = \frac{1}{2}p^2 - \epsilon_L\sqrt{P-p}\,\cos(q) + \epsilon_T\,\cos(q+Q). \tag{5.23}$$

5.3 Phase portrait analysis

5.3.1 Island overlapping

In this section we analyze the phase space of Hamiltonian (5.23). It was shown in previous chapters by numerical simulations that our system of equations, (2.8) for the non-relativistic case and (3.31) for the relativistic case, exhibits chaotic behavior. In this section we will try to support our numerical findings.

The particular technique that we will use is the so-called island overlap criterion (see [59, 60]). It consists of the following idea. A given Hamiltonian is split in two different Hamiltonians (in a more or less artificial way). Then the phase portraits of the two Hamiltonians are drawn on a common phase space. Each Hamiltonian has contours of constant energy (energy surfaces) that include closed curves (when a particle is trapped), also called islands. The width of these islands depends upon certain parameters in the Hamiltonians and/or the energy. It may happen that for certain values of the parameters, the two Hamiltonians have overlapping islands. This is an indication of chaos. A point that starts in one island may move for a certain time inside it and then suddenly jump into the other island. This is a basic mechanism for chaos and results in phase space mixing.

Applying this technique to our Hamiltonian (5.23), we define H_L (for $\epsilon_T = 0$), and H_T (for $\epsilon_L = 0$) as follows

$$H_L = \frac{1}{2}p^2 - \epsilon_L\sqrt{P-p}\,\cos(q) \tag{5.24}$$

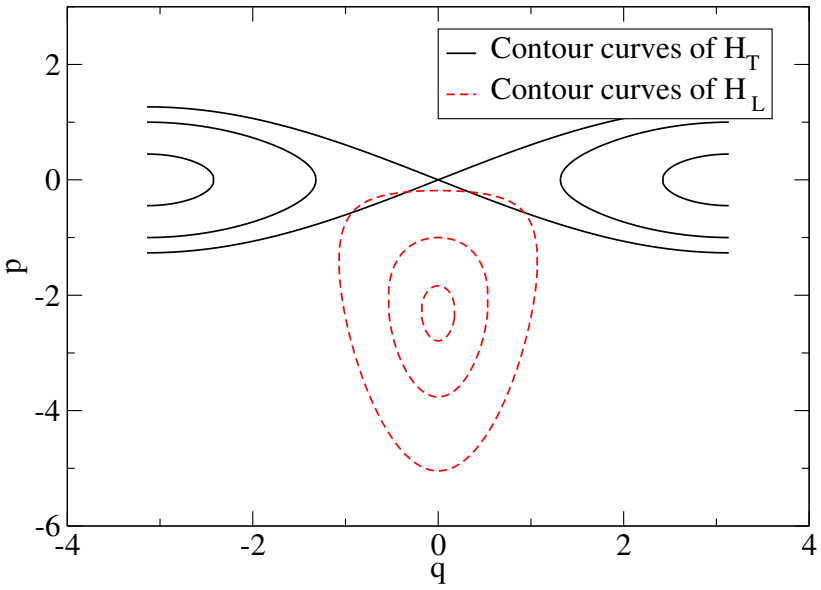

Figure 5.2: Contour plot for the Hamiltonians H_L and H_T demonstrating the island overlap technique. Overlap indicates mixing in phase space and possibility for energy transfer between the longitudinal and the transverse waves.

and

$$H_T = \frac{1}{2}p^2 + \epsilon_T \cos(q). \tag{5.25}$$

Notice that in H_L, $P = \text{const.}$. The physically interesting situation occurs when $P = 0$, since the longitudinal wave in this case grows from zero initial amplitude. In H_T we have put $Q = 0$, since $\dot{Q} = 0$ and we assume $Q(0) = 0$.

The plots for different values of the energy and for $\epsilon_L = 7$ and $\epsilon_T = 0.4$ are given in Fig. 5.2. The width of the islands of H_L is determined by the initial beam energy, while the width of the islands of H_T depends on the

amplitudes of the transverse waves. Phase space mixing occurs only above some minimal threshold for the energy of the transverse waves. Only past this threshold do the islands overlap. Energy can then be transfered between the longitudinal and the transverse waves. This phenomenon was numerically observed in Chapter 4 (cf. Fig. 4.13).

5.3.2 Surfaces of section

After discussing the consequences of island overlapping in the previous subsection 5.3.1, we now wish to make a more quantitative analysis of the Hamiltonian (5.23). We would like to plot the surfaces of section in the coordinate plane of (q, p) defined by $Q = 0$. We do as follows. Following the trajectory of the particle in the four dimensional phase space, we plot a point in the plane (q, p) where the trajectory pierces this plane. If the particle moves on a torus (H = const.), the surface of section traces out a well ordered pattern. If a particle does not stay on the same torus, it jumps in an unpredictable way and such behavior results in a chaotic pattern. This idea was developed by Poincarè in relation to studying the stability of the solar system. It has been widely used and is an established technique for stability analysis.

To find the necessary mapping in the (q, p) plane, we reduce the dimensionality of the Hamiltonian (5.23) from a four-dimensional phase space to a two-dimensional one, using the energy integral of the system and using the coordinate Q as an independent variable; in this way we can plot (q, p) for $Q = 0, 2\pi, 4\pi, ...$ To do so, we express the momentum P through the energy E (i.e we put $H = E$); this defines the Hamiltonian for our new reduced system

(see [61, 62])

$$h := P = p + \frac{1}{\epsilon_L^2 \cos^2(q)} \left(\frac{p^2}{2} + \epsilon_T \cos(q+Q) - E \right)^2 . \qquad (5.26)$$

The equations of motion following from h are

$$\begin{aligned} \frac{dq}{dQ} &= \frac{\partial h}{\partial p} = 1 + \frac{2p}{\epsilon_L^2 \cos^2(q)} \left(\frac{p^2}{2} + \epsilon_T \cos(q+Q) - E \right), \\ \frac{dp}{dQ} &= -\frac{\partial h}{\partial q} = -\frac{2}{\epsilon_L^2 \cos^2(q)} \left(\frac{p^2}{2} + \epsilon_T \cos(q+Q) - E \right) \\ &\quad \times \left(\tan(q) \left(\frac{p^2}{2} + \epsilon_T \cos(q+Q) - E \right) - \epsilon_T \sin(q+Q) \right). \qquad (5.27) \end{aligned}$$

The initial condition for the variable q is $q(0) = 0$. The initial condition for p is set so as to sample out the phase space. We pick 20 sample points along the $q = 0$ line. Special attention is given to the initial condition for which $h = 0$ (recall that the physical situation of interest is when $P = 0$); it can be found simply by solving the equation $h = 0$ for p. The number of iterations varies up to 10^4. If a singularity is encountered before this number is reached, then we plot the smaller number of iterations.

As a first surface of section plot, Fig. 5.3, the transverse waves have zero amplitude, i.e. $\epsilon_T = 0$. Similarly to the previous subsection, we have set $\epsilon_L = 7.0$ and $E = -3.0$. The curve with $h = 0$ corresponds to the out most contour of H_L in Fig. 5.2. Naturally, the surface of section and the contour plot match perfectly (by the definition of H_L). The smooth curves in this plot indicate that the system is integrable. We begin to increase the value of the parameter ϵ_T. As a result of the interaction between the two waves, an additional island appears in phase space, as shown in Fig. 5.4. The value of ϵ_T in this figure equals 0.7, but a tiny island is formed even at very low values of ϵ_T. However, as mentioned in the previous subsection, this island

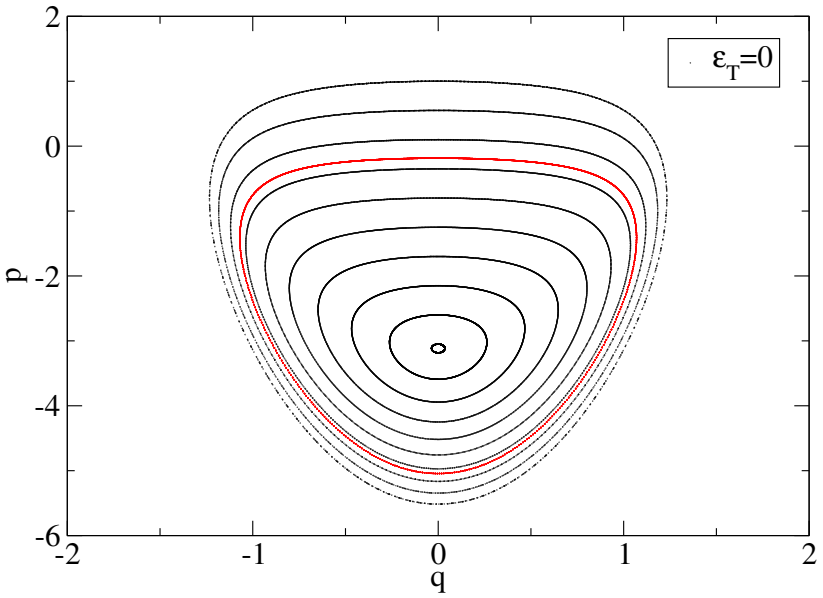

Figure 5.3: Surface of section for $\epsilon_T = 0$, $\epsilon_L = 7.0$, and $E = -3.0$. This plot corresponds to the contour plot in Fig. 5.2 for $H_L = -3.0$.

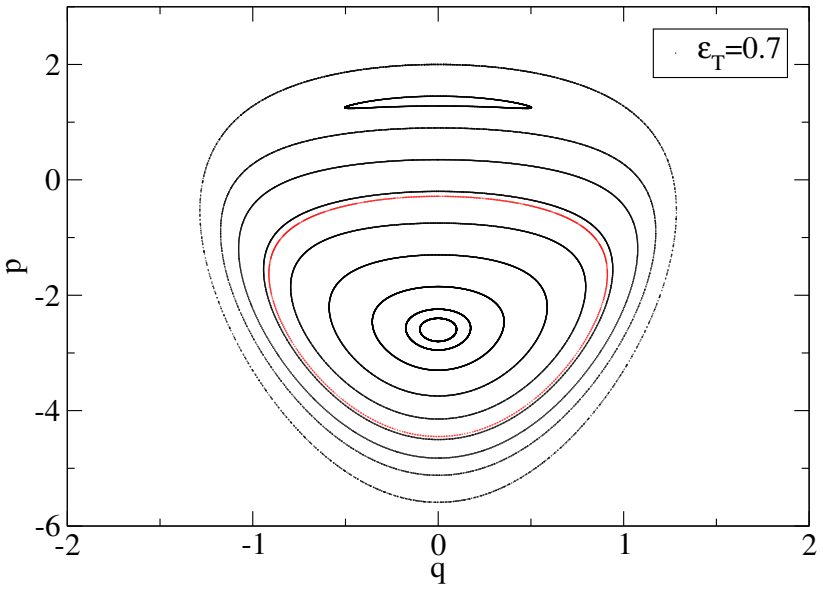

Figure 5.4: Surface of section for $\epsilon_T = 0.7$, $\epsilon_L = 7.0$, and $E = -3.0$. An additional island has formed due to the resonant interaction of the plasma wave and the electromagnetic beat wave.

needs to be given more energy (larger ϵ_T) in order to significantly influence the initial condition for $h = 0$ (the red curve). When $\epsilon_T = 0.785$, the $h = 0$ island snaps into two islands, Fig. 5.5. This is an example of a period doubling bifurcation. Further increase in ϵ_T to the value of 2.0 causes these two islands to go apart and grow in area; large chaotic regions appear and phase space mixing is present, see Fig. 5.6. As ϵ_T is increased further to 2.15, the two islands begin to approach each other. This results in the formation of chaotic layer at their boundary, see Fig. 5.7. The same is seen in the next

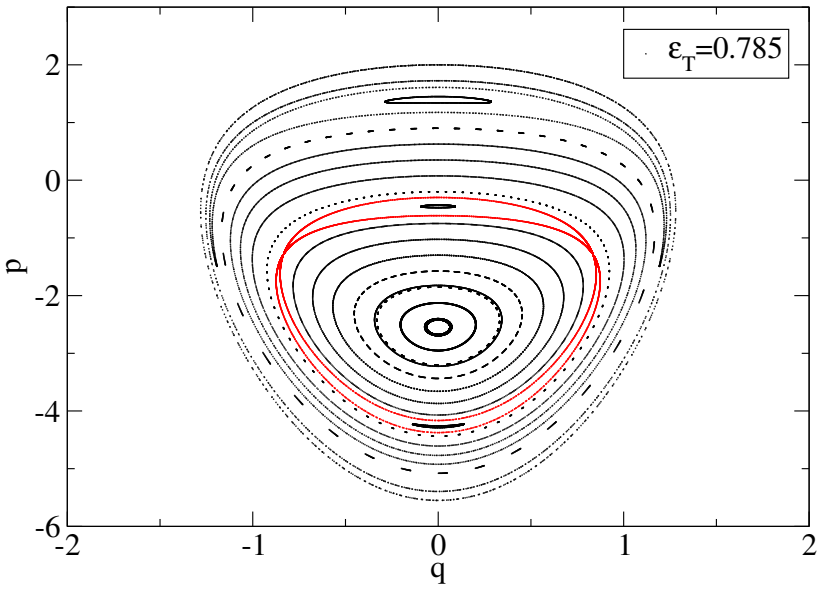

Figure 5.5: Surface of section for $\epsilon_T = 0.785$, $\epsilon_L = 7.0$, and $E = -3.0$. In this plot the initial island $h = 0$ snaps in two. This is an example of a period doubling bifurcation.

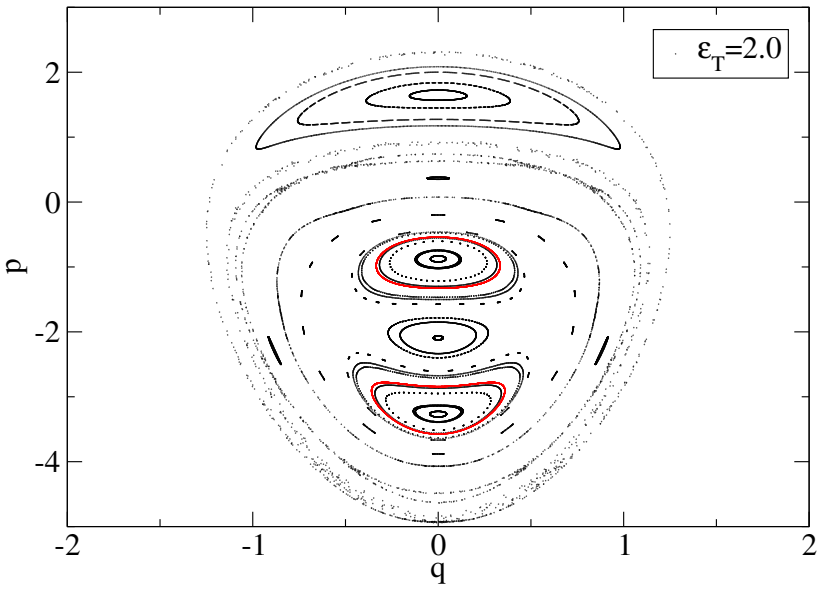

Figure 5.6: Surface of section for $\epsilon_T = 2.0$, $\epsilon_L = 7.0$, and $E = -3.0$. Chaotic regions cause phase space mixing.

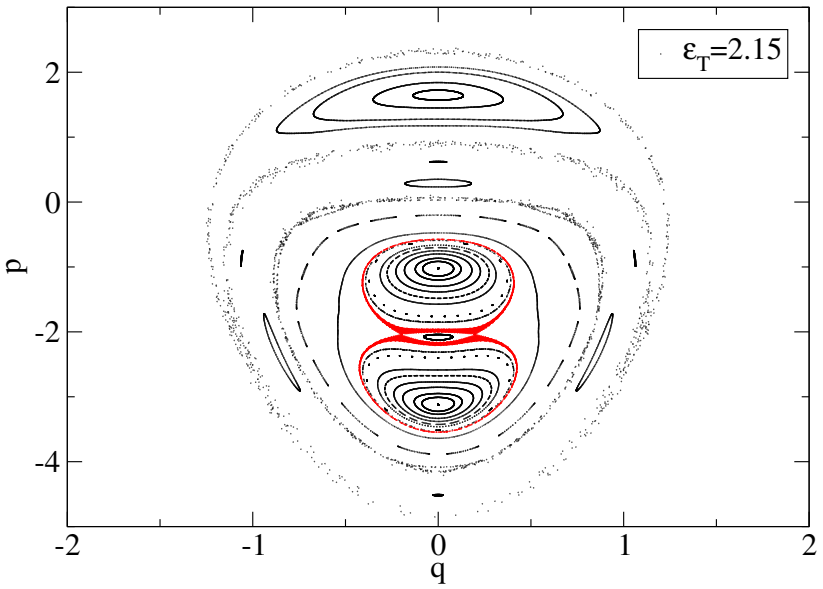

Figure 5.7: Surface of section for $\epsilon_T = 2.15$, $\epsilon_L = 7.0$, and $E = -3.0$. The boundary of two islands $h = 0$ has become chaotic.

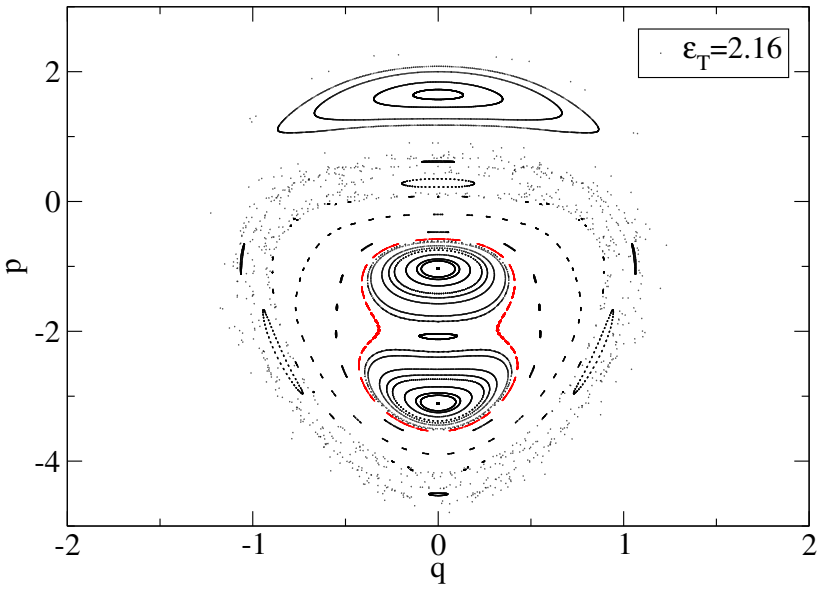

Figure 5.8: Surface of section for $\epsilon_T = 2.16$, $\epsilon_L = 7.0$, and $E = -3.0$. The two islands $h = 0$ have merged and the boundary consists of smaller islands with chaotic boundary.

Fig. 5.8 where the two islands have merged ($\epsilon_T = 2.16$) and the $h = 0$ island transforms into many small islands, each of which has a chaotic boundary. Further increase in ϵ_T to 3.01 results in chaotic regime and phase mixing for the $h = 0$ island, see Fig. 5.9. This is when energy can be transfered between the transverse waves and the particles trapped in the plasma wave.

A further increase in ϵ_T, shown in Fig. 5.10, brings the island $h = 0$ to a period three orbit. Finally, in Fig. 5.11, initial conditions near the $h = 0$ island exhibit chaotic behavior and phase space mixing when $\epsilon_L = 0.3805$. Past this

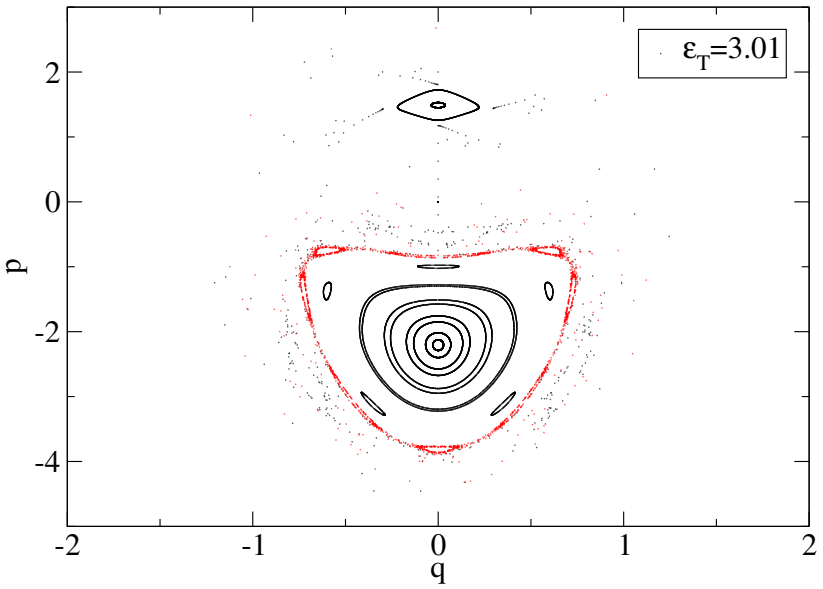

Figure 5.9: Surface of section for $\epsilon_T = 3.01$, $\epsilon_L = 7.0$, and $E = -3.0$. With further increase in ϵ_T the initial condition $h = 0$ becomes chaotic; particles with this initial energy experience phase space mixing.

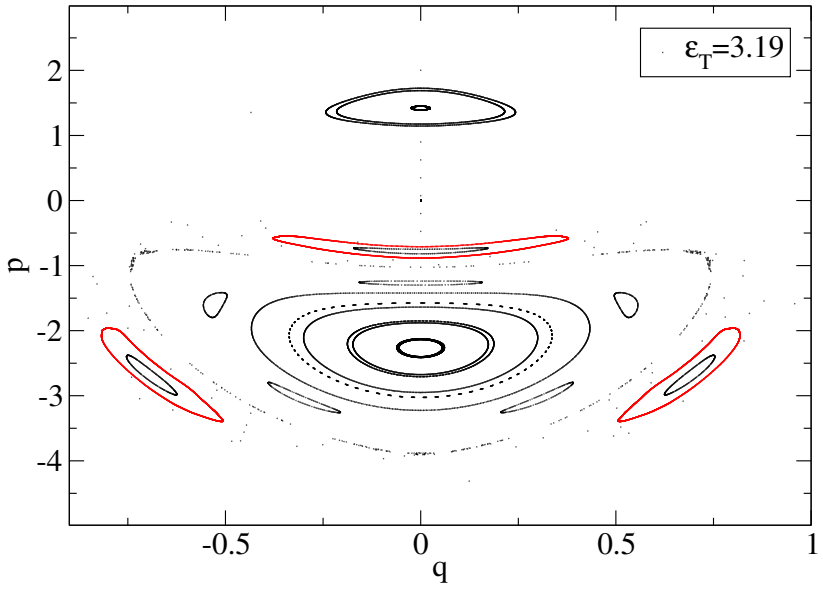

Figure 5.10: Surface of section for $\epsilon_T = 3.19$, $\epsilon_L = 7.0$, and $E = -3.0$. For this value of ϵ_T the initial condition $h = 0$ is non-chaotic.

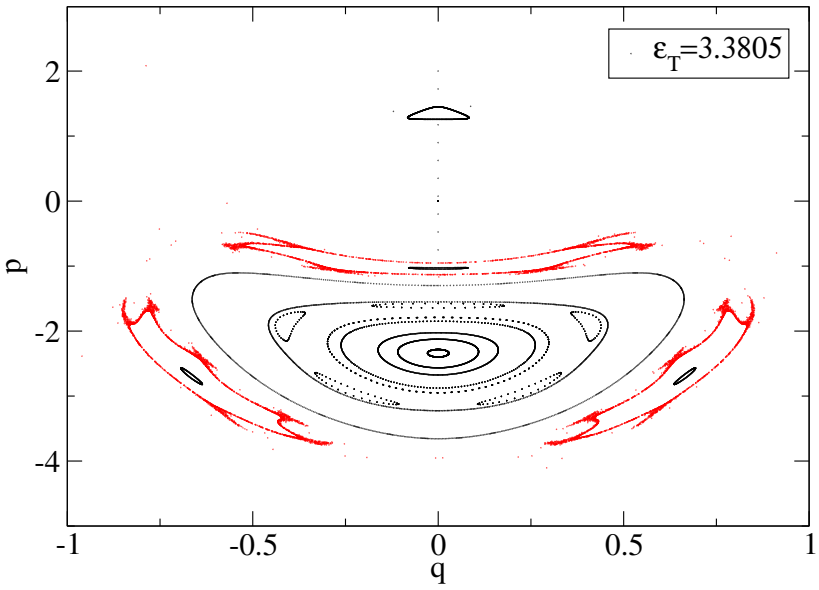

Figure 5.11: Surface of section for $\epsilon_T = 3.3805$, $\epsilon_L = 7.0$, and $E = -3.0$. This is the last chaotic stage of the initial condition $h = 0$. Past the value of $\epsilon_T = 4.97$ the equation $h = 0$ has no real solutions, therefore such values of the parameters are not physical.

point the differential solver encounters difficulties and is unable to proceed to perform the mapping after a very small number of iterations (on the order of $20 - 30$). This also is an indication of instability.

In conclusion, the system of equations (5.27) has a rich and complicated behavior. Fixing the parameter ϵ_L and changing ϵ_T leads the system from a non-chaotic to chaotic regime. We observed island breaking and reconnection, chaotic boundaries, and chaos; through the method of surfaces of section we observed chaos in the system of one electrostatic and two electromagnetic

waves. We observed phase space mixing allowing for energy transfer between electromagnetic and electrostatic waves. The chaotic regime is entered when a certain value of the parameter ϵ_T is exceeded. The latter explains the observed in Fig. 4.13 threshold.

5.4 Linear theory

We begin by determining the fixed points of the Hamiltonian (5.23) The equations of motion are

$$\begin{aligned} \dot{q} &= p + \frac{\epsilon_L}{2\sqrt{P-p}}\cos(q), \\ \dot{p} &= -\epsilon_L\sqrt{P-p}\sin(q) + \epsilon_T \sin(q+Q), \\ \dot{Q} &= -\frac{\epsilon_L}{2\sqrt{P-p}}\cos(q) \\ \dot{P} &= \epsilon_T \sin(q+Q). \end{aligned} \tag{5.28}$$

When both, $\epsilon_L \neq 0$ and $\epsilon_T \neq 0$, there are no fixed points. Since we are interested in the case when the two transverse waves have small amplitudes (i.e. we are going to study their influence perturbatively) we will find the fixed points when $\epsilon_T = 0$. Choosing $q = 0$, from the first of Eqs. (5.28) we find the following fixed point

$$q_0 = 0, \qquad p_0 = -J_0 = -\left(\frac{\epsilon_L}{2}\right)^{2/3}. \tag{5.29}$$

Next we expand the Hamiltonian (5.23) around this fixed point and keep terms up to third order (remember that in changing variables from (5.20) to obtain

(5.23) we found that $q = \zeta - \theta_L$),

$$\begin{aligned} H &= \frac{1}{2}\delta p^2 + \frac{\epsilon_L}{8J_0^{3/2}} + \frac{\epsilon_L\sqrt{J_0}}{2}\left(\delta\zeta - \delta\theta_L\right)^2 - \frac{\epsilon_T}{2}\delta\zeta^2 \\ &\quad + \frac{\epsilon_L}{4\sqrt{J_0}}\delta J\left(\delta\zeta - \delta\theta_L\right)^2. \end{aligned} \tag{5.30}$$

We make a canonical transformation of variables using a generating function of the third kind

$$F_3 = -\delta p\,\delta q' - \frac{\delta J}{\sqrt{2}}\delta Q', \tag{5.31}$$

whence the new variables are found from the relations

$$\begin{aligned} \delta\zeta &= -\frac{\partial F_3}{\partial \delta p} = \delta q', \quad \delta\theta_L = -\frac{\partial F_3}{\partial \delta J} = \frac{\delta Q'}{\sqrt{2}}, \\ \delta p' &= -\frac{\partial F_3}{\partial \delta q'} = \delta p, \quad \delta P' = -\frac{\partial F_3}{\partial \delta Q'} = \frac{\delta J}{\sqrt{2}}, \end{aligned} \tag{5.32}$$

and we can write the Hamiltonian (5.30) as

$$\begin{aligned} H &= \frac{1}{2}\delta p'^2 + \frac{1}{2}\delta P'^2 + \left(\frac{\epsilon_L}{2}\right)^{4/3}\left(\delta q' - \frac{\delta Q'}{\sqrt{2}}\right)^2 - \frac{\epsilon_T}{2}\delta q'^2 \\ &\quad + \left(\frac{\epsilon_L}{2}\right)^{2/3}\delta P'\left(\delta q' - \frac{\delta Q'}{\sqrt{2}}\right)^2. \end{aligned} \tag{5.33}$$

Because the momentum terms are diagonal (sum of squares) we can make a coordinate change using an orthogonal transformation such that the coordinates reduce to a sum of squares (the third order term will change to a third order term correspondingly) while leaving the momentum quadratic form invariant. In other words, we will achieve a diagonal form for the entire Hamiltonian. We use a generating function of the second kind to achieve this,

$$F_2 = \delta p''\left(\cos(\alpha)\delta q' - \sin(\alpha)\delta Q'\right) + \delta P''\left(\sin(\alpha)\delta q' + \cos(\alpha)\delta Q'\right). \tag{5.34}$$

The new variables are found from the relations

$$\begin{aligned} \delta p' &= \cos(\alpha)\delta p'' + \sin(\alpha)\delta P'', \quad \delta P' = -\sin(\alpha)\delta p'' + \cos(\alpha)\delta P'', \\ \delta q'' &= \cos(\alpha)\delta q' - \sin(\alpha)\delta Q', \quad \delta Q'' = \sin(\alpha)\delta q' + \cos(\alpha)\delta Q'. \end{aligned} \tag{5.35}$$

The angle α in (5.35) is found by requiring the coefficient in front of the mixed product $\delta q''\delta Q''$ to vanish. The result is

$$\tan(2\alpha) = \frac{2\sqrt{2}(\epsilon_L/2)^{4/3}}{(\epsilon_L/2)^{4/3} - \epsilon_T}, \qquad \alpha = \frac{1}{2}\arctan\left(\frac{2\sqrt{2}(\epsilon_L/2)^{4/3}}{(\epsilon_L/2)^{4/3} - \epsilon_T}\right). \tag{5.36}$$

We shall not write the Hamiltonian (5.33) in the new variables at once, but instead separate it in two parts $H = H_0 + H_1$. H_0 will contain only quadratic terms, whereas H_1 will include the terms of third order. Thus

$$H_0 = \frac{1}{2}\delta p'^2 + \frac{1}{2}\delta P'^2 + \frac{1}{2}\omega_B^2 \delta q''^2 + \frac{1}{2}\Omega_B^2 \delta Q''^2, \tag{5.37}$$

where

$$\omega_B^2 = 2\left[\left(\frac{\epsilon_L}{2}\right)^{4/3}\left(\cos(\alpha) + \frac{1}{\sqrt{2}}\sin(\alpha)\right)^2 - \frac{\epsilon_T}{2}\cos^2(\alpha)\right], \tag{5.38}$$

$$\Omega_B^2 = 2\left[\left(\frac{\epsilon_L}{2}\right)^{4/3}\left(\sin(\alpha) - \frac{1}{\sqrt{2}}\cos(\alpha)\right)^2 - \frac{\epsilon_T}{2}\sin^2(\alpha)\right] \tag{5.39}$$

and

$$\begin{aligned} H_1 = {} & \left(\frac{\epsilon_L}{2}\right)^{2/3}(-\sin(\alpha)\delta p'' + \cos(\alpha)\delta P'') \\ & \times\left[\left(\cos(\alpha) + \frac{1}{\sqrt{2}}\sin(\alpha)\right)\delta q'' + \left(\sin(\alpha) - \frac{1}{\sqrt{2}}\cos(\alpha)\right)\delta Q''\right]^2 \end{aligned} \tag{5.40}$$

Let us first look at the behavior of the frequency ω_B as a function of ϵ_T. Notice that the angle α has a jump of π at $(\epsilon_L/2)^{4/3} = \epsilon_T$. This means that the frequency ω_B will experience a jump too (and so will Ω_B), see Fig. 5.12. This jump changes the sign of ω_B^2 and the system changes behavior from a periodic to an exponentially growing one. This gives another explanation of the sharp change in the phase in Fig. 2.4 of Chapter 2. It also suggests another explanation of the threshold observed in Fig. 4.13 of Chapter 4. Beyond the

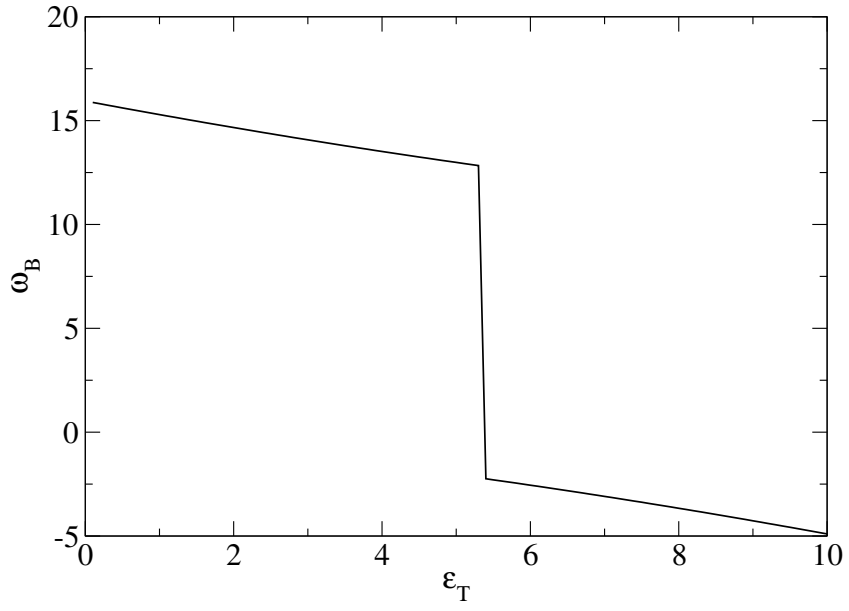

Figure 5.12: Jump in the frequency at $(\epsilon_L/2)^{4/3} = \epsilon_T$. In this plot $\epsilon_L = 7$ and the jump is at 5.3.

threshold the longitudinal wave grows at the expense of the transverse beat wave. The fact that such explanation can be given in the frame of linear theory was also suggested by the fact that the observed threshold was very low as indicated in Fig. 4.13.

5.5 Conclusions

In this last chapter we attempted to simplify, as much as possible, the many-degree-of-freedom systems (2.8) and (3.31) so that some of their basic prop-

erties could be explained. We used the "macroparticle" model to reduce the number of beam particles from N to one. Then we considered only the beat-wave of two electromagnetic waves and one electrostatic wave. Further, based on our numerical findings (see Fig. 4.12) we simplified the model assuming constant amplitudes of the electromagnetic waves, the "external wave" approximation. Thus our system was reduced to two degrees of freedom. We studied the phase portrait of the system, and using the island overlap technique showed the possibility of chaos in our system (observed numerically in Chapter 2, Fig. 2.7). Then we applied the surfaces of section method to show how with increasing of the beat wave amplitude the simplified system evolves through island braking, chaotic boundary, island merging, and chaos. This also explained why we observed a threshold for the amplitudes of the electromagnetic waves above which energy could be transfered between them and the electrostatic wave. Finally, we performed a linear analysis reducing the system to an integrable form. The linear analysis explained a jump in the phase observed in Fig. 2.4 of Chapter 2 and gave another explanation of the threshold phenomenon observed in Figs. 4.13, Chapter 4.

Future work will include the development of a canonical perturbation theory for which the basis was laid out in this last chapter. It will aim at explaining the saturation of growth that follows the stage of linear exponential growth observed in all the numerical simulations of this thesis (see e.g. Fig. 2.1).

Appendix A

Suppose an action of the form is given

$$S = \int \mathrm{d}t \left[A_i(q)\dot{q}_i - V(q) \right]. \tag{A.1}$$

We have used summation over repeated indexes. q are an even number of generalized coordinates. We would like to find the Hamiltonian equations and the Poisson bracket for this action. Let us vary the action (A.1) with respect to all coordinates

$$\begin{aligned} \delta S &= \int \mathrm{d}t \left(\frac{\partial A_i}{\partial q_j} \delta q_j \dot{q}_i + A_i(q) \delta \dot{q}_i - \frac{\partial V}{\partial q_i} \right) \\ &= \int \mathrm{d}t \left(\frac{\partial A_i}{\partial q_j} \delta q_j \dot{q}_i - \frac{\mathrm{d}}{\mathrm{d}t} \left(A_i(q) \right) \delta q_i - \frac{\partial V}{\partial q_i} \right) \\ &= \int \mathrm{d}t \left\{ \left(\frac{\partial A_j}{\partial q_i} - \frac{\partial A_i}{\partial q_j} \right) \dot{q}_j - \frac{\partial V}{\partial q_i} \right\} \delta q_i = 0. \end{aligned} \tag{A.2}$$

If we require that the variation of S vanish for every choice of δq_i, then we obtain the equations of motion

$$-\Omega_{ij}\dot{q}_j = \frac{\partial V}{\partial q_i}, \tag{A.3}$$

where we have defined

$$\Omega_{ij} = \left(\frac{\partial A_i}{\partial q_j} - \frac{\partial A_j}{\partial q_i} \right). \tag{A.4}$$

If now suppose that the matrix Ω is invertible, we can define the matrix J by

$$J_{ij} = (-\Omega_{ij})^{-1}. \tag{A.5}$$

We see that the matrix J is antisymmetric and has an even rank. Therefore it can play the role of a Poission bracket, whereas the Hamilton equations may be written in the way

$$\dot{q}_i = J_{ij}\frac{\partial V}{\partial q_i}. \tag{A.6}$$

We can see that such system may be considered as Hamiltonian, where half of the coordinates play the role of generalized coordinates, whereas the other half are the generalized momenta. Thus V is the Hamiltonian of the system and J is the Poisson bracket.

We apply this approach to the field part of the Lagrangian (3.18) to find the field part of the Hamiltonian, as well as the Poisson brackets that yield the equations of motion for the fields. The variables $f_{\mathbf{k}_L}$ and $\mathbf{a}_\mathbf{k}$ play the role of generalized coordinates, and their complex conjugate, $f^*_{\mathbf{k}_L}$ and $\mathbf{a}^*_\mathbf{k}$, are their conjugate momenta. Therefore, if we take the part of the Lagrangian which contains the fields (let for example consider only the vector potentials)

$$\begin{aligned} L_\mathbf{a} &= \frac{1}{2i}\sum_{\boldsymbol{\mu}>0}\left(\mathbf{a}_{\boldsymbol{\mu}}\cdot\dot{\mathbf{a}}^*_{\boldsymbol{\mu}} - \mathbf{a}^*_{\boldsymbol{\mu}}\cdot\dot{\mathbf{a}}_{\boldsymbol{\mu}}\right) - V(\mathbf{a}) \\ &= \frac{1}{2i}\sum_{\boldsymbol{\mu}>0}\sum_{\sigma=1}^{3}\left(-a^*_{\boldsymbol{\mu}\sigma}\dot{a}_{\boldsymbol{\mu}\sigma} + a_{\boldsymbol{\mu}\sigma}\dot{a}^*_{\boldsymbol{\mu}\sigma}\right) - V(\mathbf{a}). \end{aligned} \tag{A.7}$$

Take $q_1 = a_{\boldsymbol{\mu}1}$, $q_2 = a_{\boldsymbol{\mu}2}$, $A_1 = -a^*_{\boldsymbol{\mu}1}$, $A_2 = a_{\boldsymbol{\mu}1}$, etc. It is easy to see that the matrix Ω is block diagonal with a block for each pair of field variables $a_{\boldsymbol{\mu}\sigma}, a^*_{\boldsymbol{\mu}\sigma}$. According to formula (A.4) each block has the form

$$\Omega_{\boldsymbol{\mu}\sigma} = \frac{1}{2i}\begin{pmatrix} 0 & -2 \\ 2 & 0 \end{pmatrix}. \tag{A.8}$$

Since the matrix $-\Omega_{\mu\sigma}$ is just the σ_2 Pauli matrix, its inverse is the same as the original and the Poisson bracket is

$$J_{\mu\sigma} = \begin{pmatrix} 0 & -i \\ i & 0 \end{pmatrix}. \tag{A.9}$$

Bibliography

[1] L. Tonks and I. Langmuir. Oscillations in ionized gases. *Phys. Rev.*, 33:195, 1929.

[2] A. Vlasov. On the kinetic theory of an assembly of particles with collective interaction. *J. Phys. U.S.S.R.*, 9(1):25–40, 1945.

[3] L.D. Landau. On the vibrations of the electronic plasma. *J. Phys. U.S.S.R.*, 10:25, 1946.

[4] D. Bohm and E.P. Gross. Theory of plasma oscillations. b. excitation and damping of oscillations. *Phys. Rev.*, 75(12):1864, 1949.

[5] A.I. Akhiezer and R.V. Polovin. Theory of wave motion of an electron plasma. *Sov. Phys. JETP*, 3(5):696, 1956.

[6] V.D. Shapiro. Nonlinear theory of the interaction of a monoenergetic beam with a plasma. *Sov. Phys. JETP*, 17(2):416, 1963.

[7] T.M. O'Neil and J. H. Malmberg. Transition of the dispersion roots from beam-type to Landau-type solutions. *Phys. Fluids*, 11(8):1754, 1968.

[8] Ya. B. Fainberg, V.D. Shapiro, and V.I. Shevchenko. Nonlinear theory of

interaction between a "monochromatic" beam of relativistic electrons in a plasma. *Sov. Phys. JETP*, 30(3):528, 1970.

[9] T.M. O'Neil, J.H. Winfrey, and J.H. Malmberg. Nonlinear interaction of a small cold electron beam and a plasma. *Phys. Fluids*, 14(6):1204, 1971.

[10] N.G. Matsiborko, I.N. Onishchenko, V.D. Shapiro, and V.I. Shevchenko. On non-linear theory of instability of a monoenergetic electron beam in plasma. *Plasma Physics*, 14:591, 1972.

[11] H.E. Mynick and A.N. Kaufman. Soluble theory of nonlinear beam-plasma interaction. *Phys. Fluids*, 21(4):653, 1978.

[12] J.C. Adam, G. Laval, and I. Mendonca. Time-dependent nonlinear langmuir waves. *Phys. Fluids*, 24(2):260, 1981.

[13] P. Chen, J.M. Dawson, R.W. Huff, and T. Katsoleas. Acceleration of electrons by the interaction of a bunched electron beam with a plasma. *Phys. Rev. Lett.*, 54(7):693, 1985.

[14] T. Katsoleas, S. Wilks, J.M. Dawson, and J.J. Su. Beam loading in plasma accelerators. In *Particle Accelerators*, volume 22, page 81. Gordon and Breach Science Publishers, Inc., 1987.

[15] K. Nakajima. Plasma-wave resonator for particle-beam acceleration. *Phys. Rev. A*, 45(2):1149, 1992.

[16] B.N. Breizman, P.Z. Chebotaev, A.M. Kudryavtsev, K.V. Lotov, and A.M. Skrinsky. Self-focused particle beam drivers for plasma wakefield accelerators. In *New Modes of Particle Acceleration: Techniques and Sources*, page 75. American Institute of Physics, 1997.

[17] Yu.A. Volkov and V.B. Krasovitskii. Numerical model of a plasma with a monoenergetic relativistic electron beam. *Plasma Phys. Reports*, 26(1):70, 2000.

[18] T. Tajima and J.M. Dawson. Laser electron accelerator. *Phys. Rev. Lett.*, 43(4):267–270, 1979.

[19] Yau Wa Chan. Ultra-intense laser radiation as a possible energy booster for relativistic particles. *Pys. Lett.*, 35A(4):305–306, 1971.

[20] P. Kaw and J. Dawson. Relativistic nonlinear propagation of laser beams in cold overdense plasmas. *Phys. Fluids*, 13(2):472, 1970.

[21] M.N. Rosenbluth and C.S. Liu. Excitation of plasma waves by two laser beams. *Phys. Rev. Lett.*, 29(11):701, 1972.

[22] T. Katsoleas and W.B. Mori. Wave-breaking amplitude of relativistic oscillations in a thermal plasma. *Phys. Rev. Lett.*, 61(1):90, 1988.

[23] J.B. Rosenwig. Multiple-fluid models for plasma wake-field phenomena. *Phys. Rev. A*, 40(9):5249, 1989.

[24] J.B. Rosenwig, B. Breizman, T. Katsoleas, and J.J. Su. Acceleration and focusing of electrons in two-dimensional nonlinear plasma wake fields. *Phys. Rev A*, 44(10):R6189, 1991.

[25] B.N. Breizman, T. Tajima, D.L. Fisher, and P.Z. Chebotaev. Excitation of nonlinear wake field in a plasma for particle acceleration. In *Research Trends in Physics: Coherent Radiation Generation and Particle Acceleration*, page 263, La Jolla, California, 1992. La Jolla International School of Physics, The Institute for Advanced Physics Studies.

[26] J.-M. Rax and N.J. Fisch. Ultrahigh intensity laser plasma interaction: A Lagrangian approach. *Phys. Fluids B*, 5(7):2578, 1993.

[27] D. Farina, M. Lontano, I.G. Murusidze, and S.V. Mikeladze. Hydrodynamic approach to the interaction of a relativistic ultrashort laser pulse with an underdense plasma. *Phys. Rev. E*, 63:056409, 2001.

[28] C. Joshi, B. Blue, C.E. Clayton, E. Dod, C. Huang, K.A Marsh, W.B. Mori, M.J. Hogan, C. O'Connell, R. Siemann, D. Watz, P. Muggli, T. Katsoleas, and S. Lee. High energy density plasma science with an ultrarelativistic electron beam. *Phys. Plasmas*, 9(5):1845, 2002.

[29] N.E. Andreev and S.V. Kuznesov. Guided propagation of short intense laser pulses and electron acceleration. *Plasma Phys. Control. Fusion*, 45:A39, 2003.

[30] S.P. Le Blanc, M.C. Downer, R. Wagner, S.-Y. Chen, A. Maksimchuk, G.M. Mourou, and D. Umstadter. Temporal characterization of a self-modulated laser wakefield. *Phys. Rev. Lett.*, 77(27):5381, 1996.

[31] E. Esarey, P. Sprangle, J. Krall, and A. Ting. Overview of plasma-based accelerator concepts. *IEEE Trans. Plasma Sci.*, 24(2):252–288, 1996.

[32] J.L. Tennyson, J.D. Meiss, and P.J. Morrison. Self-consistent chaos in the beam-plasma instability. *Physica D*, 71:1, 1994.

[33] E.G. Evstatiev, W. Horton, and P.J. Morrison. Multi-wave model for plasma-wave interaction. *Phys. Plasmas*, 10(10):4090–4094, 2003.

[34] F.E. Low. A Lagrangian formulation of the Boltzmann-Vlasov equation for plasmas. *Proc. Royal Soc. London*, 248:282–287, 1959.

[35] J.P. Dougherty. Lagrangian methods in plasma physics. I. General theory of the method of averaged Lagrangian. *J. Plasma Phys.*, 4(4):761–785, 1970.

[36] H. Ye and P.J. Morrison. Action principles for the Vlasov equation. *Phys. Fluids B*, 4(4):771, 1992.

[37] K Sonnad and J. Cary. Finding a nonlinear lattice with improved integrability using lie transform perturbation theory. *Phys. Rev. E*, 69(5):056501, May 2004.

[38] C.B. Schroeder, P.B. Lee, J.S. Wurtele, E. Esarey, and W.P. Leemans. Generation of ultrashort electron bunches by colliding laser pulses. *Phys. Rev. E*, 59(5):6037, 1999.

[39] G.B. Whitham. *Linear and Nonlinear Waves*. John Wiley & Sons, Inc., 1974.

[40] D. del Castillo-Negrete. Nonlinear evolution of perturbations in marginally stable plasmas. *Phys. Lett. A*, 241:99, 1998.

[41] Y. Elskens and D. Escande. *Microscopic Dynamics of Plasmas and Chaos*. Institute of Physics Publishing, Bristol, 2003.

[42] I. Doxas and J.R. Cary. Numerical observation of turbulence enhanced growth rates. *Phys. Plasmas*, 4(7):2508, 1997.

[43] N. Padhye and W. Horton. Alfvén-wave particle interaction in finite-dimensional self-consistent field model. *Phys. Plasmas*, 6(3):970, 1999.

[44] J.D. Jackson. *Classical Electrodynamics*. John Wiley & Sons, Inc., New York, 3 edition, 1999.

[45] D. Bauer, P. Mulser, and W.-H Steeb. Relativistic ponderomotive force, uphill acceleration, and transition to chaos. *Phys. Rev. Lett.*, 75(25):4622, 1995.

[46] M.D. Tokman. Efect of the ponderomotive force of a relativistically strong wave field on charged particles. *Plasma Phys. Reports*, 25(2):140–144, 1999.

[47] I.Y. Dodin and N.J. Fisch. Relativistic electron acceleration in focused laser fields after above-treshold ionization. *Phys. Rev. E*, 68:056402, 2003.

[48] L.D. Landau and E.M. Lifshitz. *The Classical Theory of Fields*. Pergamon Press, Oxford, New York, 4 edition, 1975.

[49] V.N. Tsytovich. *Nonlinear Effects in Plasma*. Plenum Press, New York–London, 1 edition, 1970.

[50] J.M. Dawson. Nonlinear electron oscillations in a cold plasma. *Phys. Rev.*, 113(2):383, 1959.

[51] E. Frieman, S. Bodner, and P. Rutherford. Some new results on the quasi-linear theory of plasma instabilities. *Phys. Fluids*, 6(9):1298, 1963.

[52] A. Simon and N. Rosenbluth. Single-mode saturation of the bump-on-tail instability: Immobile ions. *Phys. Fluids*, 19(10):1567, 1976.

[53] V.I. Onishchenko, A.R. Linetskii, N.G. Matsiborko, V.D. Shapiro, and V.I. Shevchenko. Contribution to the nonlinear theory of excitation of a

monochromatic plasma wave by an electron beam. *JETP Lett.*, 12(8):281, 1970.

[54] J.D. Crawford and A. Jayaraman. Nonlinear saturation of an electrostatic wave: Mobile ions modify trapping scaling. *Phys. Rev. Lett.*, 77(17):3549, 1996.

[55] J.D. Crawford and A. Jayaraman. First principles justification of "Single wave model" for electrostatic instabilities. *Phys. Plasmas*, 6(3):666, 1999.

[56] N.J. Balmforth and R.R. Kerswell. Saturation of electrostatic instability in two-species plasma. *J. Plasma Physics*, 68(2):87, 2002.

[57] V.I. Arnold. *Ordinary Differential Equations*. The MIT Press, Cambridge, Massachusets, and London, England, 10 edition, 1998.

[58] F.W. Perkins and J. Flick. Parametric instabilities in inhomogeneous plasmas. *Phys. Fluids*, 14(9):2012–2018, 1971.

[59] B.V. Chirikov. A universal instability of many-dimensional oscillator systems. *Phys. Rep.*, 52(5):263–379, 1979.

[60] D. del-Castillo-Negrete and P.J. Morrison. Chaotic transport by Rossby waves in shear flow. *Phys. Fluids A*, 5(4):948–965, 1993.

[61] E.T. Whittaker. *A Treatise on the Analytical Dynamics od Particles and Rigid Bodies*. Cambridge University Press, 4 edition, 1964.

[62] P.J. Morrison. Hamiltonian description of the ideal fluid. *Rev. Mod. Phys.*, 70(2):467–521, April 1998.

Vita

Evstati Georgiev Evstatiev was born in Teteven, Bulgaria, on April 6, 1969. In 1978 his family moved to the capital city of Bulgaria, Sofia, where he attended the High School of Electronics from 1984 to 1988. He served his duty in the Bulgarian Army from 1988 to 1990, after which he entered the Faculty of Physics at Sofia University, Bulgaria. He graduated with a Master of Science degree in physics during the Fall semester of 1995. He worked as a research physicist at the Bulgarian Academy of Sciences from 1996 to September 1997 when he was accepted to begin graduate studies at The University of Texas at Austin.

Permanent Address: 7303 Wood Hollow Dr., Apt. 488,
Austin, TX 78731

This dissertation was typeset with LaTeX 2_ε[1] by the author.

[1] LaTeX 2_ε is an extension of LaTeX. LaTeX is a collection of macros for TeX. TeX is a trademark of the American Mathematical Society. The macros used in formatting this dissertation were written by Dinesh Das, Department of Computer Sciences, The University of Texas at Austin, and extended by Bert Kay and James A. Bednar.